

**EARTHQUAKE PROTECTION OF BEYLERBEYI PALACE BY
REVERSIBLE MIXED TECHNOLOGIES**

FUAT ARAS

**BOGAZIÇI UNIVERSITY
2007**

EARTHQUAKE PROTECTION OF BEYLERBEYI PALACE BY REVERSIBLE
MIXED TECHNOLOGIES

by

Fuat Aras

B.S., Civil Engineering, Istanbul Technical University, 1998

M.S., Civil Engineering, Bogaziçi University, 2001

Submitted to the Institute for Graduate Studies in
Science and Engineering in partial fulfillment of
the requirements for the degree of
Doctor of Philosophy

Graduate Program in Civil Engineering

Bogaziçi University

2007

to the wonderful memory of
my cousin, *Tansu Aras*
and
my grandfather, *H. Hüdaverdi Aras*

ACKNOWLEDGEMENTS

I would like to express my sincere thanks to my thesis supervisor, Prof. Dr. Gülay Altay for her invaluable guidance, continuous support, and helpful suggestions. She has always been supportive for the preparation of this thesis.

My sincere gratitude is also due to the members of my advisory committee Prof. Dr. Özal Yüzügüllü, Assistant Prof. Dr. Hilmi Lus, Dr. Erhan Karaesmen and Prof. Dr. Erol Güler for useful suggestions and comments.

I express my sincere thanks to the coordinator of PROHITECH, Prof. Dr. Federico M. Mazzolani and the leader of WP11, Prof. Dr. Jean. P. Jaspert.

The technical assistances of Associated Prof. Dr. Fahri Esenli, Dr. Hafez Keypour, Prof. Dr. Mustafa Erdik, Assistant Prof. Dr. Wael Mowrtage, Assistant Prof. Dr. Lidija Krstevska, Prof. Dr. Ljubomir Taskov, Prof. Dr. Ljupco Lazarov, Prof. Dr. Kiril Gramatikov, Prof. Dr. J. M. Proenca, Koce Todorov, Karin Sesetyan, and Orhan Yavuz are greatly acknowledged.

I also want to thanks to Dr. Celal Öztas, Yunus Aydin, Seyda Zirhlioglu, Erol Savran and Kamil Nalci of Regional Directorate of National Palaces for their invaluable supports.

Heartfelt thanks to Yilmaz Aras, Ali Kasay Enünlü, Selçuk Altay, Osman Kaya, Yavuz Tokmak, Ayse Aydin, and Aykut Erkal for their encouragement.

ABSTRACT

EARTHQUAKE PROTECTION OF BEYLERBEYI PALACE BY REVERSIBLE MIXED TECHNOLOGIES

The historical building stock and seismic risk of Anatolia draws considerable attention of the engineers for studying the earthquake performance of these structures and investigating appropriate protection techniques. In this respect, this study aims to examine the earthquake performance of the historic Beylerbeyi Palace which is a representative of the great buildings in the late of 19th century in Istanbul and elsewhere in the Ottoman Empire and search the possible retrofit techniques by means of reversible mixed technologies within the framework of FP6-Earthquake Protection of Historical Structures by Reversible Mixed Technologies (PROHITECH).

Starting with the mineralogical structure of the mortar and ending with mechanical properties of masonry, material identification process has been carried out. Later on Ambient Vibration Survey, (AVS) was conducted in the structure with the University of "St. Cyril and Methodius", Institute of Earthquake Engineering and Engineering Seismology. Numerical model of the palace has been constructed and calibrated according to results of AVS. Response spectrum analyses have been carried out by using three different earthquake cases, defined by accounting the site specific soil and seismic characteristics of the site. The performance of the structure was assessed as weak. Furthermore the vulnerable parts of the structure were revealed by nonlinear analyses.

Finally according to results of the analyses and considering the historical and architectural perspective of Beylerbeyi Palace three different retrofit strategies have been proposed and discussed in details. According to order of presentation, the first proposed strategy is the use of fiber reinforced polymers. The second strategy is the installation of the base isolation and the last one is the consolidation of the roof level to have the rigid diaphragm behavior with the application of fiber reinforced polymers to the required walls.

ÖZET

BEYLERBEYİ SARAYININ GERİDÖNÜSÜMLÜ KARMA TEKNOLOJILERLE DEPREME KARSI KORUNMASI

Anadolu'nun tarihi yapı stogu ve deprem riski, mühendislerin dikkatini önemli ölçüde bu yapıların deprem performanslarını belirlemeye yönelik çalışmalar yapmaya ve uygun koruma yöntemlerinin araştırılmasına çekmektedir. Bu bağlamda, bu çalışma, İstanbul ve Osmanlı İmparatorluğu içindeki diğer yerlerde, 19. yüzyıl yapılarının bir örneği olan tarihi Beylerbeyi Sarayının deprem performansının belirlenmesini ve yapının deprem etkilerine karşı olası yenilenebilir teknolojilerle takviyesinin araştırılmasını, “Tarihi Yapıların Depreme Karşı Yenilenebilir Karma Teknolojilerle Güçlendirilmesi”, isimli FP6 projesi kapsamında, amaçlamaktadır.

Yapıda kullanılan harcın minerolojik yapısıyla başlayan ve yapıdaki yigma duvarların genel mekanik özelliklerinin saptanmasıyla biten malzeme tanımlama çalışması yürütülmüştür. Daha sonra, “St. Cyril ve Methodius Üniversitesi, Deprem Mühendisliği ve Mühendislik Sismolojisi Enstitüsü” ile birlikte yapının Çevresel Titreşim Arastırması (ÇTA) yapılmıştır. Sarayın sayısal modeli hazırlanmış ve ÇTA sonuçlarına göre düzeltilmiştir. Yapının bulunduğu bölgenin yerel zemin ve deprem karakteristikleri de göz önüne alınarak tanımlanmış üç farklı deprem spektrumuna göre yapı deprem etkisi altında analiz edilmiş ve performansı zayıf bulunmuştur. İlave olarak doğrusal olmayan itme analizi ile sarayın problemlili kısımları belirlenmiştir.

Son olarak analiz sonuçlarına göre, yapının tarihi ve mimarlık özelliklerini de göz önünde bulundurarak üç farklı performans iyileştirme yöntemi önerilip, detaylı olarak tartışılmıştır. Tezdeki sunum sırasına göre ilk önerilen yöntem fiber takviyeli polimerlerin kullanılmasıdır. İkinci strateji yapı ile zeminin birbirinden ayrılmasıdır ve son olarak yapının çatı seviyesinin rijit diyafram olacak şekilde takviyesi, gerekli duvarlara fiber takviyeli polimerlerin uygulanması ile beraber önerilmiştir.

TABLE OF CONTENTS

DEDICATION.....	iii
ACKNOWLEDGMENTS	iv
ABSTRACT.....	v
ÖZET	vi
LIST OF FIGURES	x
LIST OF TABLES	xxi
LIST OF SYMBOLS / ABBREVIATIONS.....	xxiii
1. INTRODUCTION	1
1.1. Objective of the Thesis	2
1.2. Scope of the Thesis	2
2. BEYLERBEYI PALACE: HISTORY, ARCHITECTURAL AND STRUCTURAL FEATURES	5
2.1. History of Beylerbeyi Palace	5
2.2. Architecture of Beylerbeyi Palace	6
2.3. Structural Elements in Beylerbeyi Palace	13
3. DAMAGE ASSESSMENT AND MATERIAL IDENTIFICATION.....	15
3.1. Damage Assessment	15
3.2. Material Identification.....	19
3.2.1. Applicability of Non-Destructive Test (NDT) Methods	19
3.2.2. Mortar Identification Procedure	23
3.2.2.1. Thin Sections, under Polarizing Microscope	24
3.2.2.2. Scanning Electron Microscope Views and Energy Dispersive X-Ray Analysis	26
3.2.2.3. X-Ray Diffraction Analysis	31
3.2.3. Mechanical Properties of Horasan Mortar.....	32
3.2.4. Mechanical Properties of Masonry.....	36
3.2.5. Concluding remarks	44
4. AMBIENT VIBRATION SURVEY AND NUMERICAL MODEL OF THE PALACE	46
4.1 Necessity of Ambient Vibration Survey.....	46

4.2 Ambient Vibration Survey (AVS)	47
4.2.1 Procedure	47
4.2.2. Experimental results	47
4.3. Numerical Model of the Palace.....	51
4.3.1. Construction of Numerical Model.....	52
4.3.2. Modal Analysis of the Structure	56
4.4. Effect of the Exterior Wall to the Dynamic Behavior of the Structure	66
4.5. Calibration Process	67
4.5.1. First Step in Calibration	68
4.5.2. Second Step in Calibration	69
4.5.3. Third Step in Calibration	70
4.5.4. Fourth Step in Calibration	71
4.5.5. Fifth Step in Calibration	72
4.6. Interpretation of the Results	77
5. SEISMIC HAZARD AND EARTHQUAKE RISK OF THE MARMARA REGION	78
5.1 Earthquake Ground Shaking Hazard Levels.....	78
5.1.1. Serviceability Earthquake	79
5.1.2. Design Earthquake	79
5.1.3. Maximum Earthquake 14	79
5.1.4. Maximum Considered Earthquake	79
5.2 Seismic Risk of the Marmara Region.....	80
5.3. Hazard Maps	81
5.4. Geological and Geotechnical Properties of the Site on which Beylerbeyi Palace is Located	85
5.5. Concluding Remarks.....	86
6. ANALYSIS UNDER STATIC AND DYNAMIC LOADS	88
6.1. Analysis of the Structure under Static Loads	93
6.2. Analysis of the Structure under Dynamic Loads	89
6.2.1. RSA according to Turkish Earthquake Code.....	92
6.2.2. RSA, according to Design Earthquake (DE)	96
6.2.3. RSA, according to Maximum Considered Earthquake (MCE).....	98
6.2.4. Concluding Remarks	100

7. NONLINEAR PUSHOVER ANALYSIS	103
7.1. Lateral Load Pattern and Non-linear Material Properties	103
7.2. Pushover Analysis along with Longitudinal Direction.....	108
7.3. Pushover Analysis along with Transversal Direction.....	111
7.4. Concluding Remarks.....	113
8. RETROFIT OF THE STRUCTURE	114
8.1. Fiber Reinforced Polymer Overlays (FRP).....	115
8.1.1 Technical description,	115
8.1.2. Practical Methodologies and Structural Detailing	120
8.1.3. Reversibility.....	125
8.1.4. Aesthetic of Appearance	126
8.2. Base Isolation.....	126
8.2.1 Technical Description.....	126
8.2.2. Practical Methodologies and Structural Detailing	128
8.2.3. Reversibility.....	139
8.2.4. Aesthetic of Appearance	139
8.3. Consolidation of the Slabs to Have Rigid Diaphragm Behavior	139
8.3.1 Technical Description.....	139
8.3.2. Practical Methodologies and Structural Detailing	140
8.3.3. Reversibility.....	141
8.3.4. Aesthetic of Appearance	142
9. CONCLUSION	143
REFERENCES	146

LIST OF FIGURES

Figure 2.1.	The first Beylerbeyi Palace	6
Figure 2.2.	Site plan of Beylerbeyi Palace complex.....	7
Figure 2.3.	Present Beylerbeyi Palace	8
Figure 2.4.	Plan of the basement floor of the palace	8
Figure 2.5.	Plan of the first storey of the palace	9
Figure 2.6.	Plan of the second storey of the palace	9
Figure 2.7.	Vertical section of the structure along with transversal direction.....	10
Figure 2.8.	Vertical section of the structure along with longitudinal direction.....	10
Figure 2.9.	Western interaction on exterior façade versus Turkish interaction on interior face	11
Figure 2.10.	A view from Pool Saloon.....	11
Figure 2.11.	A view from Blue Saloon.....	12
Figure 2.7.	Views from two different staircases in the palace.....	12
Figure 2.13.	Foundation of the palace	13
Figure 2.14.	Splice of timber beam between the structural wall and slab beams.....	14
Figure 2.15.	Structural wall and timber slab in the roof of the structure.....	14

Figure 3.1.	Ventilation opening in the foundation floor	16
Figure 3.2.	High humidity over stones and its effects	16
Figure 3.3.	Chipped timber beams due to decay on the foundation floor	16
Figure 3.4.	Horizontal crack in the Mabeyn part	17
Figure 3.5.	Vertical crack in Mabeyn part	18
Figure 3.6.	Inclined cracks on the corners of the door	18
Figure 3.7.	Application of double flatjack testing method on a masonry wall.....	21
Figure 3.8.	Masonry configuration in the room of harem	24
Figure 3.9.	Masonry configuration in the stair case of harem.....	24
Figure 3.10.	Thin-sections	25
Figure 3.11.	Photograph of thin-section under microscope.....	25
Figure 3.12.	Mortar specimens, prepared for SEM and EDX analysis	26
Figure 3.13.	SEM views from the mortar between the bricks.....	27
Figure 3.14.	SEM views from the mortar between the bricks.....	28
Figure 3.15.	SEM views from the plaster.....	29
Figure 3.16.	EDX analysis of particle in SEM view	30
Figure 3.17.	Identified feldspar elements, EDX analysis of particle	30

Figure 3.18.	EDX analysis of binding material in SEM view.....	31
Figure 3.19.	Compression and flexure tests and failure of the specimens	34
Figure 3.20.	Stress-strain curves of the mortar specimens produced with F1	35
Figure 3.21.	Stress-strain curves of the mortar specimens produced with F2.....	35
Figure 3.22.	Masonry test specimen.....	37
Figure 3.23.	Compression test specimen with 1.8 cm mortar height and 6.5 cm brick height.....	37
Figure 3.24.	Testing of masonry specimen.....	38
Figure 3.25.	Failure of the masonry specimen	38
Figure 3.26.	Load-displacement curves for masonry specimens produced by F1 mortar.....	39
Figure 3.27.	Stress-strain curves of masonry specimens produced by F1 mortar	39
Figure 3.28.	Load-displacement curves for masonry specimens produced by F2 mortar.....	40
Figure 3.29.	Stress-strain curve of masonry specimens produced by F2 mortar.....	40
Figure 3.30.	Average stress-strain curves of the masonries produced with F1 and F2 mortar.....	41
Figure 3.31.	Determination of modulus of elasticity according to EC-6.....	42
Figure 4.1.	Location of the measurements and position of the reference point.....	48

Figure 4.2.	First Mode Shape (T=0.371 second).....	48
Figure 4.3.	Second Mode Shape (T=0.278 second)	49
Figure 4.4.	Third Mode Shape (T=0.241 second)	49
Figure 4.5.	Fourth Mode Shape (T=0.192 second).....	49
Figure 4.6.	Fifth Mode Shape (T=0.126 second)	50
Figure 4.7.	Sixth Mode Shape (T=0.120 second).....	50
Figure 4.8.	Eighth Mode Shape (T=0.095 second).....	50
Figure 4.9.	Basement of the structure	53
Figure 4.10.	Basement of the palace with timber slab members	53
Figure 4.11.	Three dimensional model of the palace	54
Figure 4.12.	Three dimensional model of the palace with timber slab.....	54
Figure 4.13.	Three dimensional model of the palace with timber slab	55
Figure 4.14.	First mode shape; Movement of the right part in transversal direction (T=0.361 sec, MPR 0.12-Y).....	61
Figure 4.5.	Second mode shape; Movement of the right part in transversal direction (T=0.317 sec, MPR0.12-Y)	61
Figure 4.16.	Third mode shape; Movement of the front part in longitudinal direction (T=0.301 sec, MPR=0.10-X)	62

Figure 4.17.	Fourth mode shape; Movement of the back part in longitudinal direction (T=0.282 sec, MPR=0.12-X)	62
Figure 4.18.	Fifth mode shape; Movement of the mid part in transversal direction (T=0.277 sec, MPR=0.075-Y)	63
Figure 4.19.	Sixth mode shape; Movement of the back part in longitudinal direction (T=0.276 sec, MPR=0.074-X)	63
Figure 4.20.	Seventh mode shape; Movement of the mid part in longitudinal direction (T=0.249 sec, MPR=0.073-X)	64
Figure 4.21.	13th mode shape; Movement of the timber slab in vertical direction (T=0.221 sec, MPR=0.000465-Z).....	64
Figure 4.22.	59th mode shape; Movement of the lower part in longitudinal direction (T=0.009 sec, MPR=0.21-X)	65
Figure 4.23.	60th mode shape; Movement of the lower part in transversal direction (T=0.009 sec, MPR=0.20-Y)	65
Figure 4.24.	Adjacent wall.....	66
Figure 4.25.	Numerical model of the palace including the external wall.....	66
Figure 4.26.	First mode in NM and AVS (The same movement with different periods).....	68
Figure 4.27.	Second mode in NM and fourth mode of AVS after the first calibration.	69
Figure 4.28.	Second mode in NM and AVS after the second calibration	70

Figure 4.29: The fourth mode of NM and the third mode of AVS after the third calibration..... 71

Figure 4.30. Determined modulus of elasticities..... 73

Figure 4.31. The first mode of calibrated model is exactly same as the first mode of AVS..... 73

Figure 4.32. Three consecutive modes (second, third and fourth modes) of calibrated model form the second mode of AVS 74

Figure 4.33. The fifth mode of the calibrated model is the same as the third mode of the AVS..... 75

Figure 4.34. Two consecutive modes (seventh and eighth modes) of calibrated model form the fourth mode of AVS 75

Figure 5.8. Fault segmentation model of the Marmara region..... 81

Figure 5.2. PGA contour map for 10% probability of exceedence in 50 years 82

Figure 5.3. PGA contour map for 10% probability of exceedence in 50 years 82

Figure 5.4. $S_a(T = 0.2 \text{ s})$ contour map for 10% probability of exceedence in 50 years 83

Figure 5.5. $S_a(T = 0.2 \text{ s})$ contour map for 2% probability of exceedence in 50 years 83

Figure 5.6. $S_a(T = 1.0 \text{ s})$ contour map for 10% probability of exceedence in 50 years84

Figure 5.7.	Sa (T = 1.0 s) contour map for 2% probability of exceedence in 50 years	84
Figure 5.8.	Code of the Drillings and lines of Seismic Refraction Analysis.....	85
Figure 6.1.	S11 stresses under vertical loads	88
Figure 6.2.	S22 stresses under vertical loads	88
Figure 6.3.	Turkish Earthquake Code based response spectra	90
Figure 6.3.	Construction of the response spectra (NEHRP).....	90
Figure 6.5.	Response spectrum of Turkish Earthquake Code	92
Figure 6.6.	S11 stresses under RSA according to TEC, in longitudinal direction	93
Figure 6.7.	S22 stresses under RSA according to TEC, in longitudinal direction	94
Figure 6.8.	S12 stresses under RSA according to TEC, in longitudinal direction	94
Figure 6.9.	S11 stresses under RSA according to TEC, in transversal direction	95
Figure 6.10.	S22 stresses under RSA according to TEC, in transversal direction	95
Figure 6.11.	S12 stresses under RSA according to TEC, in transversal direction	95
Figure 6.12.	Response Spectrum obtained for Design Earthquake	96
Figure 6.13.	S11 stresses under RSA of DE in longitudinal direction.....	97
Figure 6.14.	S11 stresses under RSA of DE in transversal direction.....	97

Figure 6.15.	Response Spectrum obtained for Maximum Considered Earthquake	98
Figure 6.16.	S11 stresses under RSA of MCE in longitudinal direction.....	99
Figure 6.17.	S11 stresses under RSA of maximum MCE in transversal direction.....	99
Figure 6.18.	Out of plane behavior and related stress concentration.....	100
Figure 6.19.	Stress concentrations at the corner of openings and a corner crack from the structure	102
Figure 6.20.	Vertical stress concentration and respective crack from the structure.....	102
Figure 7.1.	Application of the horizontal loads	104
Figure 7.2.	Nonlinear material properties for CCCM.....	107
Figure 7.3.	Terminology through the discussion.	108
Figure 7.4.	Deformed shape of the palace after pushover analysis in longitudinal direction.....	109
Figure 7.5.	Pushover curves for the walls loaded by inplane loads along with longitudinal direction	110
Figure 7.6.	Pushover curves for the walls loaded by out of plane loads along with longitudinal direction	110
Figure 7.7.	Deformed shape of the palace after pushover analysis in transversal direction.....	111
Figure 7.8.	Pushover curves for the walls loaded by inplane loads along with transversal direction	112

Figure 7.9.	Pushover curves for the walls loaded by out of plane loads along with transversal direction	112
Figure 8.1.	Stress-strain relationship of different FRPs	116
Figure 8.2.	Different types of FRP and their applications	117
Figure 8.3.	Strengthening of masonry with FRP (a) bonded strips to improve flexural and in-plane shear strength, (b) circumferentially applied unbonded strip-like tendons, providing confinement.....	118
Figure 8.4.	The specimen test set-up	119
Figure 8.5.	The tested RM3 wall (vertical applied CFRP).....	119
Figure 8.6.	Load-displacement diagram of the wall for vertically applied CFRP.....	119
Figure 8.7.	Load-displacement diagram of the wall for horizontally applied CFRP ..	120
Figure 8.8.	Critical regions with respect to horizontal stresses according to TEC	121
Figure 8.9.	Critical regions with respect to vertical stress stresses according to TEC	121
Figure 8.10.	Critical regions with respect to horizontal stresses according to DE.....	122
Figure 8.11.	Critical regions with respect to vertical stresses according to DE.....	122
Figure 8.12.	Critical regions with respect to horizontal stresses according to MCE.....	123
Figure 8.13.	Critical regions with respect to vertical stresses according to MCE.....	123

Figure 8.14.	Critical regions with respect to horizontal and vertical stresses under MCE for external left part walls.....	124
Figure 8.15.	Critical regions with respect to horizontal and vertical stresses under MCE for external sea-side walls	125
Figure 8.16.	Base isolation devices (A : HDRB, B:LRB, C, D : FPS).....	127
Figure 8.17.	Period shifting and damping effect on response reduction.....	128
Figure 8.18.	Plan lay-out of HDRB in Beylerbeyi Palace	130
Figure 8.19.	Load free area, Af.....	132
Figure 8.20.	Reduced cross-sectional area of circular bearing.....	134
Figure 8.21.	Geometry of the HDRB designed for Beylerbeyi Palace.....	135
Figure 8.22.	S11 stresses under RSA of maximum earthquake in longitudinal direction for isolated Beylerbeyi Palace with HDRB	137
Figure 8.23.	S11 stresses under RSA of maximum earthquake in transversal direction for isolated Beylerbeyi Palace with HDRB	137
Figure 8.24.	Parliament House, Wellington (Seismic retrofit, 1994).....	138
Figure 8.25.	City and County Building, Salt Lake City, Utah (Seismic retrofit, 1989).....	138
Figure 8.26.	Application of concrete over timber beams with steel connector	140
Figure 8.27.	Critical horizontal stress zones for rigid diaphragm application under MCE.....	142

Figure 8.28. Critical vertical stress zones for rigid diaphragm application under
MCE 142

LIST OF TABLES

Table 3.1.	Use of nondestructive tests.....	22
Table 3.2.	Mortar ingredients according to thin-section analysis	26
Table 3.3.	Mineralogical components the specimens according to XRD analysis	32
Table 3.4.	Mixture proportions of the ingredients in F1	33
Table 3.5.	Mixture proportions of the ingredients in F2	33
Table 3.6.	Particle size distribution of the brick powder, used for F1 type mortar....	33
Table 3.7.	Mechanical properties of laboratory made horasan mortar specimens.....	36
Table 3.8.	Identified material properties	44
Table 4.1.	Dynamic characteristics of the palace	48
Table 4.2.	Dynamic parameters of the uncalibrated model	58
Table 4.3.	Calibration process to obtain E for all structure.....	69
Table 4.4.	Calibration process to obtain E for wall in the transversal direction of right part	70
Table 4.5.	Calibration process to obtain E for wall in the longitudinal direction in sea-side	71
Table 4.6.	Obtained modes at the end of the calibration process	76

Table 5.1.	Identified soil layers under the main palace	86
Table 5.2.	Ground shaking parameters for DSHA and PSHA	87
Table 8.1.	Tension characteristics of fibres	117
Table 8.2.	Damping coefficients B_D or B_M factor	130
Table 8.3.	Relation of rubber hardness and material constants.....	131
Table 8.4.	Dynamic properties of isolated Beylerbeyi Palace	136

LIST OF SYMBOLS / ABBREVIATIONS

A	Full cross-sectional area (loaded area) of the bearing
A_0	Effective cross-sectional area
A_f	Load-free area around the bearing
B	Plan dimension of the bearing parallel to the displacement
B_M	Damping coefficient
c	Initial cohesion
d	Diameter of a circular bearing
D_M	Maximum horizontal displacement for a bearing
E	Modulus of elasticity
E1	Modulus of elasticity of masonry produced by F1 mortar formula
E2	Modulus of elasticity of masonry produced by F2 mortar formula
E_c	Compression modulus of the rubber-steel composite
E_k	Characteristic modulus of elasticity
$f_{average}$	Average compressive strength
f_k	Characteristic compressive strength of masonry
f_{min}	Minimum compressive strength
F1	The first formula of horasan mortar
F2	The second formula of horasan mortar
F_y	Yield strength of the steel plates
G	Shear modulus
G_f	Fracture energy per unit area
I_0	Intensity of earthquake
K	Stiffness matrix
k	Modified factor, in the range of 1 to 0.5
K_{eff}	Effective horizontal stiffness
K_H	Horizontal stiffness of the bearing
K_V	Vertical stiffness of the bearing
L	Plan dimension of the bearing perpendicular to displacement
M	Diagonal mass matrix
m	Ratio of compressive strength to tensile strength

M_W	Seismic moment magnitude
N	Number of rubber layer
P_{DL+LL}	Load induced by dead and live load
S	Shape factor
S_{11}	Horizontal stress
S_{12}	Shear stress
S_{22}	Vertical Stress
S_a	Spectral response acceleration
S_D	Spectral displacement
S_{D1}	The design spectral response acceleration at 1 second period,
S_{DS}	The design spectral response acceleration at 0.2 second period,
T	Period
t	Thickness of individual rubber layer
T_0, T_S	Spectral characteristic periods
T_1	Period of the first mode
T_A, T_B	Spectral characteristic periods of the soil
T_D	Target design period,
t_i, t_{i+1}	Rubber layer thickness in top and bottom of the steel plate
t_r	Total height of rubber layers
t_s	Steel plate thickness
δ_s	Horizontal displacement of the bearing
e	Strain
e_{c0} ,	Strain at end of compressive softening curve
e_{cp}	Strain at peak compressive stress
F	Friction angle
Ω	Diagonal matrix of eigenvalues
γ_{max}	Design shear strain for rubber
s	Stress
s_c	Compressive strength
s_t	Tensile strength
v	Matrix of eigenvectors (mode shapes)
γ_{eff}	Effective damping ratio

ADRB	Added Damping Rubber Bearings
AFRP	Aramid Fibre Reinforced Polymer
AVS	Ambient Vibration Survey
BSE-1	Basic Safety Earthquake-1
BSE-2	Basic Safety Earthquake-2
BSO	Basic Safety Objective
CCCM	Cracking-Crashing Concrete Model
CFRP	Carbon Fibre Reinforced Polymer
CNM	Calibrated Numerical Model
CQC	Complete Quadratic Combination
DE	Design Earthquake
DPMM	Drucker-Prager Material Model
EDX	Energy Dispersive X-Ray
FEM	Finite Element Method
FPS	Friction Pendulum System
GFRP	Glass Fibre Reinforced Polymer
HDRB	High Damping Rubber Bearings
LRB	Lead Rubber Bearings
ME	Maximum earthquake
MPR	Modal Participation Ratio
NDE	Non-Destructive Evaluation
NDT	Non-Destructive Test
NEHRP	National Earthquake Hazard Reduction Program
NM	Numerical Model
PGA	Peak Ground Acceleration
PROHITECH	Earthquake Protection of Historical Structures by Reversible Mixed Technologies
RMT	Reversible Mixed Technologies
RSA	Response Spectrum Analysis
SE	Safety Earthquake
SEM	Scanning Electro microscope
TEC	Turkish Earthquake Code

UBC	Uniform Building Code
UV	Ultrasonic pulse velocity
XRD	X-Ray Diffraction analysis

1. INTRODUCTION

With its permanent occupancy over 8000 years Anatolia is the cradle of civilization. Since Hittites the region has been occupied by different tribes, resulting with the establishment of many countries and empires. Roman, Byzantine, Seljuk and Ottoman empires are the most significant civilizations in the history that had brought Anatolia to its historical structure stock. There are many churches, bridges, school, mosques, cisterns, public baths, palaces and pavilions, defying the centuries with their magnificence. Istanbul, as the capital of Byzantine and Ottoman empires has an important and special place among the other cities in Turkey with respect to cultural heritage.

Over the course of history Anatolia has been the site of numerous destructive earthquakes. At least 70% of the region is under-risk of earthquake. Between 1902 and 2005, 128 earthquakes hit the region causing more than 80.000 deaths. Most of the historical documentation is related to damages suffered in Istanbul. The earthquake history of the city reveals that; it experiences with a medium earthquake ($I_0 = VII - VIII$) in every 50 years and with a strong earthquake ($I_0 = VIII - IX$) in every 300 years. Moreover recent extensive geophysical studies have clearly delineated the presence of a single major tectonic entity crossing the Marmara Sea and the studies on the stress transfer related to the 1999 Kocaeli earthquake have indicated the heightened probabilities for a major earthquake in the region. The probability of having an $M_w 7 +$ earthquake is in the vicinity of 70% in the next 30 years [1].

In those conditions, protection of the historical heritage structures against earthquake becomes a primary concern. A combination of both scientific and cultural knowledge and experience is indispensable for the study of all architectural heritages. For this reason, a multidisciplinary approach must be employed and archaeologists, architects, art historians and civil engineers should work together in any restoration project in order to preserve the structure without damaging the historical fabric [2].

Being aware of the importance of the historical heritage structures and seismic danger of Mediterranean region, 16 institutions from 12 countries, mostly belonging to the

South European and Mediterranean area, have participated in a research project, named as “Earthquake Protection of Historical Structures by Reversible Mixed Technologies”, (PROHITECH). The project tackles the very important subject of the seismic protection of the historical and monumental buildings namely of constructions dating back from ancient age up to mid of the 20th century. The main objective of the project is to develop suitable methodologies for the use of reversible mixed technologies in the seismic protection of existing construction with particular emphasize to building of historical and artistic interest [3].

Bogaziçi University has participated in the PROHITECH as Turkish team and proposed Beylerbeyi Palace, presenting the sign of earthquake oriented damages, as a study case in order to perform analysis of feasibility of seismic protection interventions by means of reversible mixed technologies

1.1. Objective of the Thesis

The main objective of this thesis is to develop suitable methodologies for the use of reversible mixed technologies in seismic protection of Beylerbeyi Palace. Built between 1861 and 1865, the palace is the most magnificent Ottoman structure on the Asian shore of the Bosphorus. The analysis of the structure poses important challenges because of the complexity of the geometry, the variability of the properties of the construction material, difficulty of the experimental survey, use of different building techniques, and the lack of the knowledge on the existing damage sources. Furthermore its cultural value and desire to preserve it for the future generations, demands a high level of protection against any possible earthquakes. In these respects the works need a scientific approach to be remunerated.

1.2. Scope of the Thesis

Starting with this introduction part on which study plan is also presented, the study is organized into nine chapters. Each chapter also contains the relevant literature review.

The second part is dedicated to historical importance, architectural characteristics and structural features of the structure. The knowledge of historical fabric is technically of importance to evaluate the possible intervention strategies and search the applicability of them. There is no doubt that, the best intervention has to not harm what has survived until today [4].

Damage assessment and material characteristics of the palace are the subject of the third chapter. The existing damages in the palace were investigated and material characteristics were tried to be identified. For the mathematical model mechanical characteristics of material are in great importance. Starting from the mineralogy of the mortar, a laboratory based investigation was performed, till compression tests over reproduced masonry specimen. Mechanical properties of the timber used in the palace were determined by a literature survey.

The fourth chapter presents the ambient vibration survey, construction of the numerical model, and the calibration of the numerical model. The ambient vibration survey analysis has been performed with University "St. Cyril and Methodius", Institute of Earthquake Engineering and Engineering Seismology. Modal frequencies of the palace were determined [5]. Secondly numerical model of the palace was prepared in SAP2000 and LUSAS finite element analysis tools with material characteristics explained in the previous chapter and modal analysis was performed to obtain the modal frequencies and period. Finally moduli of elasticity of the masonry walls were altered in the numerical model in order to catch the mode shapes and frequencies, obtained in ambient vibration survey.

The seismic risk and geotechnical characteristics of the site on which Beylerbeyi Palaces sits, was presented in the fifth chapter. Several works have been carried out in Kandilli Observatory and Earthquake Research Institute of Bogaziçi University. With general tectonic setting of the Marmara region, Northwest part of Turkey, earthquake risk and its effects were discussed [1]. Detailed soil investigation report was prepared by Regional Directorate of the National Palace, state establishment, responsible from the protection of the Beylerbeyi Palace [6]. As the result of the mentioned information ground shaking parameters were determined.

The earthquake performance of the palace was checked by linear response spectrum analysis. Three different ground shaking parameters were defined. The first one is based on Turkish Earthquake Code and other two are Design Earthquake and Maximum Considered Earthquake defined probabilistically [7, 8, and 9]. It was determined that the structure is not capable to resist the specified ground motion and it should be consolidated. These results were presented in the sixth chapter.

In the seventh chapter non-linear pushover analysis results were presented. The performance of the structure under expected earthquake proves that stresses are beyond of the linear limits, determined in the third part. In that condition, the non-linear behavior of the structure is in great importance.

As the results of the performed efforts, possible retrofit strategies were evaluated in the eighth chapter. Within the technical upgrading of the palace two important aspects of rehabilitation were emphasized. These are:

- Preservation of Structural Integrity of existing buildings under severe or exceptional seismic actions.
- Improvement of building seismic performance by means of Reversible Mixed Technologies (RMT).

Reversible Mixed Technologies (RMT) are based on the integration of structural members of different materials and/or construction methods into a single construction. The basic feature of RMT is that their application should be always completely recoverable, that is reversible, if required. This is considered as an essential design requirement in order to prevent historical and monumental buildings from unsuitable rehabilitation operations [3]. In this study three retrofitting techniques were evaluated to apply to the palace. These are the use of fiber reinforced polymer, the installation of base isolation systems and the consolidation of the slabs.

The last chapter of the study is the conclusion part on which the obtained results have been presented.

2. BEYLERBEYI PALACE: HISTORY, ARCHITECTURAL AND STRUCTURAL FEATURES

2.1. History of Beylerbeyi Palace

By establishing an imperial estate, the Ottoman sultans had carried on a tradition dating from the Byzantines in Beylerbeyi area. In the 17th century Ahmed I (1603-1617) and Murad IV (1623-1640) were both frequent visitors here, staying in lodges built for their use. Ahmet III (1703-1730) and his successor Mahmud I (1730-1754) was even fonder of Beylerbeyi and restored and enlarged the existing building on the estate. A description of Beylerbeyi during the reign of Ahmed III reveals that there was a complex of structure here including a ornamental fountain flowing into a pool, tiled and domed pavilions, a prayer room, a Turkish bath with glass panes, a pavilion with a sadirvan (fountain for ablutions) overlooking the pool, a domed building with a view of the sea for the Valide sultan (sultan's mother) a small two floor building for the sultan's favorite wife, accommodations for the woman servants and housekeepers, a pavilion for a female readers of Koran, an imperial kasir (small summer palace or lodge) under pistachio trees, a hunting gate, and a pavilion for the janissary commander on the waterfront. Figure 2.1 is the illustration of the first Beylerbeyi Palace depicted by J. Schranz [10].

In 1734 the boathouse was enlarged and the gardens laid out anew and in 1735 a new pavilion was built. The following year Mahmut I apparently spent several weeks here. Between 1740 and 1748 large sums were spent on building and alterations at the palace complex. In 1760, the palace furniture was repaired [10].

Beylerbeyi's popularity waned in the second half of the 18th century to point where Mustafa III (1757-1774) had the palace demolished and sold off the land. The curious reason given for this sale was that a house standing adjacent to the palace prevents it being enlarged [10].

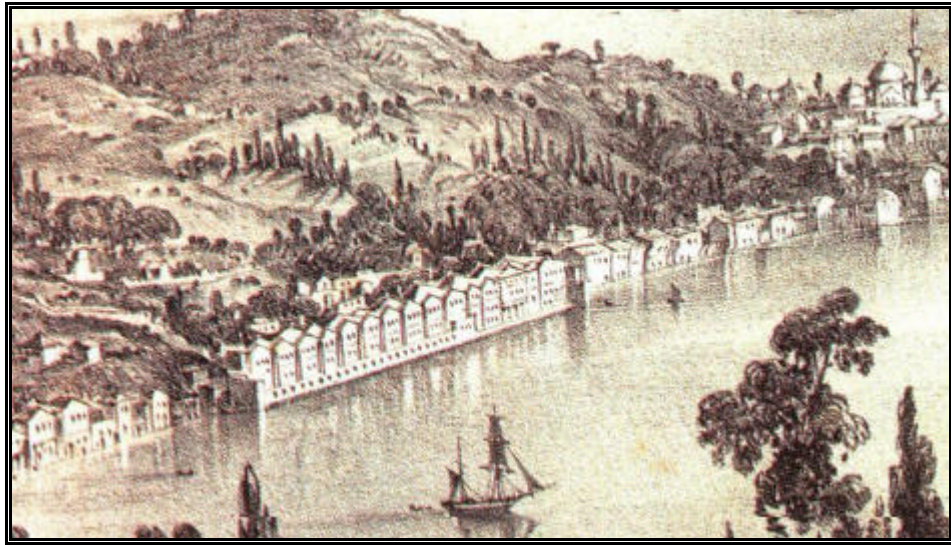


Figure 2.1. The first Beylerbeyi Palace [10]

The late 18th and early 19th centuries mark a turning point in the history of the Ottoman Empire. Uprisings toppled the reformist and music loving Selim III from the throne and declared the reign of Mustafa IV. While Mustafa IV ordinance the execution of Selim III and Prince Mahmud another party of uprisings toppled him. Selim III was murdered and Prince Mahmud became Mahmud II as the Ottoman sultan. The murder of Selim III so grieved his young nephew Mahmud II, that he could no longer bear the associations of Topkapi Palace. Wishing to break with the past and escape the memory of his uncle's death, he sought a site for a new palace. Beylerbeyi was finally selected and the land which had previously had been sold was repurchased and construction of a new palace began. Construction of the timber palace commenced in 1829 and was completed in 1832. In 1851, during the reign of Abdulmecid, who succeeded Mahmut II, a fire broke-out here and the sultan moved to Çiragan palace for a brief while [10].

2.2. Architecture of Beylerbeyi Palace

Frequent fires were the greatest ravagers of the Ottoman architectural heritage, particularly in Istanbul where the use of timber was prevalent. Countless palaces, pavilions, kasirs, and houses have been burnt to ashes, leaving only their names and stories behind. Fires affected the lives of sultans as well as the lives of ordinary people, and it was this fear which prompted Sultan Abdulaziz to have the timber palace of Beylerbeyi

demolished in 1861 and started to build the present palace of stone on the site. The construction of the palace complex was completed in 1865. The complex includes the present Beylerbeyi Palace, Yellow Pavilion, Stable Pavilion, Sea Pavilions and pools. Sultan Abdulaziz did not touch the Tunnel Structure and Marble Pavilion which were built in the first palace complex because they have no fire risk.

All structures in the palace complex are independent of each other. Yellow Pavilion and Marble Pavilion are around the big pool, Stable Pavilion is on the Southern part of the complex and the main palace is on the shore with two Sea Pavilions. Figure 2.2 shows the lay-out of the complex.

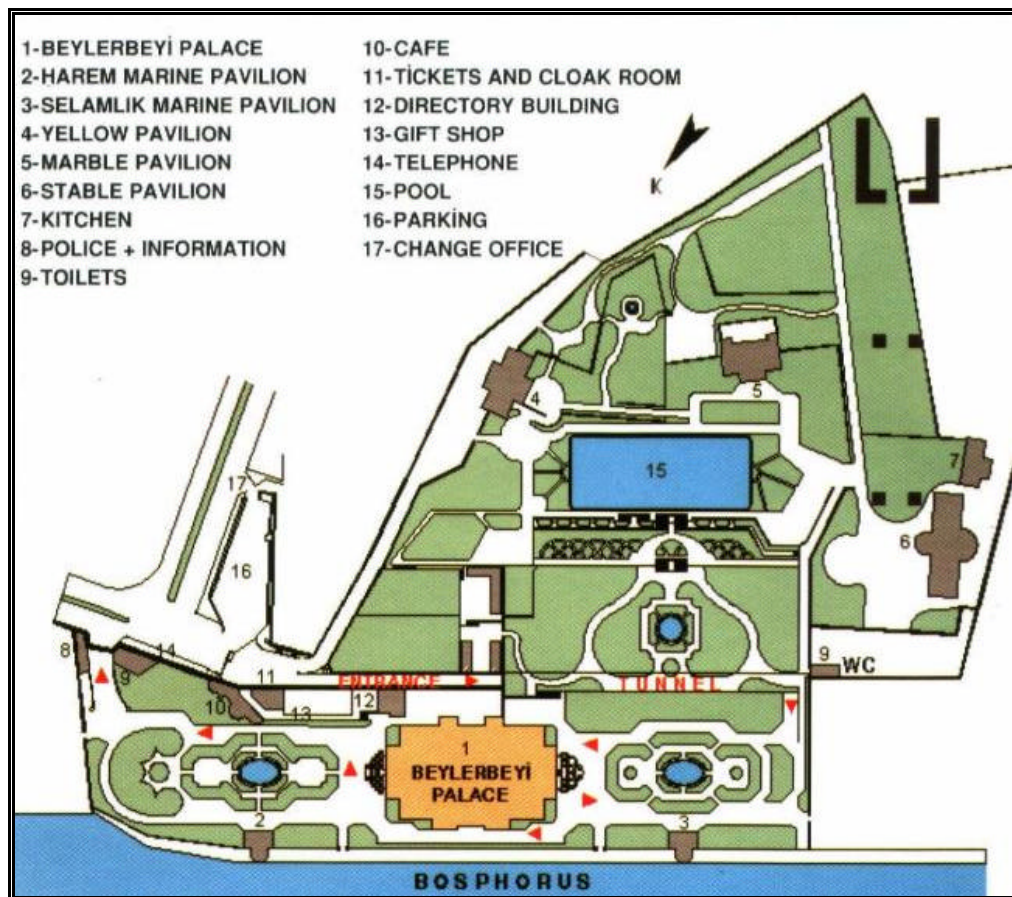


Figure 2.2. Site plan of Beylerbeyi Palace complex [10]

Designed by the well known Ottoman architect Sarkis Balyan, the palace was generally reserved for summer use by the sultans or to accommodate foreign heads of state visiting the Ottoman capital. There is no heating system in the palace. This may be due to the danger of fire, which destroyed the first palace partially (Figure 2.3).



Figure 2.3. Present Beylerbeyi Palace

Three-story main structure, with a basement and two ordinary floors is divided into two parts, namely Mabeyn, official part on which the imperial works were carried out and Harem, the private part on which sultans live with their families. These two parts have different entrances. The palace has three entrances, six state rooms and 26 smaller rooms. The building has a 72m length along the shore 48 m in the perpendicular direction. Figure 2.4-2.6 show the architectural plans of the structure while Figure 2.7 and 2.8 illustrate the vertical sections of the structure along with transversal and longitudinal directions. The story heights in the basement change between 1.5 and 2.5 m and this floor is partially underground while in the ordinary floors they are vary between 7 and 9 m.

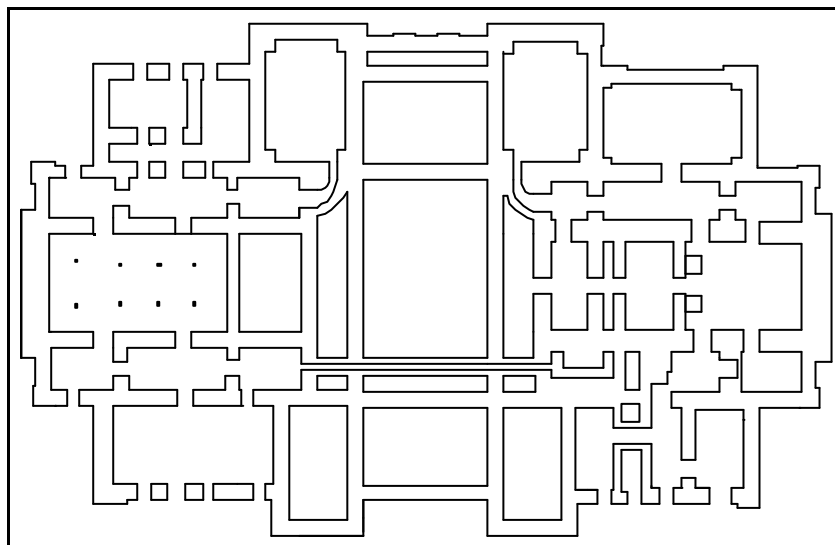


Figure 2.4. Plan of the basement floor of the palace

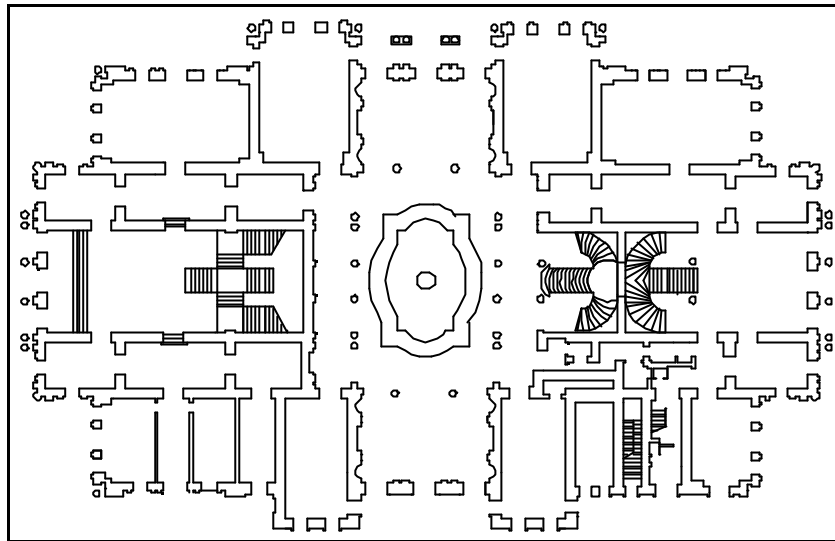


Figure 2.5. Plan of the first storey of the palace

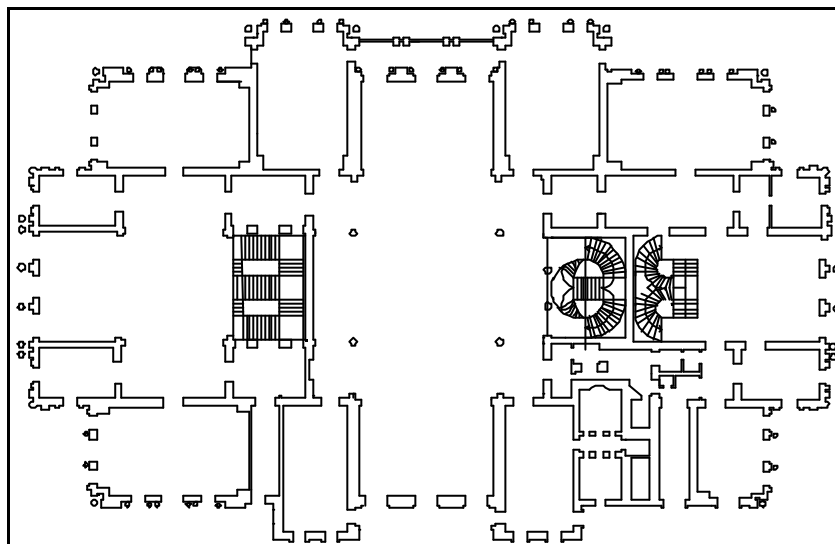


Figure 2.6. Plan of the second storey of the palace

There is a clear difference in aesthetics of Mabeyn and Harem part of the palace. Mabeyn part rooms are decorated with more fascinating furniture, curtains than Harem part rooms. Moreover in Mabeyn part the walls are covered with timber and stucco plaster was used while the ordinary plaster was used for the Harem. In that respect it can be inferred that, in the Ottoman tradition state works were in more importance than those of related to their family.

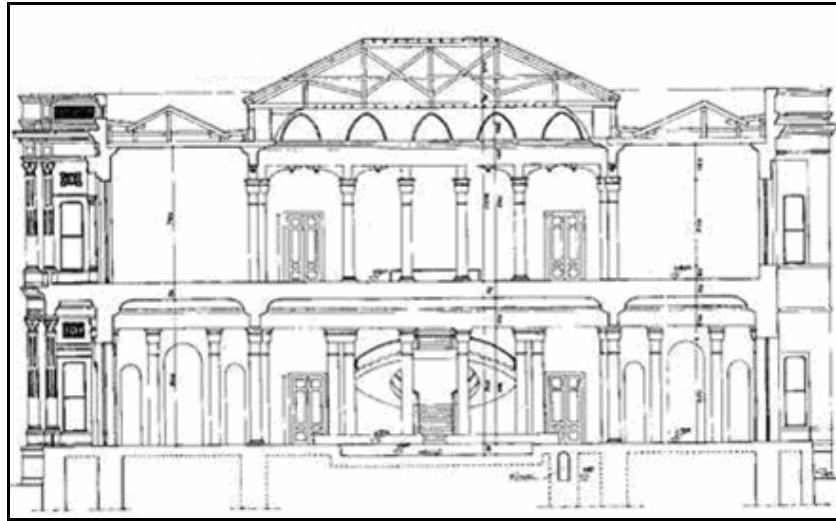


Figure 2.7. Vertical section of the structure along with transversal direction

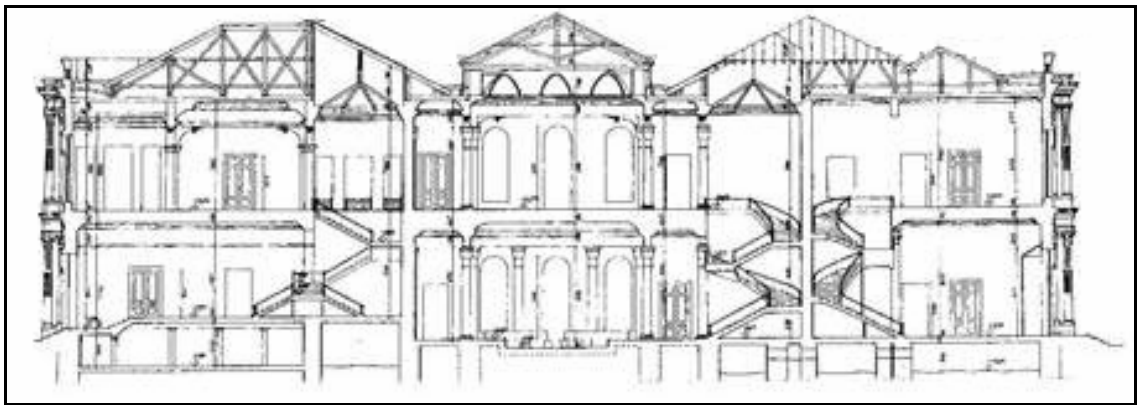


Figure 2.8. Vertical section of the structure along with longitudinal direction

The 19th century Beylerbeyi Palace illustrates the distinct western influence on Ottoman architecture over this period. Many European architects who worked in Anatolia during that century played a part of that influence which is clearly seen in the palaces of Dolmabahçe, Çiragan and Beylerbeyi. While the exterior side of Beylerbeyi palace reflects the western architectural style, the interior plan complies with traditional Turkish vernacular architecture (Figure 2.9). The exterior façade is covered by küfeki stone. On the interior wall surface of Mabeyn part, special stucco plasters with drawings and wood covering with carvings are used while Harem part walls are cover with normal plaster and paintings [10].



Figure 2.9. Western interaction on exterior façade versus Turkish interaction on interior face

The palace contains two main saloons, namely pool saloon and blue saloon. The pool saloon is located in the first story of the structure and takes its name from the pool located at the centre while the blue saloon is on the second story with blue columns. The pool was designed as the source of cooling in the summer seasons. Both saloons are piece of art with respect to decoration, drawings and carvings on the ceilings and walls (Figure 2.10-2.11). There are four different stair systems with their magnificent style and appearance in the palace. Two of them are in Mabeyn part and other two are in Harem part (Figure 2.12).



Figure 2.10. A view from Pool Saloon



Figure 2.11. A view from Blue Saloon



Figure 2.12. Views from two different staircases in the palace

Beylerbeyi Palace has hosted so many presidents, diplomats and distinguished guests for years. French Queen, Eugenie (1869), Emperor of Austria-Hungary, Joseph (1869), Shah of Persia, Nasireddin (1873), Montenegro Prince, Nikola (1874), and Shah of Iran, Riza Pehlevi (1934) are among them. The last guest of the palace is Mustafa Kemal Atatürk in 1936 [10].

2.3. Structural Elements in Beylerbeyi Palace

Three-story structure is mainly made of masonry walls and timber slabs. The basement floor of the Harem part enables to identify the masonry which is composed of lime mortar and stones. This part of the palace has no architectural function thereby no plaster was used and system is clearly seen. The timber floor is also visible. Thicknesses of the walls are changing between 2 m and 1 m and it is often 1.4 m on that floor. These walls are also forming the foundation system of the palace. Figure 2.13 shows the details from that floor.

It is determined that the slab of the structure is mainly composed of two types of timber cross-sections. 20*20 cm² beams (supporting beam) were located on the masonry walls and 8*40 cm² beams (slab beam) with 40 cm spacing lie between two walls perpendicular to wall direction. Oak was used for the supporting beam while slab beams were produced from fir. Details can be seen in Figure 2.14.



Figure 2.13. Foundation of the palace

The first and second storey of the structure is made of masonry walls, consists of lime mortar and brick, marble and wood columns and timber slabs. The thickness of the walls in the first storey is generally 80 cm while it is 60 cm in the second floor. Cast iron clamps were used within the walls to increase the out of plane stability of the structure. The exterior face of the structure was covered by küfeki stone while interior faces were veneered with stucco and lime plaster and timber cover.



Figure 2.14. Splice of timber beam between the structural wall and slab girders

The roof of the palace verifies the slab configuration in the basement. On the other hand the first story slab configuration could not be examined. Figure 2.15 illustrates the interior side of the roof of the palace.



Figure 2.15. Structural wall and timber slab in the roof of the structure

3. DAMAGE ASSESSMENT AND MATERIAL IDENTIFICATION

Analysis of a historical structure is indeed a difficult and challenging task. Precise understanding of the problem is essential since each structure may experience different types of damages and have different material characteristics and construction techniques. In that respect it is very difficult to make generalizations about historical structures. As one of the most magnificent historical structures within the cultural heritage treasury of Turkey, Beylerbeyi Palace deserves a special care to assess existing damages and the material properties.

3.1. Damage Assessment

A detailed damage survey was carried out in the palace. It should be emphasized that the structure is under the protection of the state establishment, Regional Directorate of National Palaces. The directorate is spending valuable effort and time to save the structure against aging and atmospheric conditions. In that respect many minor restoration works have been carried out for both interior and exterior sides of the structure.

Damage survey of the basement storey revealed the existence of high humidity level although it has several ventilation openings (Figure 3.1). Especially Harem part of the basement has been affected and snowy segments took form on the surface of stones as proven by Figure 3.2. The high level of humidity affected both the timbers slab system, by causing decay and masonry walls by affecting the mechanical properties. In order to prevent the propagation of decay on timber members, affected parts were chipped and some members were replaced by new timber beams during the restoration works (Figure 3.3). For the prevention of high humidity which causes deterioration of stone, mortar and timber, ventilation of the basement floor with suitable machinery equipment can solve the problem. Recent studies have revealed the efficiency of the ventilation against high humidity [11].



Figure 3.1. Ventilation opening in the foundation floor



Figure 3.2. High humidity over stones and its effects



Figure 3.3. Chipped timber beams due to decay on the foundation floor

In the first and second floors of the structure several cracks were observed. Since no restoration process has been carried out in the mabeyn part of the palace, everything is original on the other hand in the harem part of the palace repair works were performed to cover the cracks. For that reason most of the detected cracks are in the mabeyn part on the stucco plaster. Since the reproduction of stucco plaster is impossible nowadays, authorities do not touch the cracks to repair them. Similarly the timber coverings of the rooms in mabeyn part have very wide cracks which are hard to interpret the effect of them over structural safety. If the cracks stem from the damage occurred on the wall beneath the covering, special care must be spent. Other wise they only disturb the beauty of the rooms. Through Figures 3.4 - 3.6 the observed cracks are shown. The cracks can be classified into three categories. These are;

- The horizontal cracks,
- Vertical cracks on the side of the windows,
- Inclined cracks on the corners of the openings.

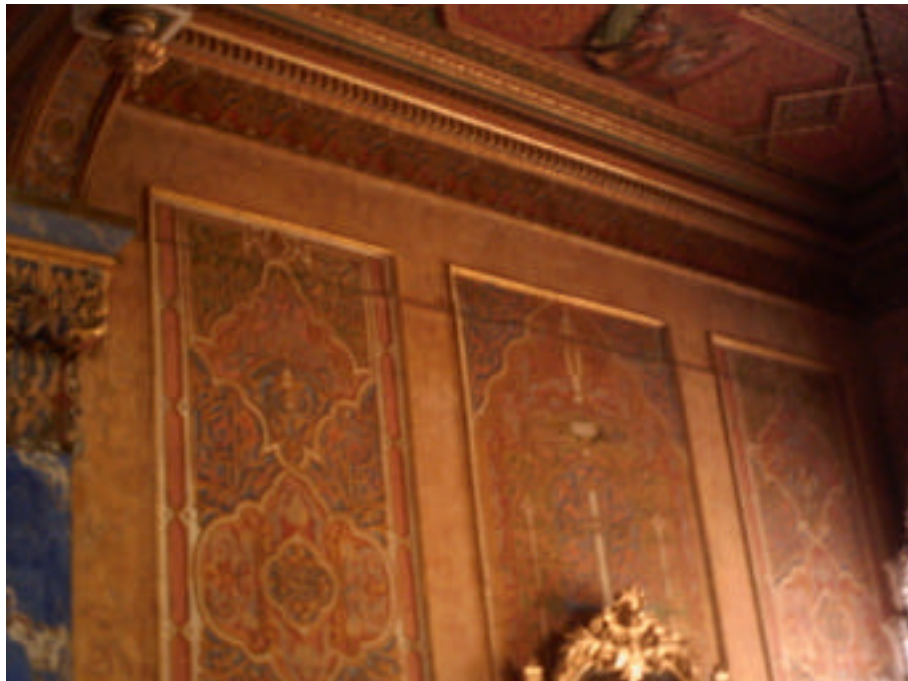


Figure 3.4. Horizontal crack in the Mabeyn part

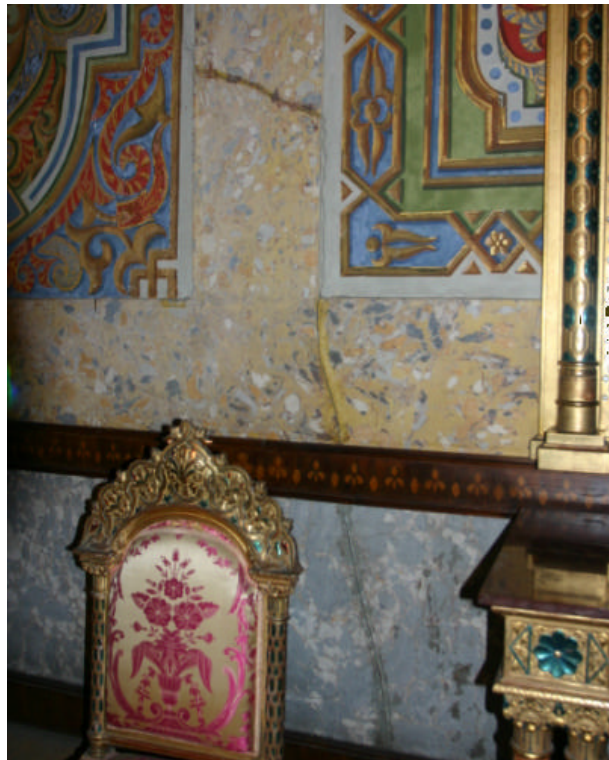


Figure 3.5. Vertical crack in Mabeyn part

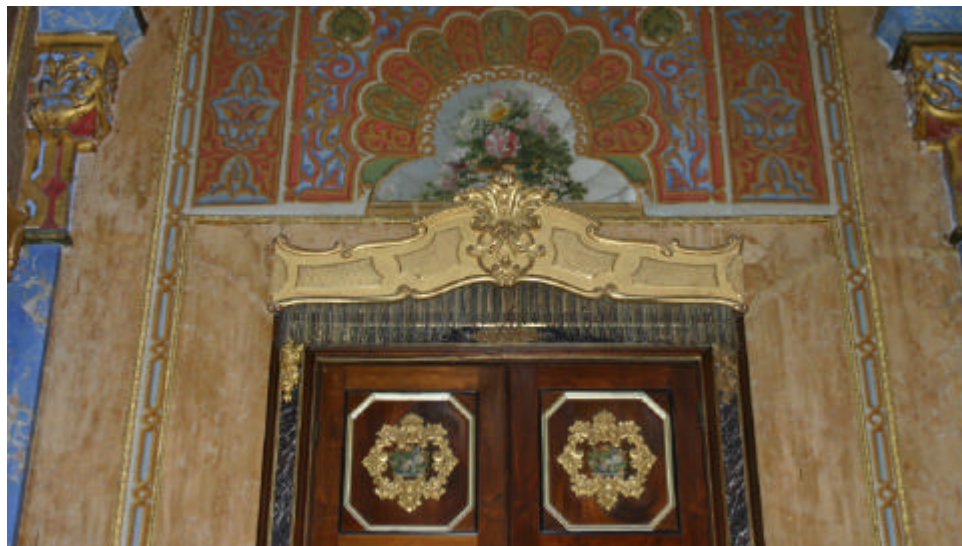


Figure 3.6. Inclined cracks on the corners of the door

Not only is the existence of the damage but also the reasons of them in importance. The existing damages may stem from four reasons, namely, aging effects, atmospheric conditions, the horizontal earthquake loads, and ground settlements. In order to contribute the structural system iron reinforcement were also used. Oxidation of them should also be accounted as a damage factor and of course this damage can also be included in either

aging or atmospheric conditions effect. Numerical analysis can reveal the origin of the damages and material properties are the essential parameters for the numerical model of the palace.

3.2. Material Identification

Mechanical characteristics of the material, composing the structure are the basic and important input data needed for the analysis. In order to make a correct assessment the initial point is the determination of the mechanical properties of the material used in the structural carrying system. In particular, compressive and tension strengths, their modulus of elasticity, Poisson ratio and unit weight are of primary concern [4].

In this study special care was spent to obtain the mechanical properties of the masonry composed of brick and lime mortar. It is expected that, the behavior of the structure, under seismic load, will be governed by walls of the first and second stories. Moreover thick stone masonry in the basement floor is not as critical as thin, brick masonry of the first and second stories. Another material that should be characterized with respect to mechanical properties is timber which forms the slab of structure. There are many researches about mechanical properties of the different type of timber. For these reasons the mechanical properties of the stone masonry and timber material can be determined by a literature survey.

3.2.1. Applicability of Non-Destructive Test (NDT) Methods

Generally material properties can be identified by a series of destructive and non-destructive test for a structure. In case of historical structures destructive tests are out of question while non-destructive tests are applied successfully. Schmidt hammer, flatjack methods, in-plane shear and ultrasonic pulse tests are some of common nondestructive test methods, applied to obtain the mechanical properties of masonry.

The Schmidt Hammer test is the quickest, simplest, and least expensive method for NDE of solid clay unit, i.e., brick masonry. Correlation between the rebound number and the compressive strength of clay brick masonry is required. The Schmidt Hammer is most

ideally suited to the measurement of material uniformity over large areas of a structure. It must be accompanied by a limited number of destructive tests to calibrate the results if an indication of the actual masonry strength is required [12].

The flatjack test is being recognized as a powerful tool for NDE of the structural properties of masonry. The test has been successfully applied to cut stone masonry. No other NDE test method offers direct physical measurement of material and structural properties without any reliance on empirical correlations. The two main types of flatjack tests are the in-situ stress or single flat jack test and the in-situ deformability or double flatjack test [12].

Evaluation of the in-situ compressive stress is a simple process of stress relief induced by the removal of a portion of a mortar bed joint followed by restoration of the original state of stress by pressurizing a flatjack inserted in the slot created by the removal of the mortar [12].

The deformation properties of masonry may be evaluated by inserting two parallel flatjacks, one directly above the other separated by several courses of masonry, and pressurizing them equally, thus imposing a compressive load on the intervening masonry. The deformations of the masonry between the flatjacks are then measured for several increments of load. The results are used to calculate the masonry deformability modulus. If some damage to the masonry is acceptable, the masonry may be loaded to failure to determine the maximum strength [12]. Figure 3.7 shows the application of double flatjack test over an existing masonry structure [13].

The in-place shear test, often called the push test, is designed to measure the in-situ joint shear resistance between masonry units and mortar joints. It requires the removal of a single masonry unit and a head joint on opposite sides of a test unit. The test unit is then displaced horizontally relative to the surrounding masonry using a hydraulic jack and the horizontal force required to cause the first movement of the test unit is recorded. The test may be considered nondestructive, because the removed unit and mortar joints may be replaced to their former appearance [12].

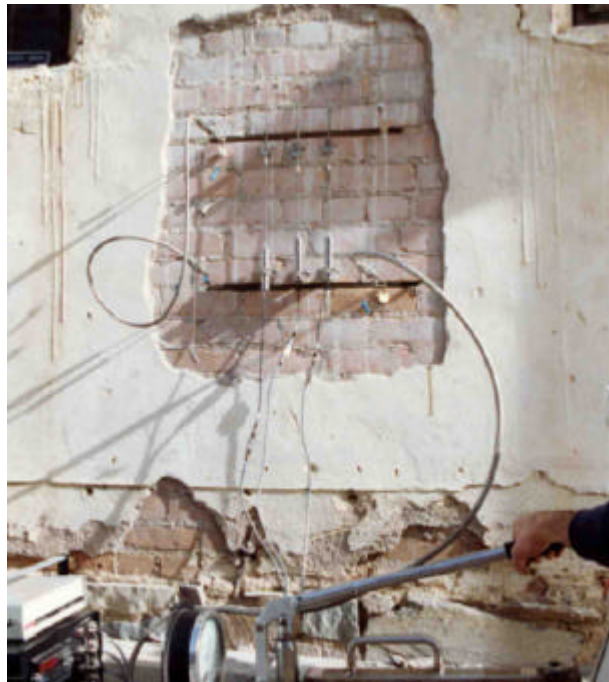


Figure 3.7. Application of double flatjack testing method on a masonry wall [11]

The ultrasonic pulse velocity (UV) technique uses electroacoustic transducers to pass a high frequency (50,000 Hz) stress wave through masonry. This technique has good potential for evaluation of masonry structures and is most useful for the location of relatively small flaws in otherwise uniform masonry materials. In certain cases, it may be possible to obtain an estimate of masonry compressive strength from ultrasonic pulse velocity measurements. However, very careful interpretation of the signal is required along with a meticulous visual survey in order to interpret the data properly. It is recommended that pulse velocity techniques be used in conjunction with other NDE tests such as the flatjack test for determining the state of stress and deformability in walls and also with destructive tests to verify the deformability and strength [12].

Table 3.1 lists each NDE technique along the top and gives the desired information along the left side, which are grouped under the headings of material properties and condition. A simple matrix of dots indicates which techniques are useful for measuring each of the desired quantities. A filled dot indicates the technique is useful while an unfilled dot indicates that the technique is useful, but may be affected by conditions such as loading and crack distributions in the walls. Thus, the techniques with unfilled dots should be used in tandem with others to strengthen the reliability of the results [12].

Table 3.1. Use of nondestructive tests [12]

REQUIRED INFORMATION FOR STRUCTURAL EVALUATION		NONDESTRUCTIVE TESTING TECHNIQUES								
		Schmidt Hammer	Single Flatjack	Double Flatjack	In-Plane Shear	Modified Shear Test	Ultrasonic Pulse	Mechanical Pulse	Magnetic Methods	Visual
MATERIAL PROPERTIES	Compressive Strength (Direct)			●						
	Compressive Strength (Indirect)	●					○	○		
	Deformability			●						
	Joint Shear Strength				○	●				
	Coulomb Shear Relationship					●				
CONDITION	Voids between Wythes						●	●		
	Cracks in Outer Wythes						○	○		○
	In-Situ Stress		●							
	Material Uniformity	●					●	●		○
	Location of Reinforcement								●	
●		Useful for evaluation								
○		Useful, but may require additional information regarding loading conditions and crack distributions								

Architectural and historical aspects of Beylerbeyi palace do not permit any of non-destructive test methods to be applied to determine the mechanical properties. Even the simplest strategy, Schmidt hammer requires peeling of the plaster. Since both exterior and interior façade of the walls are covered by stones, special stucco plaster and timber the application of non-destructive test methods seems unacceptable. It is impossible to recreate the magnificent stucco plaster and carving on the façade of the walls.

In that condition another procedures should be employed to identify the mechanical properties of the material. The basic and logical procedure was perceived as reproduction of the masonry specimen with the same configuration and origin of the material. Thereby desired engineering properties of the material can be identified by performing laboratory tests.

As stated before the walls of the palace is composed of the lime mortar, stone and brick. In order to produce the masonry specimen, the configuration (thickness of the mortar and bricks) must be verified. Secondly identification process for lime mortar must be performed. After the production of the specimen the required tests should be performed to obtain basic material properties.

3.2.2. Mortar Identification

The oxidation of metal clamps used within the masonry caused swelling and finally cracking of the wall in a room and stair case in harem part. This damage ended up with the separation of about 50*50 cm² wall part in the room. This event enabled us to determine the masonry configuration and have ruins from the original mortar of the structure. Both mortar and plaster particles were taken to analyze the origin of the mortar. The average mortar thickness is about 18 mm and brick height was measured as 65 mm. Figure 3.8 and 3.9 show the masonry configuration in the room and stair case in harem part respectively

More recently developed mortar characterization schemes have optical microscopy as the first step in identifying the aggregates, of various mineral additions, binder type, and binder-related particles and in describing the pore structure. Optical microscopy is also a valuable aid for damage diagnosis of degraded historic mortars and for the study of the interfacial zone, the bonding and possible reaction rims between aggregates, brick or stone and the mortar [14].

A Scanning Electro Microscopy (SEM) analysis together with an X-Ray Diffraction (XRD) analysis is the most valuable second step in the characterization process of historic mortars. SEM analysis can be performed on mortar fragments or on polished epoxy-impregnated sections. With a scanning electro microscope, equipped with an Energy Dispersive X-Ray (EDX) -detector, valuable information can be obtained on the mineral phase composition [14].

For these reasons chemical and mineralogical composition of mortar from Beylerbeyi Palace was determined by Thin-Section analysis, Scanning Electron Microscope-Energy Dispersive X-Ray (SEM-EDX) analysis and X-Ray Diffraction (XRD) analysis. Through all investigations Associated Prof. Dr. Fahri Esenli of Mining Faculty of Istanbul Technical University spent valuable time to interpret the results.



Figure 3.8. Masonry configuration in the room of harem



Figure 3.9. Masonry configuration in the stair case of harem

3.2.2.1. Thin Sections, under Polarizing Microscope. For the characterization of mortar, the study of thin sections under the polarizing microscope is a very efficient analytical technique. A thin section is made by grinding down a slice of rock which has been glued to a glass slide until it reaches a thickness of about 0.03mm (30 microns). At this thickness most minerals become more or less transparent and can therefore be studied by a microscope using transmitted light. In this study five thin sections were prepared and investigated. Figure 3.10 shows three enlarged views of the prepared thin sections and Figure 3.11 shows the photograph of the first thin section, taken under petrography microscope.



Figure 3.10. Thin-sections

Thin-section analysis showed that, about 60% of the mortar is binding material and remaining part is the grains. The general grain size is about 500 μm and less. It occasionally reaches to 1 mm. These grains contain mineral particles, quartz particles and clearly identified brick powder particles. Table 3.2 summarizes the identified ingredients of the thin-sections.

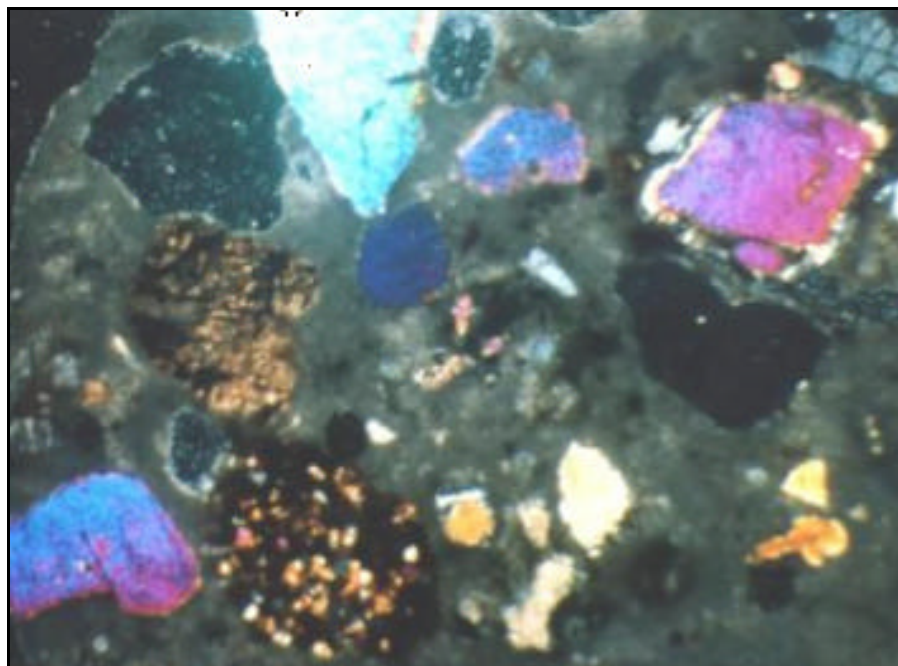


Figure 3.11. Photograph of thin-section under microscope

Although the brick powder can be recognized in thin-section analysis, it is hard to say that the determined ratios are the initial proportion of the brick powder since the quartz particles may come from the brick grains. Brick aggregates also contain Calcite [15].

Table 3.2. Mortar ingredients according to thin-section analysis

Sample Code	Components		
	Binding Material %	Quarts and Calcite Particles %	Brick Particles %
TS-1	50	45	5
TS-2	50	35	12
TS-3	60	30	8
TS-4	65	25	6
TS-5	67	25	6
Average	58.4	32	7.4

3.2.2.2. Scanning Electron Microscope Views and Energy Dispersive X-Ray Analysis.

Scanning Electron Microscope is a widely used technique to study surface topography. The mortar specimens were searched under Philips XL30ESEM-FEG&EDAX, Environmental Scanning Electron Microscope and Energy Dispersive X-Ray device. Figure 3.12 shows the polished specimens. The first two specimens with bigger grain size belong to the mortar taken between the bricks and the third one is the plaster mortar. Mineralogical structure of the ingredients of the mortar were tried to be identified on enlarged views thanks to EDX.



Figure 3.12. Mortar specimens, prepared for SEM and EDX analysis

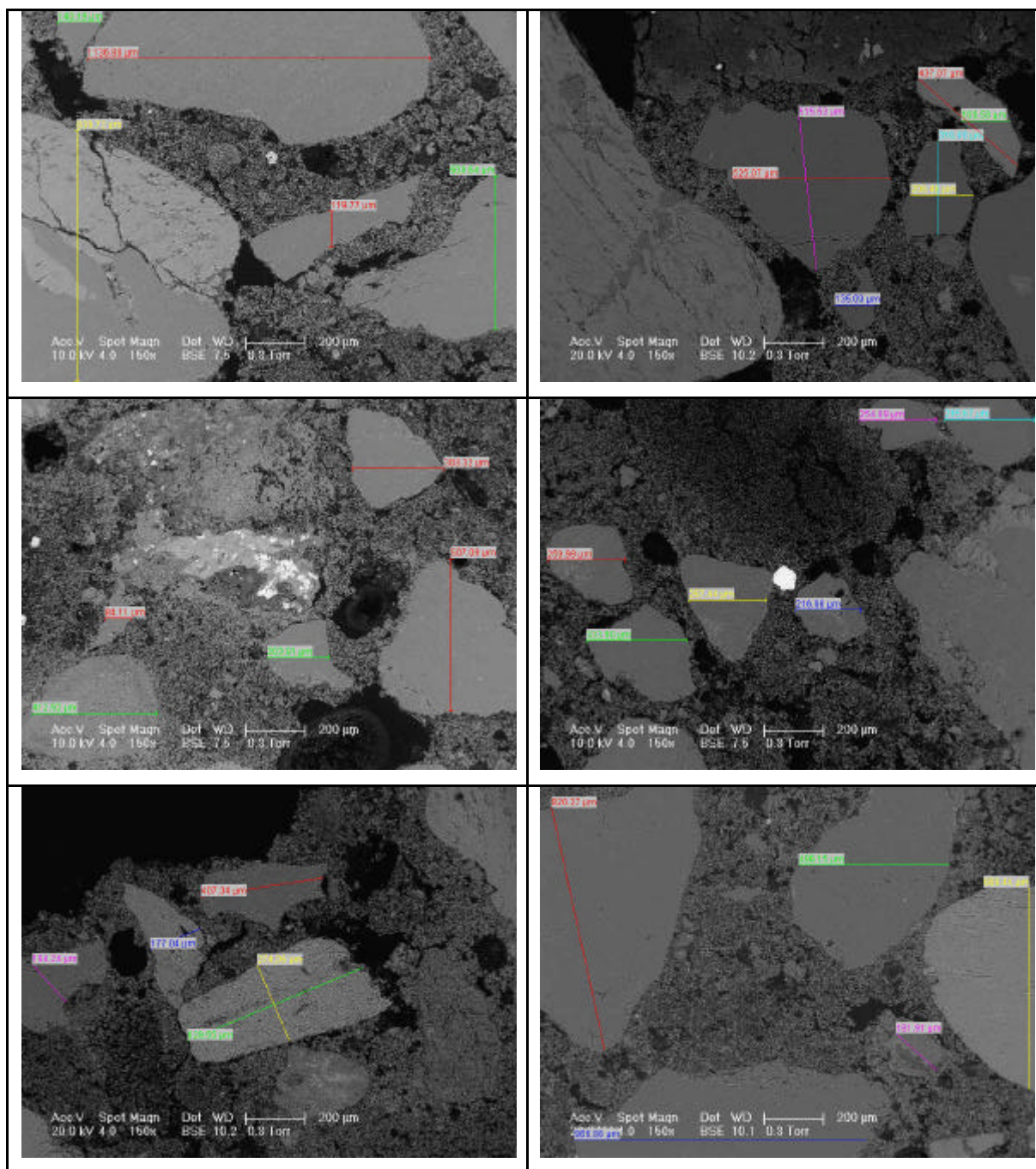


Figure 3.13. SEM views from the mortar between the bricks

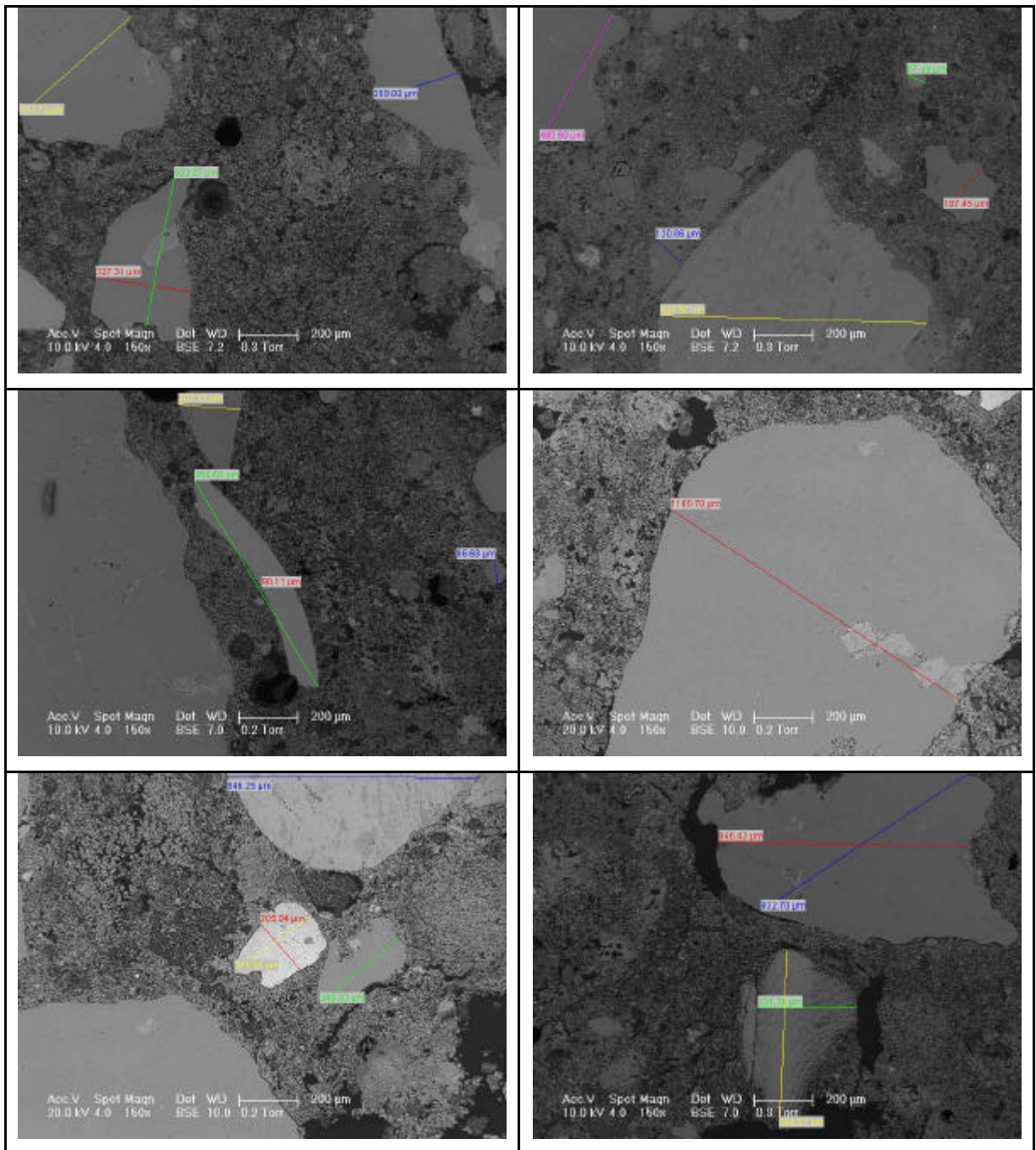


Figure 3.14. SEM views from the mortar between the bricks

Good connection between particles and binding material was observed through the SEM views. No gap or cracks were determined. Particle size distribution can easily be determined from SEM views (Figures 3.13 – 3.15). It is seen that the grain particle size, used in mortar is grater than that used in plaster. According to SEM views the maximum size is determined as about 1800 μm.

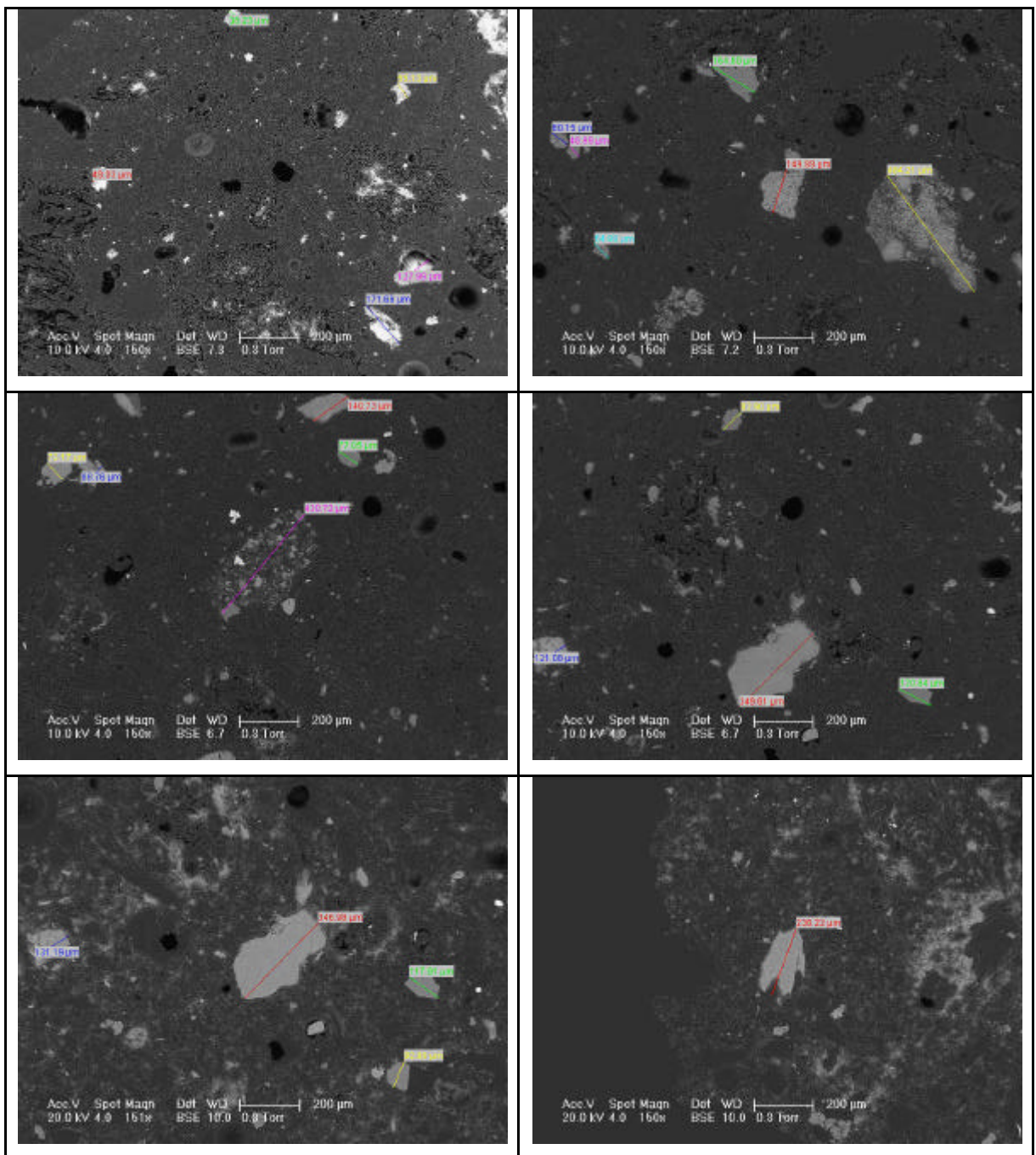


Figure 3.15. SEM views from the plaster

The EDX analyses were performed simultaneously with the SEM. It was determined that the mineralogical origin of the particles is quartz, SiO_2 and derived from the aggregates containing sand and brick powder. Figure 3.16 represents the EDX analysis for a particle, seen in SEM view as in gray color. Wt % column shows the weight ratio of the each element and oxides. Occasionally feldspar minerals were seen through the EDX patterns of aggregates (Figure 3.17).

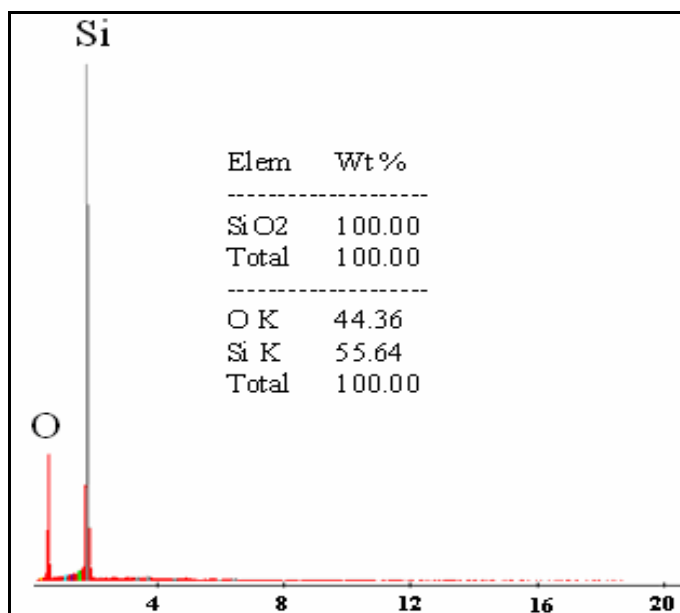


Figure 3.16. EDX analysis of particle in SEM view

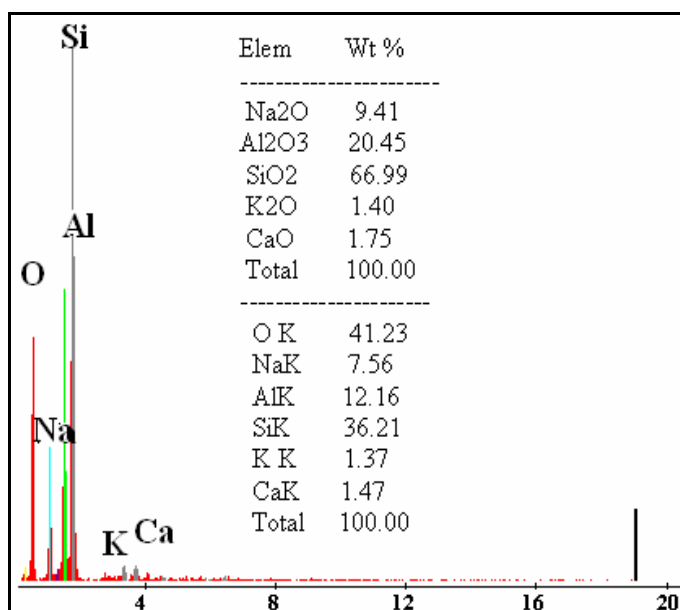


Figure 3.17. Identified feldspar elements, EDX analysis of particle

EDX analysis showed that the origin of the binding material between the particles is calcite minerals. Calcite is originated from carbonated lime [15]. Figure 3.18 shows the EDX analysis, applied to the darker region (binding material) on the SEM view.

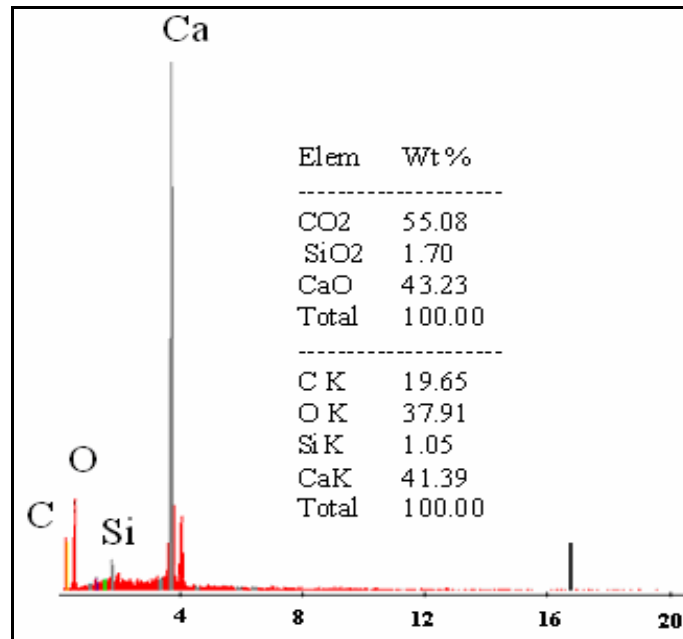


Figure 3.18. EDX analysis of binding material in SEM view

3.2.2.3. X-Ray Diffraction Analysis. X-ray Diffraction (XRD) clarifies the nature of the mineralogical phases present in the sample [16, 17, and 18]. Pulverized mortar specimen were analyzed under Rigaku D/Max-Ultima+/PC XRD device. XRD analysis verified the existence of calcite and quartz elements. Six specimens were analyzed and it is seen that each of them consists of quartz, calcite and feldspar minerals with varying ratios. Table 3.3 summarizes identified component ratios for each specimen. These specimens were taken from the two different room of the palace and all specimens belong to mortar between bricks.

The average of ratios indicates that, about 65% of the horasan mortar is calcite derived from carbonated lime, 30% of the mortar is quartz, derived from aggregates, and 5% is feldspar, (Na, K, Ca), (Si, Al)O elements.

The same kinds of mineralogical analysis were performed to mortar ruins of Dolmabahçe palace taken from different parts of the palace. The first mortar ruin was taken from beneath of balcony marble covering and composed of 25-30% lime, 45% crushed brick and 10% fine sand. The second ruin is taken from muayede saloon's pendantive and composed of 40% lime, 30% crushed brick, fine sand and in a very small

percentage fiber. The third ruin was from exterior side of the dome of the muayede saloon and composed of 35-40% lime and crushed brick. Finally the mortar specimen from the sea-side of perimeter wall of stair of the muayede saloon consists of 45% lime, 50% marble powder and fiber [19].

Table 3.3. Mineralogical components of the specimens according to XRD analysis

Sample Code	Mineralogical Component		
	Calcite %	Quartz %	Feldspar %
W-01	60	30	10
W-02	30	65	5
W-03	53	43	4
W-04	85	10	5
T-01	75	20	5
T-02	90	5	5
Average	65.5	28.8	5.7

The results of the mortar identification process revealed that the mortar of the Beylerbeyi Palace is typical lime mortar, used in Ottoman time known as Horasan mortar. In Turkey and Balkan region there are many structures, including Hagia Sophia, Süleymaniye Mosque, Selimiye Mosque, Blue Mosque, Dolmabahçe Palace, Beylerbeyi Palace, Aynalikavak Pavilion, Mustafa Pasha Mosque, L alas Pasha Mosque, Çifte Minaret Madrasa, Yesil Madrasa, Gök Madrasa, Ishak Pasha Castle, constructed by using this type of mortar. Although some damages observed, these structures are defying the centuries with their magnificence.

3.2.3. Mechanical Properties of Horasan Mortar

Two different horasan mortar formulas were used to produce the test specimens. In the first formula (F1), the mortar is the combination of slaked lime, brick powder and water (Table 3.4) [20]. The second formula (F2) is used for the restoration works of the historical structures by Regional Directorate of National Palaces in Turkey. The state establishment is responsible from historical palaces and pavilions, including Dolmabahçe and Beylerbeyi Palaces. The mortar is the combination of slaked lime, brick powder, fine

sand, fiber, and water (Table 3.5). In both F1 and F2 the maximum size of the sand and brick powder grain is 2 mm. Particle size distribution of the brick powder is presented in Table 3.6.

Horasan can also be produced with crushed brick and aggregates with bigger grain size. This mixture is named as horasan concrete and detailed information can be found in Akman et. al. study [18]. Brick powder were mainly used for rendering and for the upper layers of floors, but crushed bricks with large grain size were recommended not only for masonry walls, arches and foundations, where high humidity or water were present, but also to improve the performance of mortars and conglomerates in normal conditions [21].

Table 3.4. Mixture proportions of the ingredients in F1 [20]

Ingredients	Lime	Brick Powder	Water
Mixture Proportion (by Weight)	1.00	1.22	2.10

Table 3.5. Mixture proportions of the ingredients in F2

Ingredients	Lime	Brick Powder	Fine Sand	Water	Fiber
Mixture Proportion (by Volume)	4.00	4.00	2.00	1.50	0.05

Table 3.6. Particle size distribution of the brick powder, used in F1 and F2 type mortars

Pulverized Brick										
Sieve size (mm)	20	16	8	4	2	1	0.5	0.25	0.125	0.074
% Passing	100	100	100	100	98.5	68.2	42.2	17.5	4	0.08

Before mixing the ingredients, lime slurry was formed by mixing the slaked lime and water and it was left to stand 24 hours. Then the brick powder and other ingredients were added to the mixture. Three-5cm*5cm*5cm cubic specimens and 4cm*4cm*16cm

prismatic test specimens were created for each type of formula. All specimens were kept in humidity cabinet for the first seven days. After six-month curing, the compression and flexure tests were performed. Figure 3.19 illustrates the testing procedures and failed specimens.

During the compression tests the applied load and measured displacement were recorded and stress-strain diagrams were obtained for each specimen. Figures 3.20 and 3.21 show the stress-strain diagrams for mortar produced with F1 and F2 formulas respectively. At the failure point similar crack patterns were observed for both types of mortar specimens. The average compressive strength for both kind of mortar is roughly the same and they are 4.54 MPa and 4.68 MPa for F1 and F2 respectively. On the other hand the strain capacities are different. The average ultimate strain for F1 mortar is measured as 0.04 while that is 0.055 for F2 mortar. Secant modulus of elasticity for mortars was also determined as the slope of the line intersects the origin and one third of the maximum stress on stress-strain curve of each specimen. Average modulus of elasticity for F1 was determined as 1127 MPa while it is 473 MPa for F2.

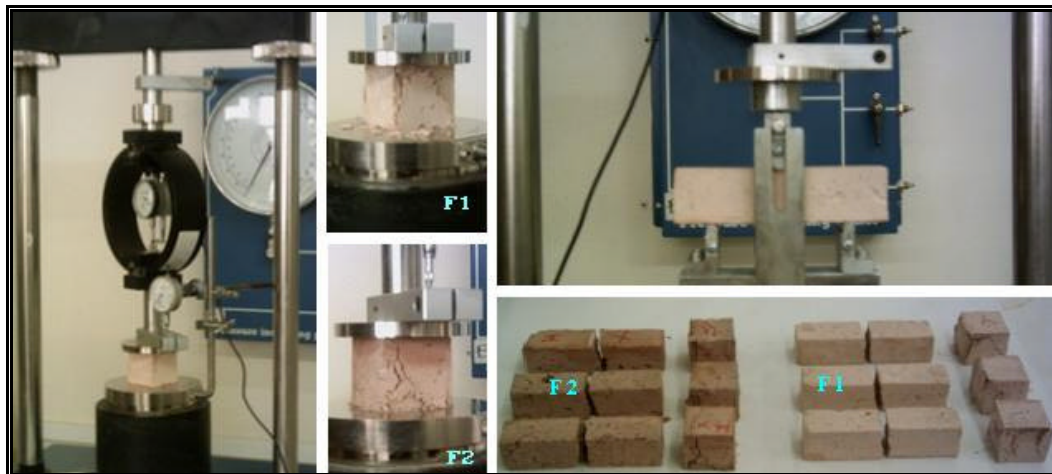


Figure 3.19. Compression and flexure tests and failure of the specimens

Flexure tests were also performed to determine the flexural strength of the mortar. For each mortar type three specimens were tested on three point flexure jig. The specimens have showed very brittle behavior and via single vertical crack, occurred just under the application point of the load they failed. Average flexural strength of the F1 and F2 are determined as 1.57 MPa and 1.71 MPa respectively.

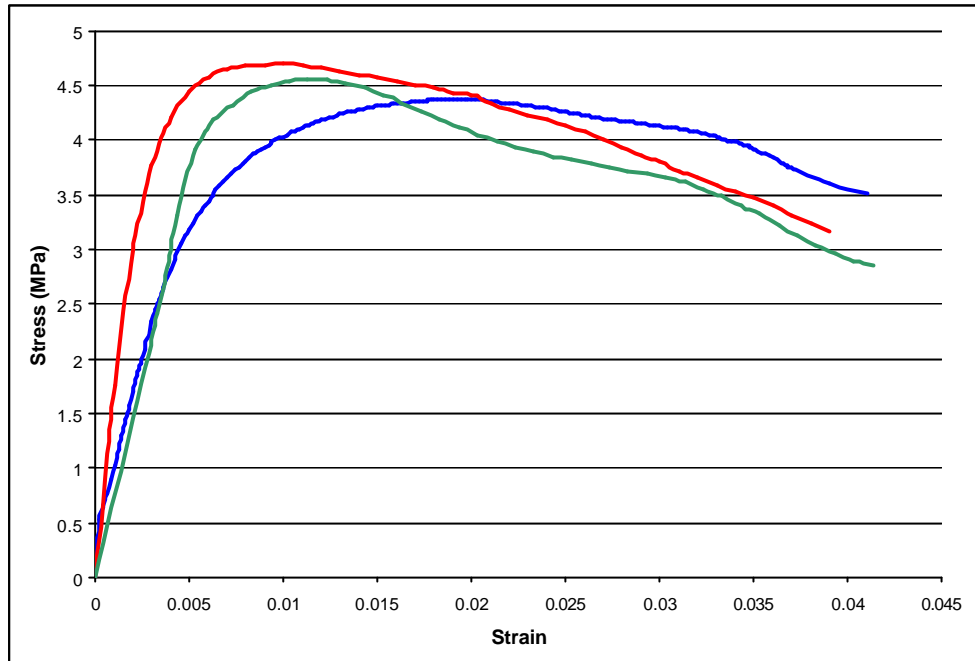


Figure 3.20. Stress-strain curves of the mortar specimens produced with F1

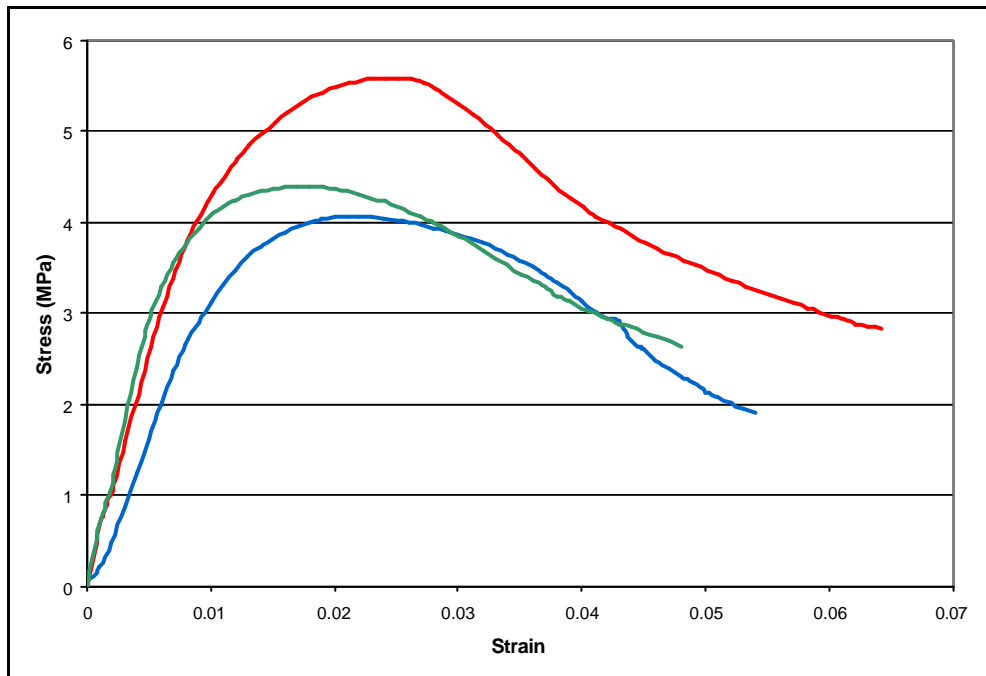


Figure 3.21. Stress-strain curves of the mortar specimens produced with F2

Determined mechanical properties for each test are summarized in Table 3.7. It is interesting to note that mortar of F2 formula has greater strain capacity and flexural strength while the modulus of elasticity is less than mortar of F1. It can be inferred from the test results F2 mortar is more ductile than F1 and related to the flexural strength the tensile strength of F2 is greater than that of F1. This may be the result of the addition of fiber to the mortar. This reveals the reason of addition of hay or goat and horse hair to the mortar in the old times in Anatolia.

Table 3.7. Mechanical properties of laboratory made horasan mortar specimens

Specimen	Compressive Strength (Mpa)	Strain at Maximum Stress	Ultimate Strain	Modulus of Elasticity (Mpa)	Flexural Strength (Mpa)
F1-1	4.37	0.019	0.041	902	1.86
F1-2	4.69	0.010	0.039	1748	1.32
F1-3	4.55	0.011	0.041	730	1.53
F1 Average	4.54	0.013	0.040	1127	1.57
F2-1	4.06	0.022	0.054	312	1.63
F2-2	5.59	0.025	0.064	508	1.79
F2-3	4.39	0.017	0.048	599	1.71
F2 Average	4.68	0.021	0.055	473	1.71

4.2.4. Mechanical Properties of Masonry

Within this study test specimens were created according to European Norm, EN 1052, methods of tests for masonry [22]. According to specification for the compression test at least three specimens of 1.5-unit length and 3-unit height should be tested (Figure 3.22). The characteristic compressive strength of masonry f_k is determined as the smaller value of either $f_k = f_{average} / 1.2$ or $f_k = f_{min}$ [22].

Three masonry specimens with F1 type of mortar formula and three masonry specimens with F2 type mortar formula were produced and tested after six month from the production (Figure 3.23). Normal clay burnt brick were used in the specimens. The tests were performed in the laboratory of Bogazici University. One load cell and two

displacement cell were used to measure the applied load and obtained displacement. The displacement cells were placed to opposite face of the specimen in the longer direction. Figure 3.24 shows the testing procedure. Figure 3.25 illustrate the failure of masonry specimen after testing.

Applied load and obtained displacement were recorded. The load-displacement graphs were converted to stress-strain basis by dividing the load to initial specimen area and displacement to initial specimen height. Figure 3.26 shows the load-displacement curve of the masonry produced by F1 while stress-strain curve is illustrated in Figure 3.27. Load displacement curve and stress curve for masonry, produced by F2 are shown in Figure 3.28 and 3.29 respectively. The average s-e curves of masonry produced with two different types of mortar are also illustrated in Figure 3.30 for the sake of comparison.

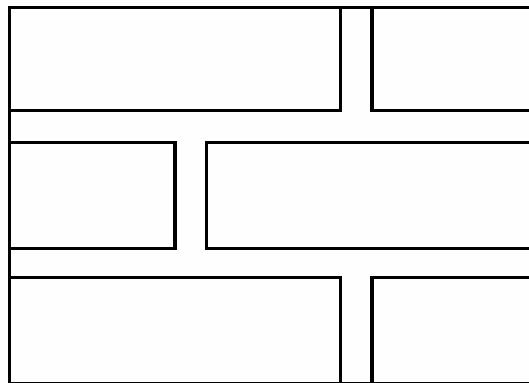


Figure 3.22. Masonry test specimen [22]



Figure 3.23. Compression test specimen with 1.8 cm mortar height and 6.5 cm brick height



Figure 3.24. Testing of masonry specimen



Figure 3.25. Failure of the masonry specimen

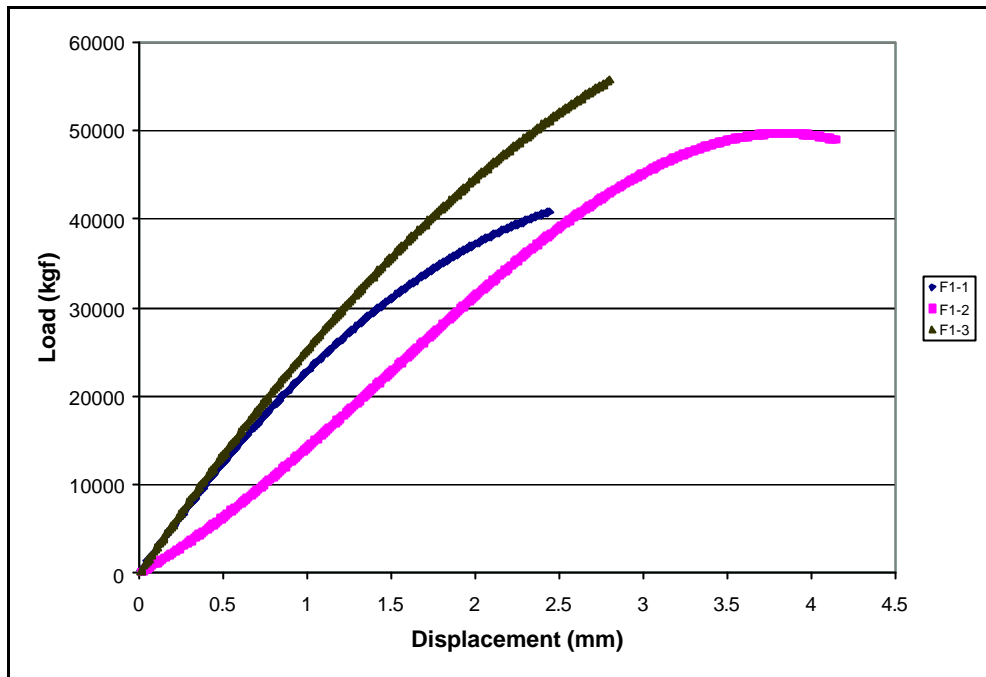


Figure 3.26. Load-displacement curves for masonry specimens produced by F1 mortar

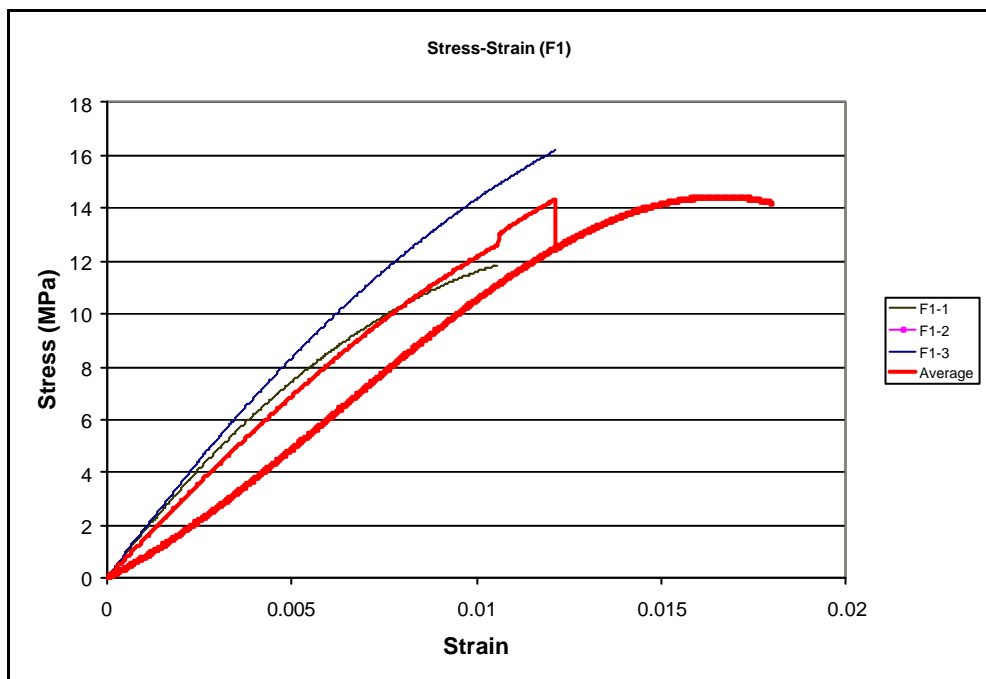


Figure 3.27. Stress-strain curves of masonry specimens produced by F1 mortar

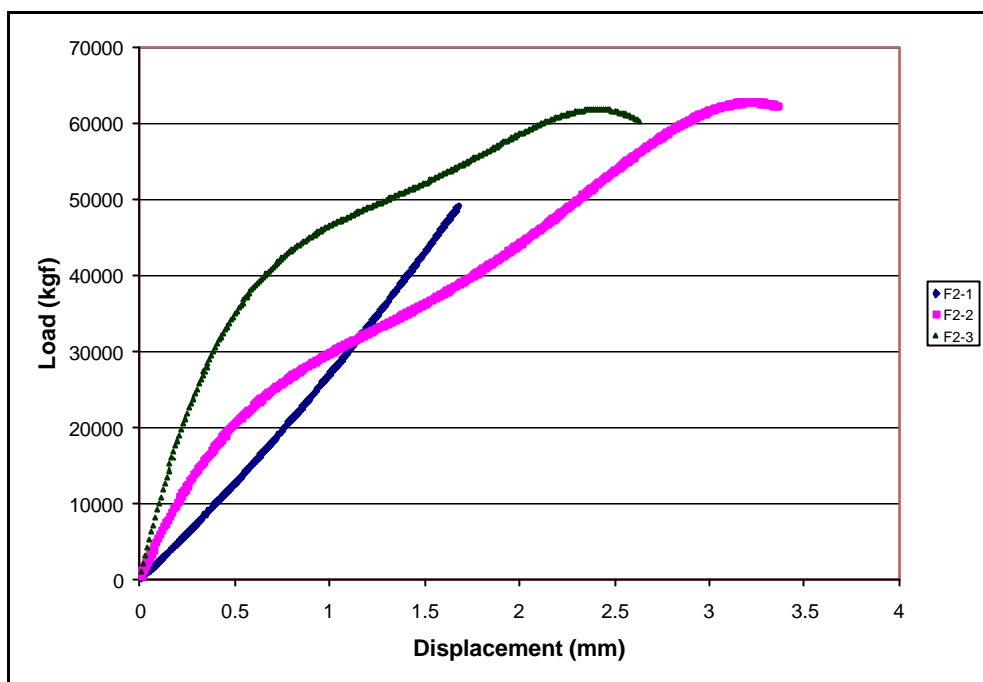


Figure 3.28. Load-displacement curves for masonry specimens produced by F2 mortar

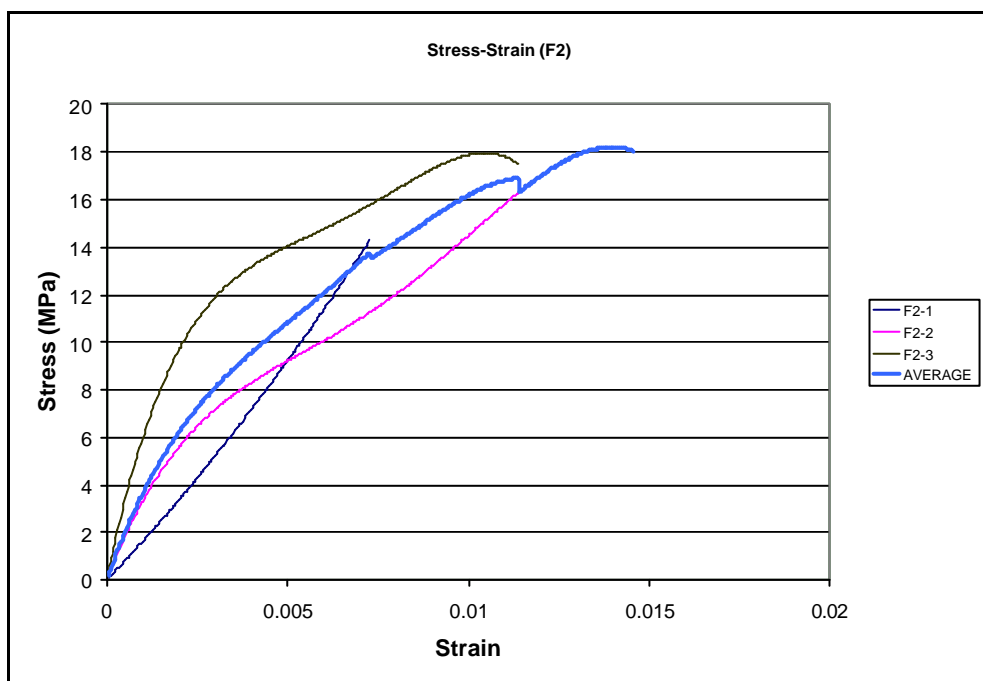


Figure 3.29. Stress-strain curve of masonry specimens produced by F2 mortar

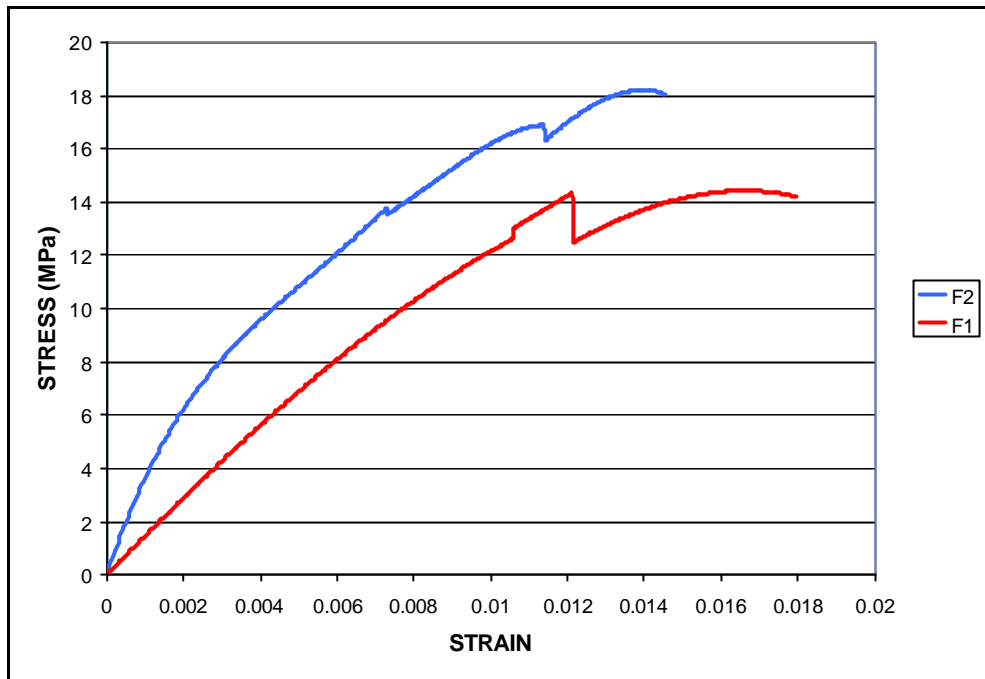


Figure 3.30. Average stress-strain curves of the masonry specimens produced by F1 and F2 mortar

For each graph there are two discontinuous points were observed. Each one of these represents the failure of one specimen. For example, according to the first discontinuous point in F2 graph when the average strength of the masonry specimens is 13.77 MPa, the first specimen was failed. For this reason from that point on the average was taken according to two specimens. The second irregular point is the point on which the second specimen was failed. For this reason the last portion of the average stress-strain graph was totally taken from the F2-2 graph, shown in Figure 4.32.

The characteristic compressive strength of masonry f_k is determined as the smaller value of either $f_k = f_{\text{average}} / 1.2$ or $f_k = f_{\text{min}}$ as indicated in EN1052 [22]. According to test results the average compressive strength and minimum compressive strength were obtained as 14.16 MPa and 11.86 MPa respectively for masonry specimens produced with F1 type of mortar. For the masonry produced with F2 type of mortar the values were obtained as 16.82 and 14.28 respectively. When the EN1052's approach was used to determine the maximum compressive strength of masonry smaller values were coming from $f_k = f_{\text{average}} / 1.2$ formula. Thereby the compressive strength for masonry produced with F1 type mortar was obtained as 11.8 MPa and it is 14.02 MPa for masonry produced with F2 type mortar.

According to Eurocode-6, Design of Masonry Structures, the characteristic modulus of elasticity (E_k) is defined as a secant modulus at service load conditions, i.e. at 1/3 of the maximum vertical load [23]. Modulus of elasticity for each type of masonry calculated at the load level of 1/3 of the compression strength. Figure 3.31 illustrates the calculation. In the illustration E1 and E2 are calculated as 1455 MPa and 3545 MPa respectively.

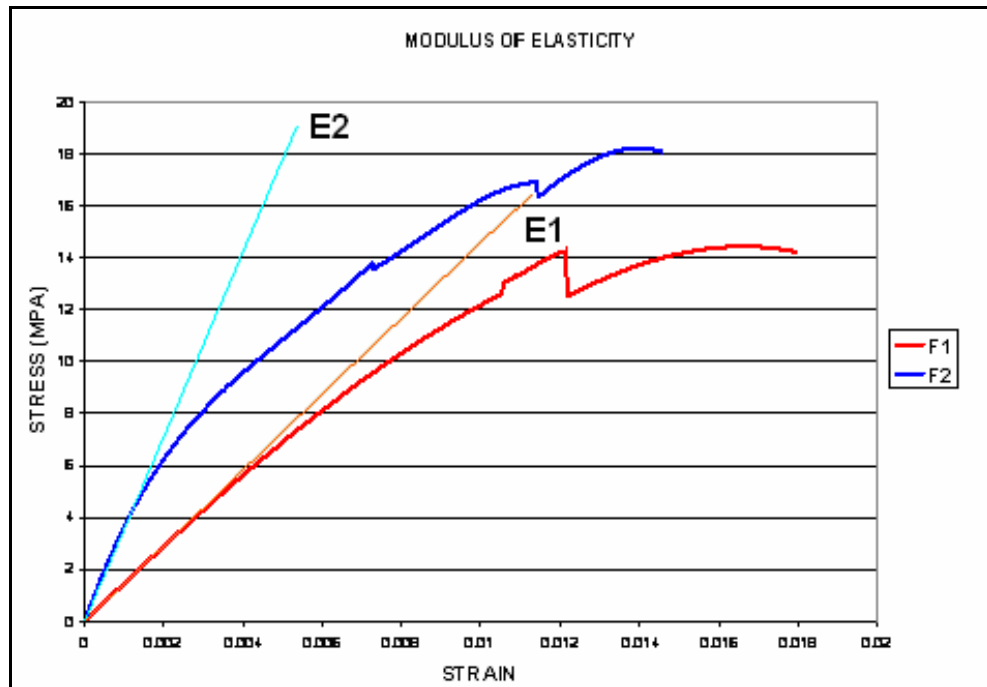


Figure 3.31. Determination of modulus of elasticity according to EC-6

As indicated in EC-6 in the absence of the value of E_k , determined by tests, it can be taken into consideration as [23];

$$E_k = 1000 * f_k \quad (3.1)$$

However the test performed by Miha Tomazevic, written in his book, "Earthquake-Resistant Design of Masonry Buildings", showed that, the values of modulus of elasticity, assessed by Equation 3.1 were sometimes far away from the reality [24]. It was noted that;

$$200 f_k < E_k < 2000 f_k \quad (3.2)$$

The same conclusion can be made by our test. If EC-6 approach is applied to obtain E, they were calculated as around 11800 MPa and 14020 MPa for masonry with F1 and F2 mortars respectively. As can be noted these values are so much greater than the modulus of elasticity values calculated from stress-strain diagrams. Modulus of elasticity value is going to be taken as 1455 MPa for masonry with F1 and 3545 for masonry F2.

Tensile strength may also be estimated from compressive strength of the material. For masonry a good estimation for the tensile strength can be taken between 5% and 7% of its compressive strength. If the tensile strength of the masonry is assumed as 7% of the compression strength, they will be obtained as around 0.82 MPa and 0.98 MPa for masonries with F1 and F2 mortar respectively. Besides flexure tests, applied to mortar specimen are directly related to tensile strength. In literature, the tensile strength of the material is taken as the half of the flexural strength. In that respect the tensile strength of the mortars can be obtained 0.785 MPa and 0.855 MPa for F1 and F2 respectively. These values can also be taken as the tensile strength of the masonry since the mortar is the weakest material in masonry. When two different approaches are compared, it is seen that, the values are in good agreement.

By the experiments, the basic material properties were determined for modeling and assessment of Belerbeyi palace. The identified material properties, modulus of elasticity, compression and tension strength are shown in Table 3.8.

Table 3.8. Identified material properties

Specimen No	Compressive Strength (Test, Mpa)	Compressive Strength (EN 1052, MPa)	Modulus of Elasticity (EN 1052, MPa)	Tensile Strength (7% of Compressive Strength, MPa)	Tensile Strength (Half of the Flexural Strength of mortar, MPa)
F1-1	11.86	11.8	1455	0.82	0.785
F1-2	14.43				
F1-3	16.19				
F2-1	14.28	14.02	3545	0.98	0.855
F2-2	17.96				
F2-3	18.21				
Average		12.91	2500	0.9	0.82

It should be remembered that, the masonry specimens have been produced and tested the obtained mechanical properties do not belong to original structure. There may be differences in mechanical properties of the original structure and reproduced and tested specimens. These differences may stem from the following reasons.

- It is well known that the horasan mortar gain strength with time because of the long carbonation duration of lime used as an ingredients. The specimens were produced at the beginning of September 2005 and tested in March 2006.
- Although the chemical and petrography analysis reveal the origin of the mortar as horasan mortar, the ingredient ratios are different from the general mortar formulas, F1 and F2. This difference is important and it affects the mechanical properties.
- The bricks used in the production of the test specimens normal bricks and they must have different mechanical properties with the historical bricks used in the construction of Beylerbeyi Palace. Nevertheless it is observed that the bricks of Beylerbeyi Palace are in good conditions and the mechanical properties should be close to recently produced bricks.
- Another important reason is the behavior of the material under service load. The mechanical properties, are dependent on the load apply to the structure. That is the reason why the in-situ tests are more reliable than the laboratory test.

The produced specimens do not represent the effects of the cast iron reinforcement. The configuration and the locations of the reinforcement were not known. Moreover due to oxidation problem it may totally lose its effect. In these conditions ignorance of the reinforcement is a good engineering approach.

3.2.5. Concluding Remarks

The engineering philosophy always requires using the all available access. Only available method to determine the mechanical properties of the wall was the employed testing strategy. As the result of the tests, the modulus of elasticity of the masonry wall composed by brick and horasan mortar was determined as 2500 MPa. Compressive strength is determined as 12.91 MPa but in order to avoid cracks, observed in the testing

this value is assumed as 10 MPa. Tensile strength is assumed as 0.85 MPa. The unit mass of the masonry is measured as 2.24 t/m³ and poisson ratio is assumed as 0.3.

For the basement story of palace which is composed of stones masonry a different type of material is defined with 50000MPa modulus of elasticity and 2.65 t/m³ unit mass [17].

Two types of wood were used in the slabs. It is determined that the cushion beams, on the walls are oak and slab beams, between the cushion beams are from fir. Modulus of elasticity of oak, in Turkey was determined as 12500 MPa and that of fir was 9700 MPa. The unit mass for both types of timber was taken as 0.72 t/m³ [25 - 26].

4. AMBIENT VIBRATION SURVEY AND NUMERICAL MODELING FOR THE PALACE

4.1. Necessity of Ambient Vibration Survey

Due to many uncertainties, associated with the construction system, material properties, modeling techniques, analysis method and soil interaction, evaluation of a historical structure is indeed a difficult task. However sophisticated measurement techniques, on the real structure enable engineers to learn the real behavior of the structure. The findings can later be used to check the accuracy of the assessment method. Moreover the results were used to adjust the assessment tools. In this study Ambient Vibration Survey (AVS) technique has been adopted as the sophisticated measurements and assessment of the safety of Beylerbeyi Palace has been done by performing analysis on numerical model of the structure.

This study was totally grown up within the sixth framework project, PROHITECH. At every stage, from the beginning to the end, we had the chance of changing ideas, discussing techniques, deciding the strategy and interpreting the results with the masters of the engineers from twelve countries, sixteen institutions. The ambient vibration survey, applied to Beylerbeyi Palace is one of the joint projects, carried by the collaboration of Macedonian and Turkish team together. The experimental results were interpreted by Macedonian team from University "St. Cyril and Methodius", Institute of Earthquake Engineering and Engineering Seismology

AVS provides an inexpensive means of obtaining dynamic characteristics, namely natural periods and mode shapes, of existing structures. It is very useful to assess the accuracy of analytical model of real, complex structures for which structural drawings may be incomplete, building material properties may not be known, the extent of deterioration with time is undetermined and soil-structure interaction is poorly understood. AVS provides a fast, non-destructive, effective and inexpensive means of obtaining in-situ response of existing structures. None of the disadvantageous, mentioned in the application of non-destructive test methods exists in the application of AVS. The obtained dynamic

parameters from AVS would be used to calibrate the numerical model to give the same dynamic parameters.

4.2. Ambient Vibration Survey (AVS)

4.2.1. Procedure

Ambient Vibration Testing method is widely applied and popular full-scale testing method aiming to measure the dynamic characteristics of a structure. Wind, traffic noise or some other impulsive forces like wave loading can be assumed as ambient forces. The method can be performed without disturbing the structure's normal function.

Experimental testing of the Beylerbeyi Palace has been performed by ambient vibration measurements for two orthogonal directions. Longitudinal direction is the parallel direction to the sea-side along with the structure's longer-side whereas the transversal direction is the perpendicular direction, along with the shorter side of the structure, to the shoreline. For definition of the structure's dynamic characteristics such as natural frequencies, mode shapes of vibration and damping coefficients, this is an obligation.

4.2.2. Experimental Results

For the ambient measurements four different levels were determined through the height of the structure. These levels are ground level, base of the first storey, base of the second storey and roof level of the palace. On each level six different points were determined to have measurements. All points are illustrated on Figure 4.1. T1 was selected as reference point in the process and one seismometer was moved to all determined points to measure the vibration along with transversal and longitudinal directions.

The measured vibrations were processed by ARTeMIS software in order to determine the dynamic parameters. Table 4.1 summarizes the obtained dynamic characteristics of the palace while the obtained mode shapes are illustrated through Figure 4.2 – 4.8 [5].

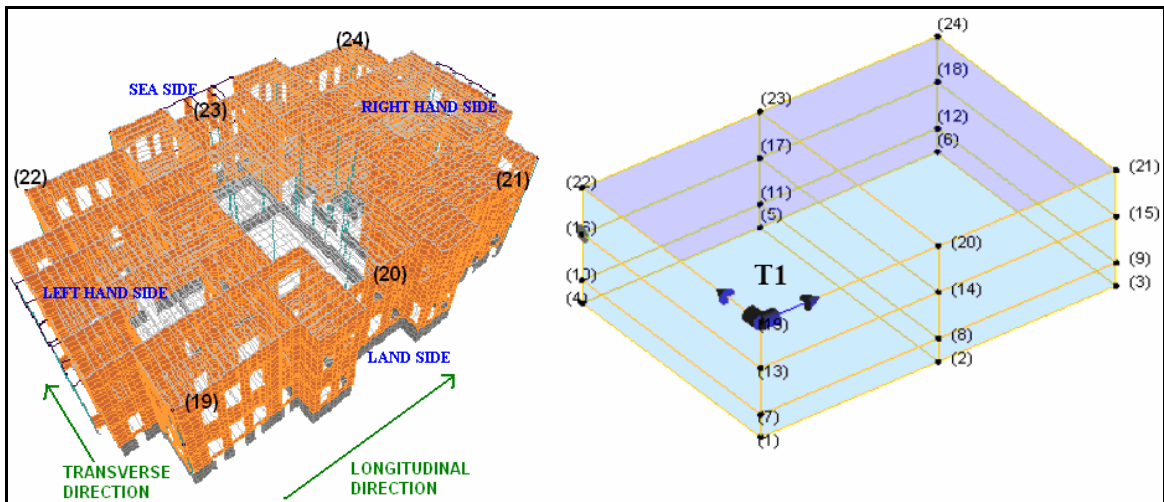


Figure 4. 1. Location of the measurements and position of the reference point

Table 4.1. Dynamic characteristics of the palace [5]

Mode	Freq. [Hz]	Period [s]	Damping Ratio (%)
Mode 1	2.697	0.371	2.653
Mode 2	3.593	0.278	2.6
Mode 3	4.147	0.241	1.937
Mode 4	5.208	0.192	2.516
Mode 5	7.927	0.126	2.542
Mode 6	8.339	0.120	2.397
Mode 6	10.56	0.095	1.045
Mode 8	14.55	0.069	2.549

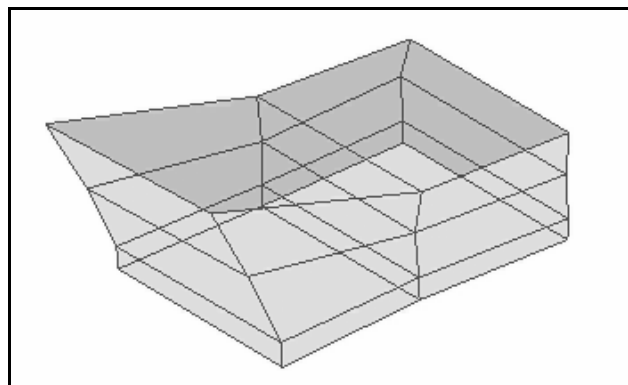


Figure 4.2. First Mode Shape (T=0.371 second) [5]

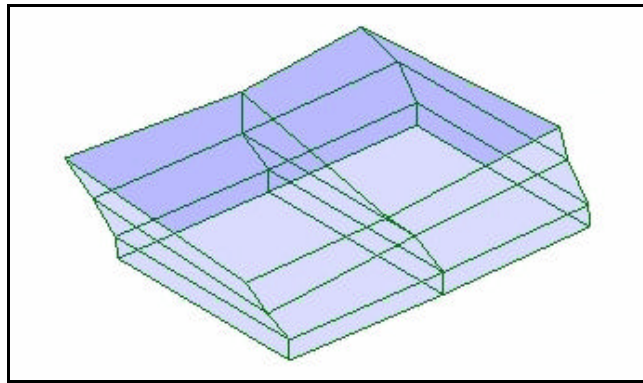


Figure 4.3. Second Mode Shape ($T=0.278$ second) [5]

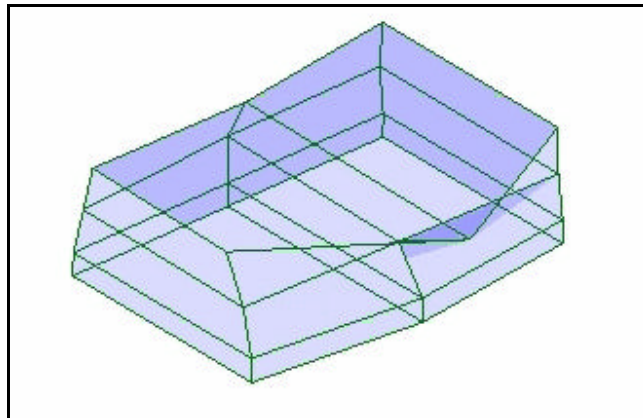


Figure 4.4. Third Mode Shape ($T=0.241$ second) [5]

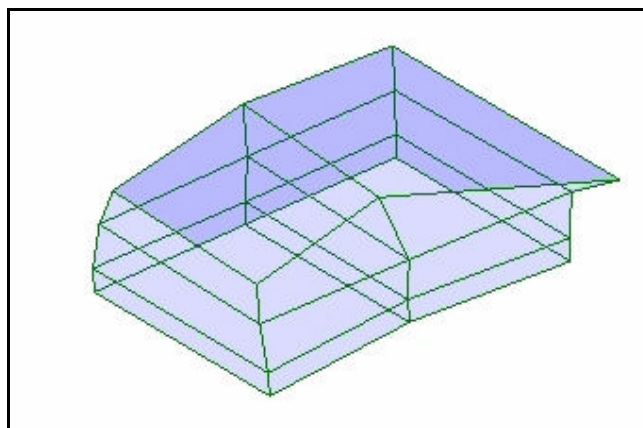


Figure 4.5. Fourth Mode Shape ($T=0.192$ second) [5]

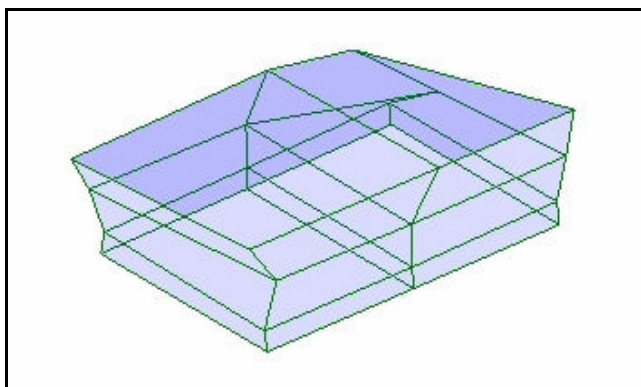


Figure 4.6. Fifth Mode Shape ($T=0.126$ second) [5]

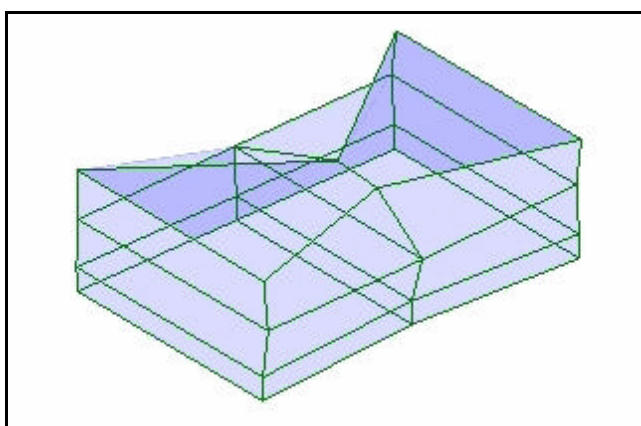


Figure 4.7. Sixth Mode Shape ($T=0.120$ second) [5]

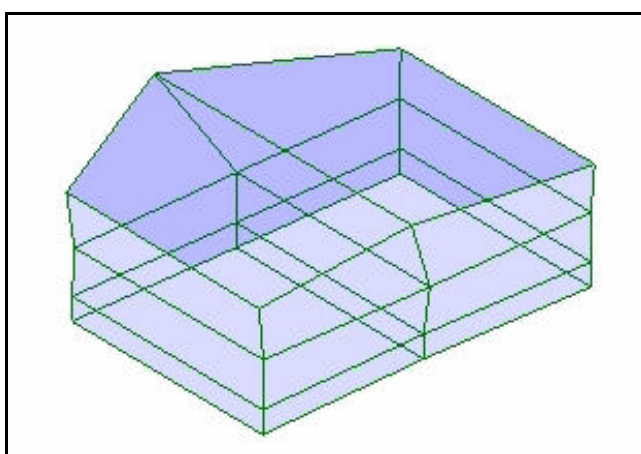


Figure 4.8. Eighth Mode Shape ($T=0.095$ second) [5]

As can be seen from the obtained data, the first natural frequencies for both orthogonal directions are well separated: for transversal vibration 2.7 Hz and for longitudinal vibration 3.6 Hz. The obtained mode shapes are showing complex vibration of the structure even it is with regular and symmetric shape in plan and in elevation. The effect of the exterior wall should be investigated. It may be the main reason for such a complex behavior [6].

Secondly no soil-structure interaction was verified. Thereby the numerical model can be prepared by assuming fixed based supports at the base. The obtained results can be further used for calibration and improving of the mathematical model to be used for analytical investigation of the stability of the Palace [6].

4.3. Numerical Model of the Palace

The analysis of a historical structure (e.g., masonry building) has many similarities, as well as many differences, compared to the analysis of a modern structure (e.g., reinforced concrete shear wall building). Similarities refer to the general assumptions and the mathematical models used; while differences refer to the material properties, the structural system characteristics (e.g., monolithic connections), and the distribution of inertial (e.g., earthquake) loads along the height of the structure.

The complex geometry—most of the historical buildings usually have—generate sizeable variations in stiffness due both to heterogeneities in masonry work and to abrupt changes in cross section among the component elements, making it impossible to carry out accurate computations through the application of conventional material strength techniques. In such cases, it is concluded that only the use of the finite element method (FEM) enables the deriving of credible computational results. Although it is possible to conduct closed for solution technique on one and two dimensional structural members [27] in this case it is not practical.

4.3.1. Construction of Numerical Model

Reflecting the determined architecture, structural carrying system and identified material properties, three-dimensional numerical model has been prepared by using SAP2000 and LUSAS computer package programs [28-29]. The masonry walls were model by shell elements and frame elements were used for the column and timber slab members. In both model, the structure was assumed to have fixed support at the base in the light of the results of AVS and geotechnical report, mentioned in previous stages.

The most important aspect of the model is the definition of the timber slab. When the stiffness of the timber members are compared to that of walls whose thicknesses varying between 2 m and 0.6m it maybe thought that the modeling of slabs is useless. However the results of the AVS showed that the timber slabs are effective and they are supplying a connection between the walls. On the other hand it is impossible to say that there is a rigid diaphragm action on the slabs. For this reason it is a must to add the timber slabs to the model. It should not be forgotten that the timber is an orthotropic material and material characteristics vary according to direction. On the other hand in the analyses it was observed that isotropic or orthotropic materials do not affect the global behavior of the structure. The important parameters are those measured in the element axis.

For the Finite Element Model (FEM) it is an obligation to connect every member by joints [27-28]. In this respect in order to model 8*40 cm² timber beams with 40 cm spacing, the maximum size of shell elements should be restricted to 40 cm. This causes incredibly high-sized model which is very hard to run. In order to overcome this problem, instead of 8*40 cm² with 40 spacing timber beams it is appropriate to use 20*40cm² beams with one meter spacing. This enables to increase the minimum size of the shell elements to 1 m and decrease the number of the elements. Thereby fast model will be ready to run. Through Figures 4.9 - 4.12 Numerical Model (NM) is illustrated in SAP2000 and Figure 4.13 shows the model in LUSAS.

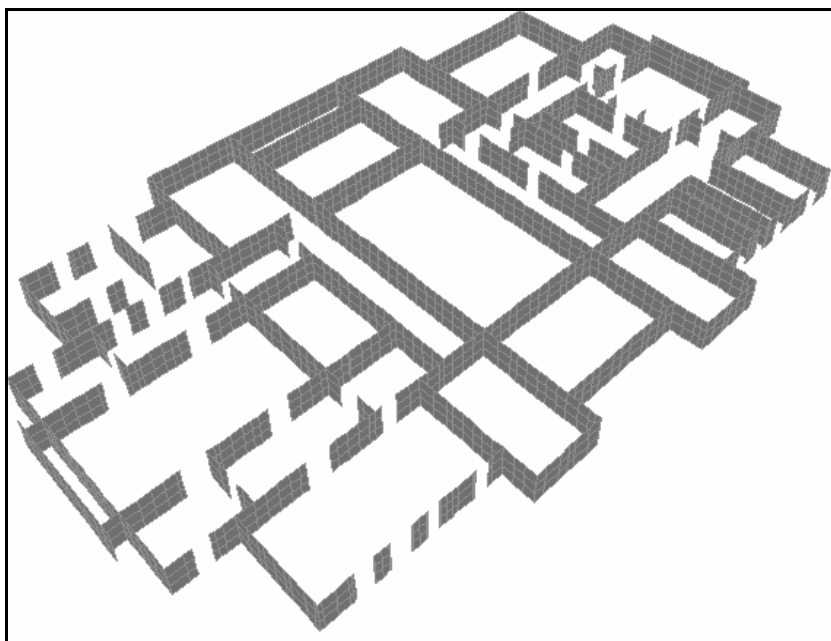


Figure 4.9. Basement of the structure [28]

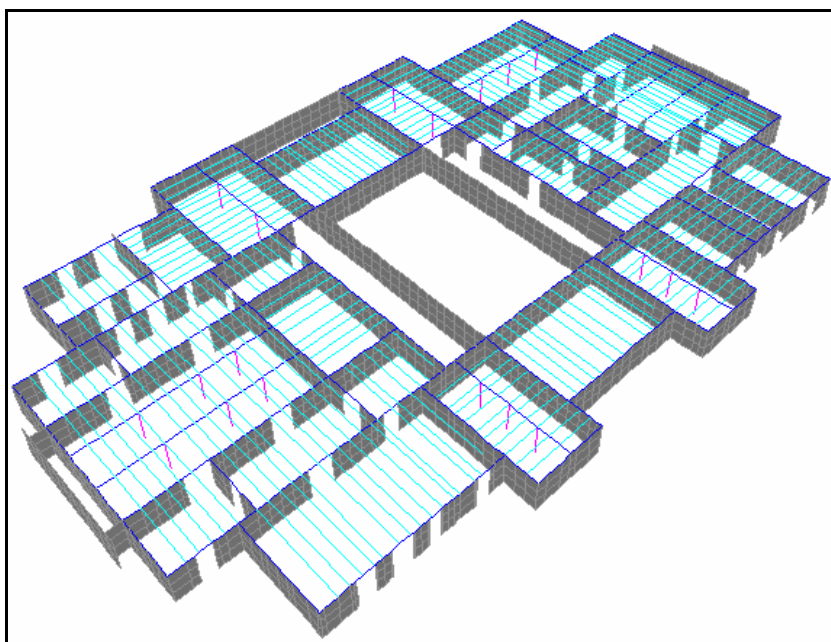


Figure 4.10. Basement of the palace with timber slab members [28]

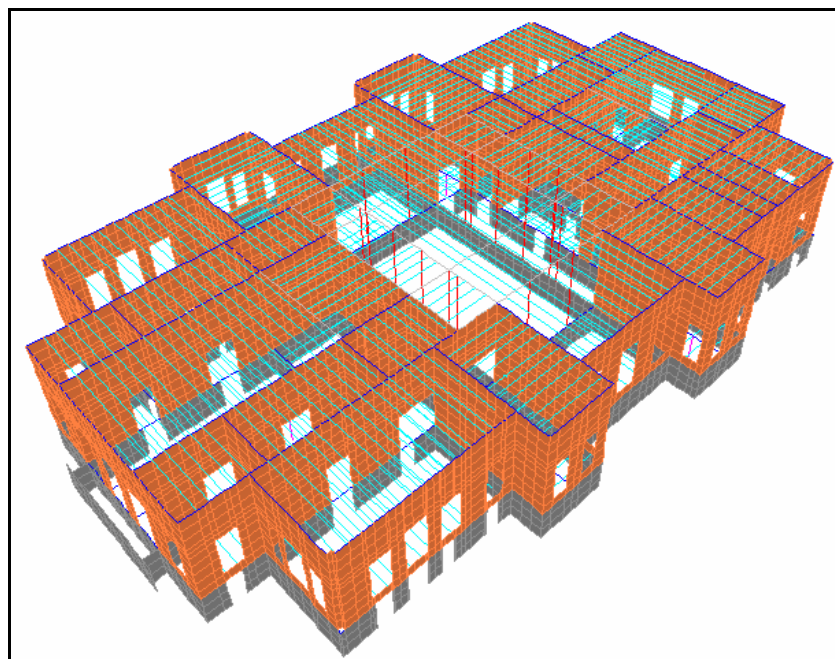


Figure 4.11. Basement and the first floor of the palace [28]

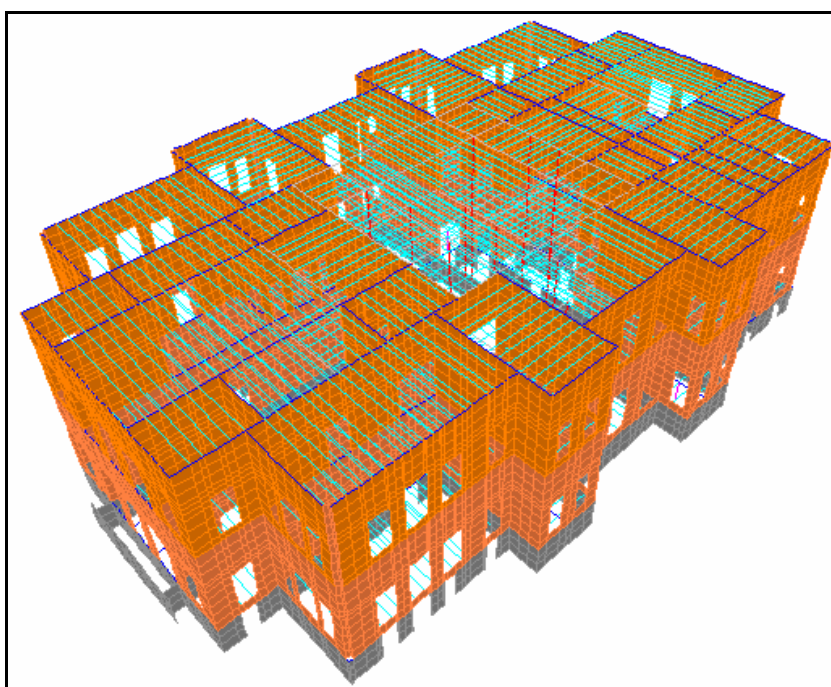


Figure 4.12. Three dimensional model of the palace with timber slab [28]

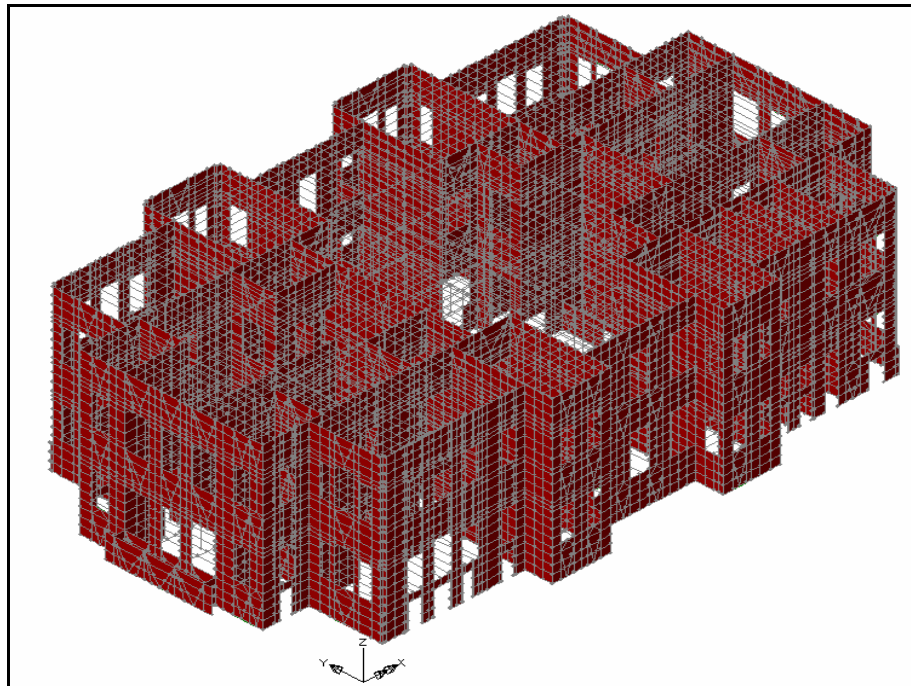


Figure 4. 13. Three dimensional model of the palace with timber slab [29]

Through the numerical analysis SAP2000 and LUSAS programs were used together. The reasons of using two different packages in the analysis of Beylerbeyi Palace, can be ordered as follows;

- From the definition of the geometry to interpretation of the results, the packages have different styles. Modeling of a historical structure is a complicated task and it is very easy to have some mistakes and error in numerical model. Use of two different programs can help to check the mistakes and correct them.
- Non-linear analysis can estimate the real behavior of the structure and it is possible to have that kind of analysis in LUSAS.
- Definition of the geometry, assignment of the loads and interpretation of the results are straightforward in SAP2000. For this reason it is suitable to model Beylerbeyi Palace which has a complex geometry and load bearing system.

4.3.2. Modal Analysis of the Structure

After assigning the additional masses and loads, induced by façade covering, plaster, roof, live load, slab beams and cover load, modal analysis was performed for the real structure. Additional masses and loads are explained below;

- Façade Load; the exterior side of the Beylerbeyi Palace is covered by küfeki stone, which is the main construction stone in Ottoman time. It is assumed that the küfeki stone has only load and mass contribution to the wall. Unit mass of the küfeki stone was determined as 2.15 gr/cm^3 and 10 cm thickness is assumed for façade.[19]
- Plaster Load; Plaster is identified as horasan plaster with a unit mass of 1.8 gr/cm^3 and it is assumed that each wall has $2*5 \text{ cm}$ plaster thickness. The load assigned with mass and load contribution to the model [19].
- Roof Loads; 75 kg/m^2 load is assumed to apply as roof loads [30]. In order to eliminate the mode of the timber slab beams, this load is assigned to cushion beams. Because of the roof system of the structure the loads were distributed to the cushion beams like two-way slab system.
- Live Load; Two different live load values are assumed related to function of the structure. 3.5 kN/m^2 is assigned to the open-visit areas and 2 kN/m^2 is assigned to close-visit areas. The loads are assigned to cushion beams. Related to slab system configuration the loads distributed as one-way slab system [30].
- Slab Beams and Cover Loads; The weight and mass of the slab beams were assumed as zero in order to eliminate the dynamic effect of them. For the global behavior of the palace it is effective. For this reason the weight and mass of them should be included somehow. In the model the weight and mass were applied to the cushion beams. The unit mass is taken as 0.7 gr/cm^3 [25-26].

After assigning the specified loads the dynamic analysis was performed to identify the modes. Modal analysis is completely linear analysis and used to determine the vibration modes of a structure. These modes are useful to understand the behavior of the

structure. There are two types of modal analysis, namely, Eigenvector analysis and Ritz vector analysis.

- Eigenvector analysis determines the un-damped free-vibration mode shapes and frequencies of the system. These natural modes provide an excellent insight into the behavior of the structure. Eigenvector analysis involves the solution of the generalized eigenvalue problem in which K is the stiffness matrix, M is the diagonal mass matrix, Ω^2 is the diagonal matrix of eigenvalues, and v is the matrix of corresponding eigenvectors (mode shapes) [28, 31 and 32].

$$[K - \Omega^2 M]v = 0 \quad (4.1)$$

- **Ritz-vector** analysis seeks to find modes that are excited by a particular loading. Ritz vectors can provide a better basis than do eigenvectors when used for response-spectrum or time-history analyses that are based on modal superposition [28].

The spatial distribution of the dynamic load vector serves as a starting load vector to initiate the procedure. The first Ritz vector is the static displacement vector corresponding to the starting load vector. The remaining vectors are generated from a recurrence relationship in which the mass matrix is multiplied by the previously obtained Ritz vector and used as the load vector for the next static solution [28].

For the dynamic analysis of Beylerbeyi Palace, Ritz-vector analysis was performed since it gives better results than do eigenvector analysis. The modal analysis was performed for 60 modes in order to catch 90% mass participation factor. Minimum 90 percent mass participation is an obligation for a numerical model to have according to Turkish Earthquake Code in order to make, the modal analysis to represent the overall behavior of the structure [7]. Table 4.2 summarizes the dynamic data of the analysis.

Table 4.2. Dynamic parameters of the un-calibrated model

MODE	Period (Sec)	Mass Participation Ratio in X	Mass Participation Ratio in Y	Total Mass Participation Ratio in X	Total Mass Participation Ratio in Y
1	0.361	0.000	0.120	0.000	0.120
2	0.317	0.003	0.120	0.003	0.230
3	0.301	0.100	0.005	0.110	0.240
4	0.282	0.120	0.001	0.220	0.240
5	0.277	0.000	0.075	0.220	0.310
6	0.276	0.074	0.002	0.300	0.310
7	0.249	0.073	0.000	0.370	0.310
8	0.242	0.000	0.012	0.370	0.330
9	0.236	0.003	0.000	0.370	0.330
10	0.229	0.000	0.000	0.370	0.330
11	0.227	0.014	0.002	0.390	0.330
12	0.224	0.001	0.011	0.390	0.340
13	0.221	0.000	0.000	0.390	0.340
14	0.216	0.034	0.000	0.420	0.340
15	0.211	0.000	0.060	0.420	0.400
16	0.207	0.000	0.000	0.420	0.400
17	0.202	0.000	0.047	0.420	0.450
18	0.197	0.000	0.008	0.430	0.450
19	0.196	0.000	0.003	0.430	0.460
20	0.195	0.000	0.010	0.430	0.470
21	0.191	0.000	0.002	0.430	0.470
22	0.185	0.007	0.000	0.430	0.470
23	0.185	0.000	0.000	0.430	0.470
24	0.181	0.003	0.005	0.440	0.480
25	0.177	0.008	0.006	0.440	0.480
26	0.174	0.014	0.000	0.460	0.480
27	0.169	0.003	0.000	0.460	0.480
28	0.167	0.001	0.012	0.460	0.490
29	0.164	0.019	0.001	0.480	0.490
30	0.164	0.000	0.009	0.480	0.500

Table 4.2. Dynamic parameters of the un-calibrated model (Continue)

MODE	Period (Sec)	Mass Participation Ratio in X	Mass Participation Ratio in Y	Total Mass Participation Ratio in X	Total Mass Participation Ratio in Y
31	0.160	0.014	0.000	0.500	0.500
32	0.155	0.000	0.011	0.500	0.520
33	0.149	0.000	0.003	0.500	0.520
34	0.144	0.001	0.001	0.500	0.520
35	0.139	0.002	0.016	0.500	0.540
36	0.135	0.027	0.002	0.530	0.540
37	0.132	0.000	0.019	0.530	0.560
38	0.129	0.017	0.000	0.540	0.560
39	0.121	0.010	0.000	0.550	0.560
40	0.120	0.000	0.003	0.550	0.560
41	0.111	0.000	0.008	0.550	0.570
42	0.109	0.011	0.000	0.570	0.570
43	0.100	0.004	0.002	0.570	0.570
44	0.099	0.002	0.007	0.570	0.580
45	0.091	0.000	0.007	0.570	0.580
46	0.087	0.011	0.000	0.580	0.580
47	0.079	0.028	0.000	0.610	0.580
48	0.077	0.000	0.016	0.610	0.600
49	0.069	0.006	0.001	0.620	0.600
50	0.068	0.001	0.012	0.620	0.610
51	0.057	0.000	0.008	0.620	0.620
52	0.056	0.010	0.000	0.630	0.620
53	0.044	0.000	0.014	0.630	0.640
54	0.043	0.010	0.000	0.640	0.640
55	0.032	0.000	0.020	0.640	0.660
56	0.031	0.019	0.000	0.660	0.660
57	0.019	0.000	0.054	0.660	0.710
58	0.019	0.054	0.000	0.710	0.710
59	0.009	0.210	0.000	0.920	0.710
60	0.009	0.000	0.200	0.920	0.920

The dynamic properties and mode shapes of the structure have revealed important characteristics of the structural behavior. These characteristics distinguish Beylerbeyi Palace from a regular and basic structure. They are ordered as follows;

- Timber slabs could not supply the diaphragm behavior to the structure. For these reason local modes are observed. For example the first mode is only the movement of the left hand side of the structure in the transversal direction and the movement is limited by the second story. Thereby the mass participation factor is just about 10% for the first mode. At the end of the 60 modes 92% mass participation is obtained.
- Due to small mass gathered on the storey levels, lumped mass behavior is not observed. This cause, some modes are the movement of the wall segments, between the storey levels.
- Timber slab frames, which were included in the model, are effectuating the modes themselves although it was tried to be prevented by assigning zero mass. However the modes have very small mass participation factor as expected (Figure 4.21).
- Due to high stiffness difference between the basement and the normal stories the movement of the basement floor at the first modes could not be observed. 59th and 60th modes are representing the movement of the basement in the transversal and longitudinal direction with high modal mass participation ratio which the basement has (Figure 4.22 and Figure 4.23).

Important mode shapes of the palace are illustrated below with their period (T) and modal mass participation ratio (MPR) with movement direction. It can be said that, the first modes of the structure are related to the second and first stories of the palace while basement floor is participating in dynamic behavior through the 59th and 60th modes. This observation demonstrates the effect of the stiffness in modal behavior (Figures 4.14-4.23).

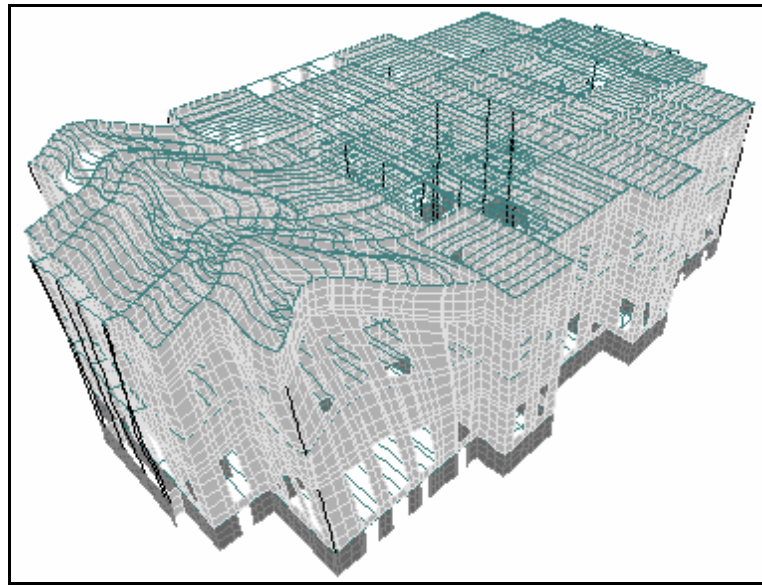


Figure 4.14. First mode shape; Movement of the left part in transversal direction

($T=0.361$ sec, $MPR=0.12$ -Y)

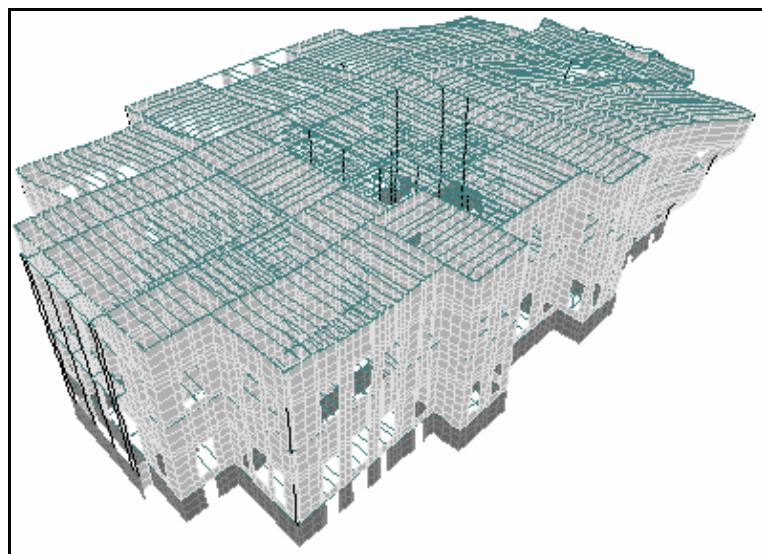


Figure 4.15. Second mode shape; Movement of the right part in transversal direction

($T=0.317$ sec, $MPR=0.12$ -Y)

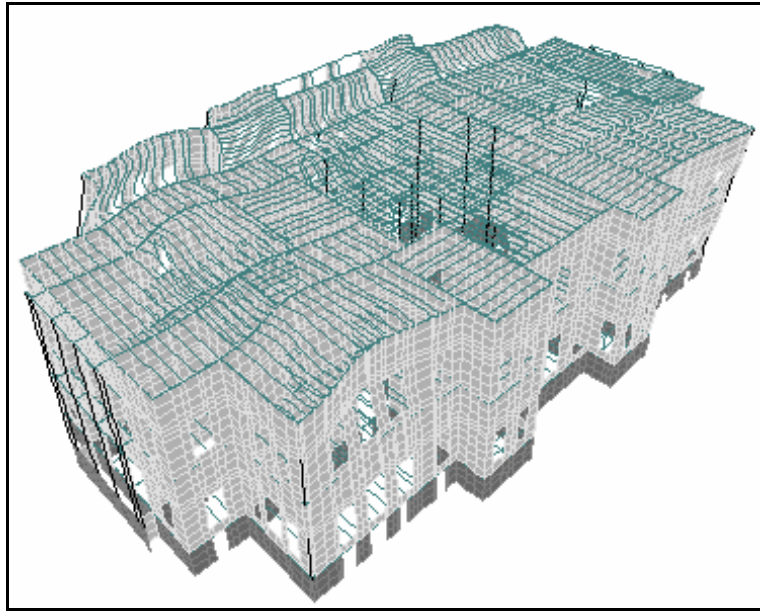


Figure 4.16. Third mode shape; Movement of the sea-side in longitudinal direction

($T=0.301$ sec, $MPR=0.10-X$)

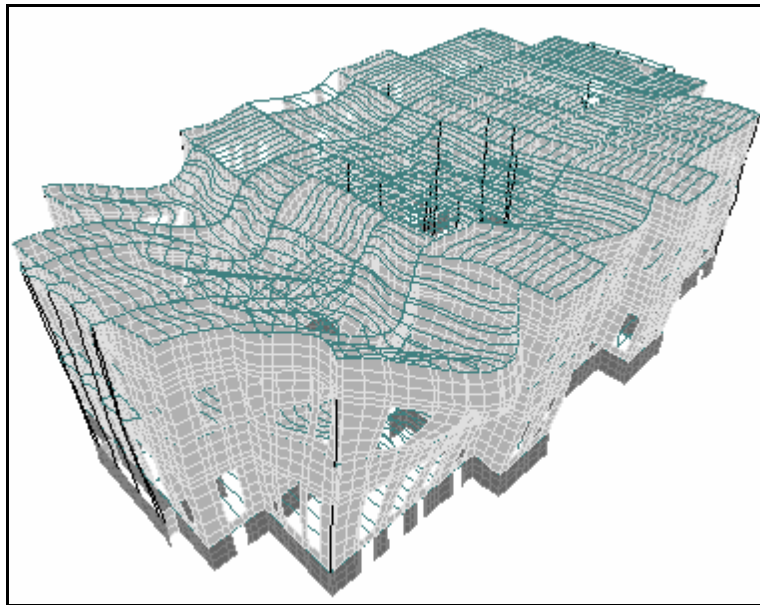


Figure 4.17. Fourth mode shape; Movement of the land-side in longitudinal direction

($T=0.282$ sec, $MPR=0.12-X$)

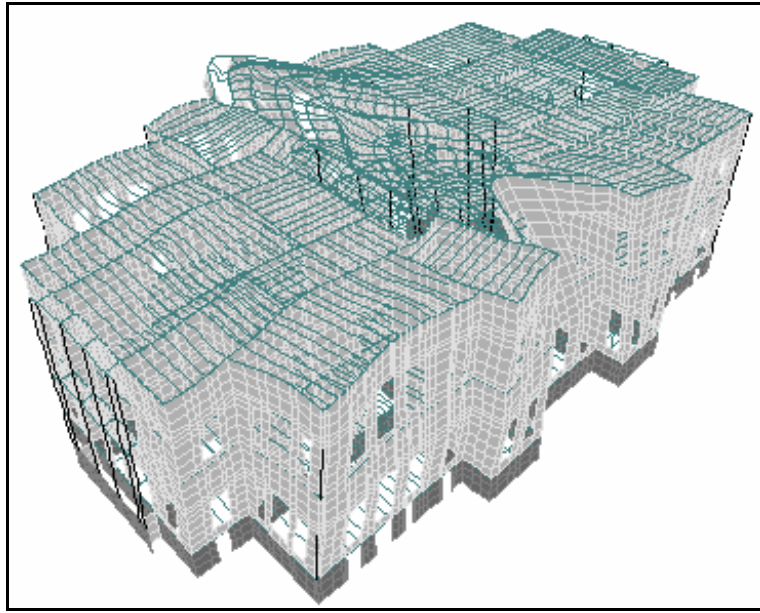


Figure 4.18. Fifth mode shape; Movement of the mid part in transversal direction

($T=0.277$ sec, $MPR=0.075$ -Y)

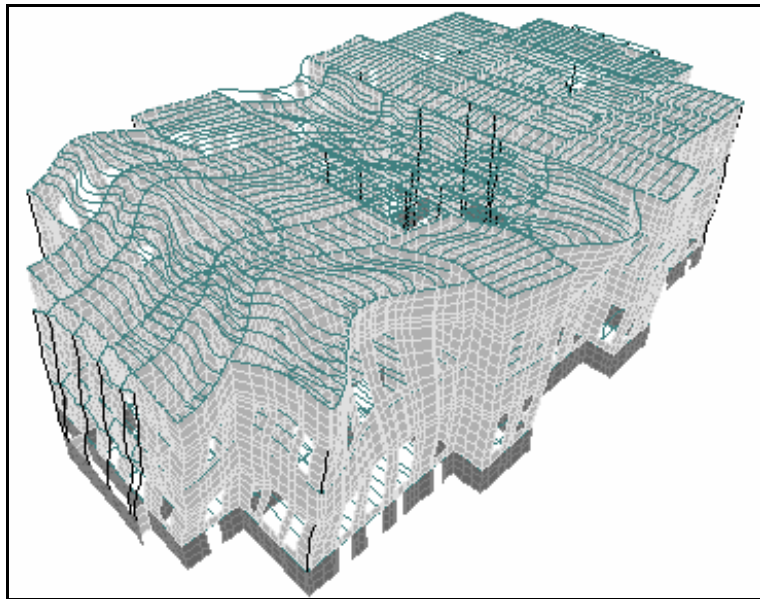


Figure 4.19. Sixth mode shape; Movement of the land-side in longitudinal direction

($T=0.276$ sec, $MPR=0.074$ -X)

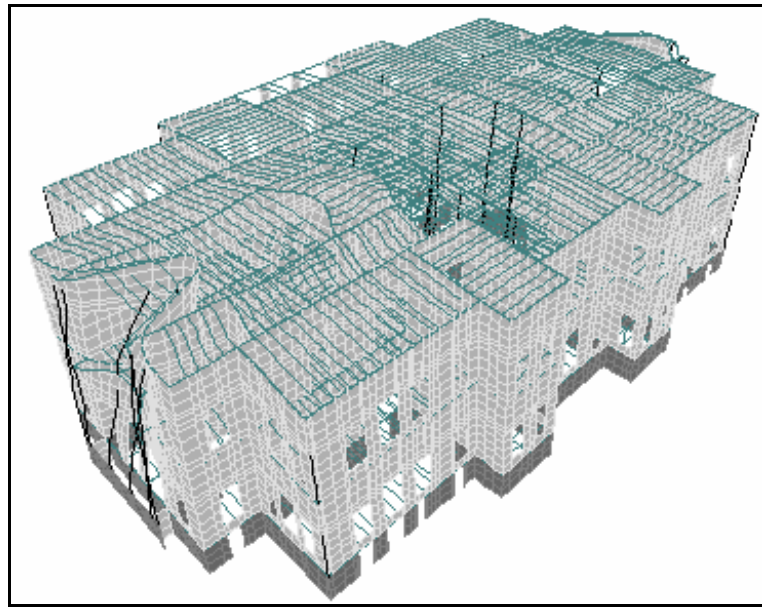


Figure 4.20. Seventh mode shape; Movement of the mid part in longitudinal direction
($T=0.249$ sec, $MPR=0.073-X$)

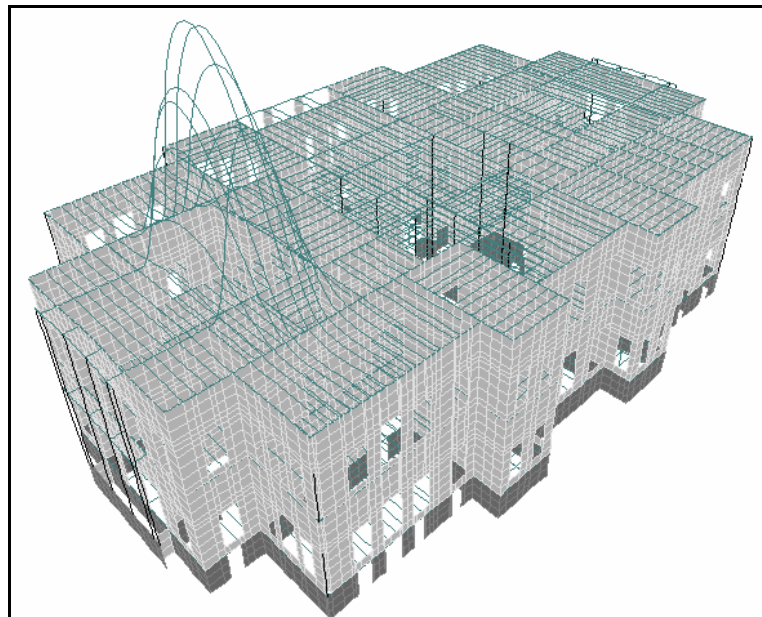


Figure 4.21. 13th mode shape; Movement of the timber slab in vertical direction
($T=0.221$ sec, $MPR=0.000465-Z$)

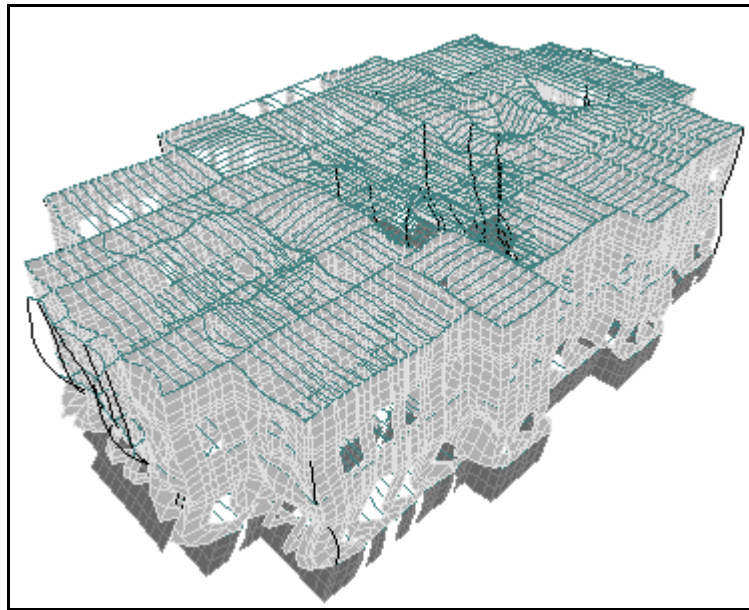


Figure 4.22. 59th mode shape; Movement of the lower part in longitudinal direction
($T=0.009$ sec, $MPR=0.21-X$)

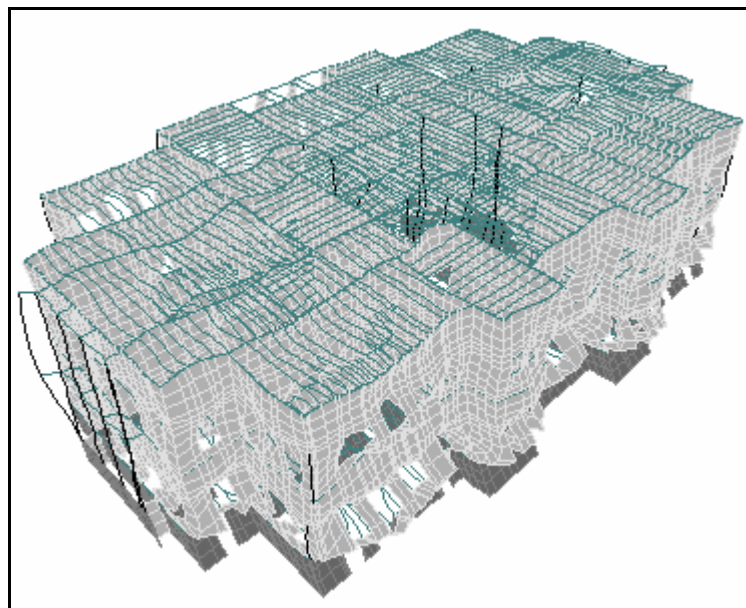


Figure 4.23. 60th mode shape; Movement of the lower part in transversal direction
($T=0.009$ sec, $MPR=0.20-Y$)

There is a structural wall joining the structure in the transversal direction (Figure 4.24). This wall can change the all dynamic behavior of the structure. For this reason the palace should be modeled with the external wall and its effect should be searched.

4.4. Effect of the Exterior Wall to the Dynamic Behavior of the Structure

In this part of the study, effect of the external wall intersecting the palace was investigated. The wall is joining the palace in the land side of the structure and separating the Harem and Mabeyn gardens. Its thickness is about 1.5 m. Figure 4.24 shows the wall.



Figure 4. 24. Adjacent wall

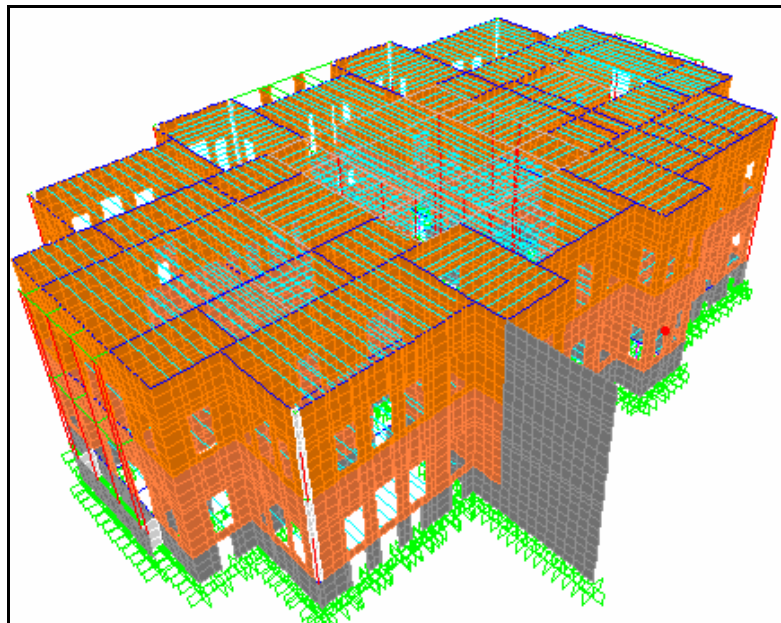


Figure 4.25. Numerical model of the palace including the external wall

At the conclusion part of the AVS, it was stated that, the complex behavior of the palace might stem from the neighboring wall [6]. For this reason the investigation is in

importance. A numerical model was prepared and modal analysis was performed to determine the dynamic properties of the structure including the neighboring wall. Figure 4.25 illustrates the prepared model.

At the end of the analysis, it was determined that, the addition of the neighboring wall has no effect in the modal behavior of the structure. All the mode shapes and modal frequencies of the two structures, namely the structure in which the neighboring wall is included and the structure without neighboring wall are the same. The main reason behind that is the lack of rigid diaphragm action on the storey levels. The lack of rigid floors causes the neighboring wall to affect only the dynamic behavior of the adjacent wall extended in the same direction. This effect did not affect the global behavior of the structure. For this reason it is concluded that in numerical model, there is no need to include the neighboring wall.

The comparison of the mode shapes, obtained from numerical analysis to those of obtained from AVS can appraise the accuracy of the Numerical Model (NM). It was seen that the first mode shapes is exactly the same for two different approaches while there is a slight difference in the period (Figure 4.2 and 4.14). The second mode of the numerical analysis, movement of the right part of the palace does not fit the second mode of AVS, movement of the structure in longitudinal direction (Figure 4.3 and 4.15). For this reason NM needs to have some alterations to catch the second and further modes of AVS.

4.5. Calibration of Numerical Model of the Structure

Modeling is a piece of art to transfer the real structure to computer atmosphere. During this process all the existing conditions and physics of the problem should be evaluated well. For the modeling of a historic structure number of the associated parameters is more than that of a regular structure. Moreover all available structural parameters are suspicious with respect to accuracy.

In this study in order to make the NM to represent the real behavior of Beylerbeyi Palace, AVS results were used. For the NM the most suspicious parameter was grasped as the modulus of elasticity of the masonry, related to dynamic behavior of the structure.

Because the used modulus of elasticity was obtained from the laboratory tests, performed over reproduced masonry specimens. As explained in previous chapter test results may give different values than the real characteristics. In addition, the use of iron reinforcement may differ in the modulus of elasticity from wall segments to wall segments. For this reason in the calibration process of the numerical model only parameter to alter is the modulus of elasticity of the masonry.

The calibration process is explained below as a bunch of step. In each step, mode shape of NM and AVS were shown and calibration process was summarized in a table. Finally the results of the calibration were explained after the table. It is important to note that; after each step of calibration the model was run and further steps' dynamic parameters were obtained in calibrated model.

4.5.1. First step in Calibration

For the first mode of both AVS and NM is the same type of movement (Figure 4.26). On the other hand there is a small difference in the period value. The first calibration aims to conceal the discrepancy in the period. The calibration coefficient (Cal Coef) is calculated as the square of the ratio of the periods due to the fact that [31, 32];

$$T = 2 * p \sqrt{\frac{m}{K}} \quad (4.2)$$

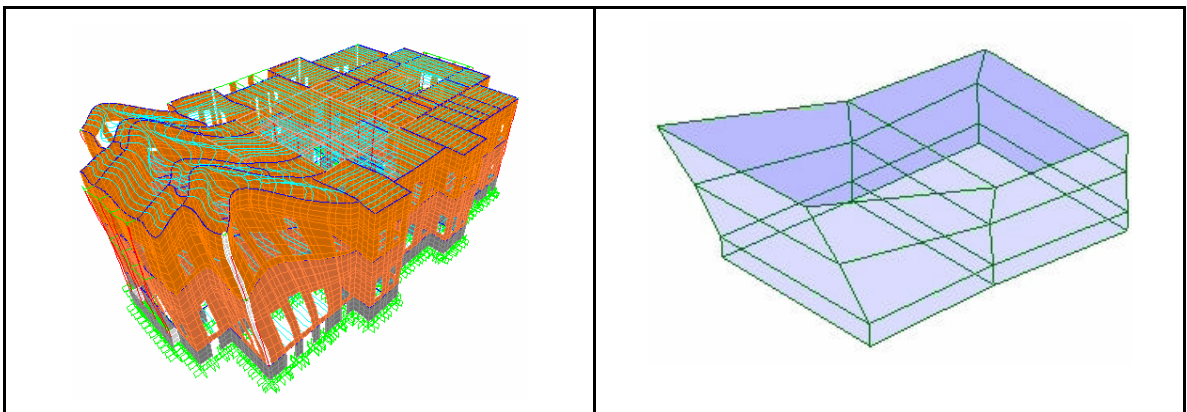


Figure 4.26. First mode in NM and AVS (The same movement with different periods)

Modulus of elasticity of the structure, E was decreased to $0.95 \times 2500 = 2375$ MPa in order to obtain the first mode period as 0.371 second (Table 4.3).

Table 4.3. Calibration process to obtain E for all structure

System	Explanation	Period (S)	Ratio	Cal. Coef.
AVS	1 st Mode	0.371	0.97	0.95
NM	1 st Mode	0.361		

4.5.2. Second Step in Calibration

As can be seen in Figure 4.27, second mode shapes are totally different for NM and AVS results. In the NM the second mode is the movement of the right hand side while it is the longitudinal movement in AVS. For this reason, in numerical model this mode should be shifted to higher modes. This can be achieved by increasing the E of the moving part. Since the movement is in the transversal direction, only the wall along with that direction will be altered. AVS results indicate that movement of the right hand side in transversal direction belongs to fourth mode. In this respect the calibration should be performed between the second mode of the NM and fourth mode of the AVS as illustrated in Table 4.4 to shift the second mode of NM to the fourth mode of AVS

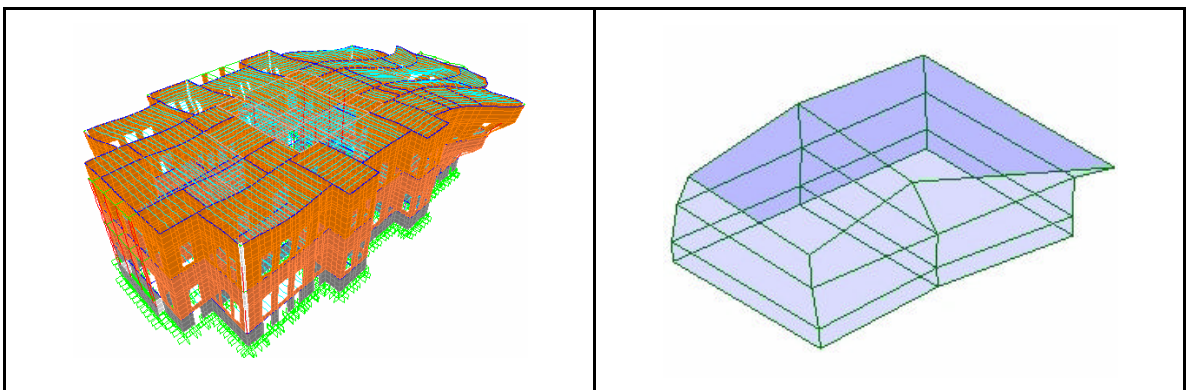


Figure 4.27. Second mode in NM and fourth mode of AVS after the first calibration.

Value of E of the wall in the transversal direction of the right hand side of the structure is increased by 2.87 and new E is calculated as $2.87 \times 2365 = 6787$ MPa. This alteration has caused to have the second mode shape of the structure as the movement of

the sea side along with longitudinal direction and the third mode as the movement of the left side along with longitudinal direction. Moreover the fourth mode is the movement of the mid part in transversal direction, fifth mode is the movement of the land side in longitudinal direction, sixth mode is the out of plane movement of the entrance wall in the left part and finally seventh mode is the movement of the right part in the transversal direction. Here it is interesting to note that these modes represent movements in the first four modes of AVS. In other words, second, third and fifth modes are forming the second mode of the AVS, the fourth mode is the third mode of AVS and finally seventh mode belongs to the fourth mode of AVS. Since no measurement has been taken from the entrance wall, it is impossible to detect the sixth mode.

Table 4.4. Calibration process to obtain E for wall in the transversal direction of right part

System	Explanation	Period (S)	Ratio	Cal. Coef.
AVS	4 th Mode	0.192	1.693	2.87
NM	2 nd Mode	0.325		

4.5.3. Third Step in Calibration

Third calibration is based on to fit the second mode of the NM to AVS (Figure 4.28). For this reason modulus of elasticity of the exterior walls, in the sea side of the palace, along with the longitudinal direction, is going to be increased as shown in Table 4.5.

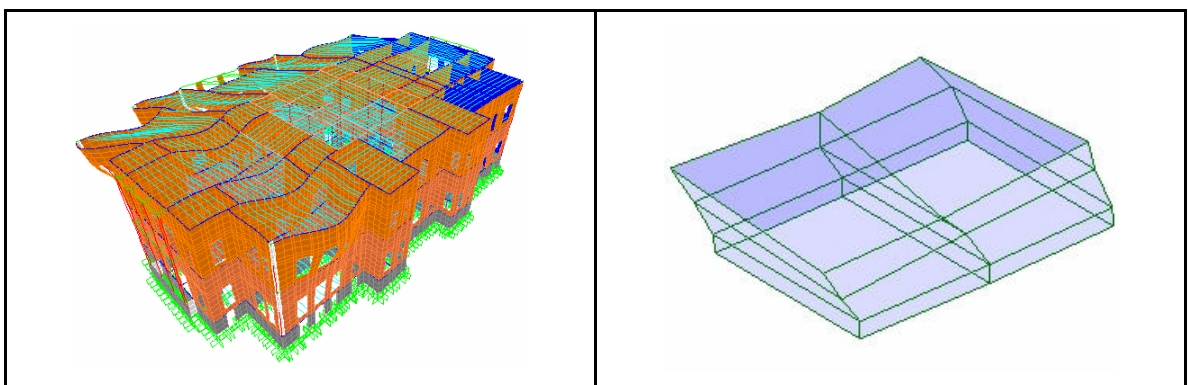


Figure 4.28. Second mode in NM and AVS after the second calibration

Table 4.5. Calibration process to obtain E for wall in the longitudinal direction in sea-side

System	Explanation	Period (S)	Ratio	Cal. Coef.
AVS	2 nd Mode	0.278	1.111	1.23
NM	2 nd Mode	0.309		

E of the wall in the longitudinal direction of the sea side of the structure is increased by 1.23 and new E is calculated as $1.23 \times 2365 = 2910$ MPA. This alteration has not changed the mode shapes.

4.5.4. Fourth Step in Calibration

The next calibration aims to change the order of the fourth and fifth mode in order to make three consecutive modes to form the second AVS mode. If this can be achieved, the third mode of AVS will appear directly. For this reason the active walls in the fourth mode of NM will have bigger modulus of elasticity. For this aim, calculated modulus of elasticity, for the third step, is going to be used. Figure 4.29 shows the active mass in the fourth mode and its respective mode in AVS.

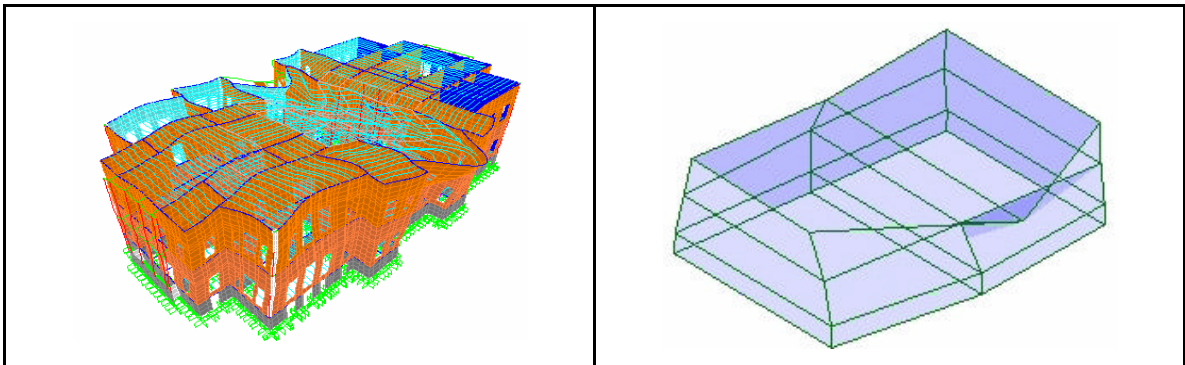


Figure 4.29. The fourth mode of NM and the third mode of AVS after the third calibration

Final alteration gave the desired order of mode shapes. According to that order, the first mode shape of NM and AVS are exactly the same, second mode of AVS was formed by second, third and fourth mode of NM, third mode of AVS is the fifth mode of NM and finally the fourth mode of AVS is formed by seventh and eighth mode of the NM. The sixth mode of the NM is the movement of the entrance in the longitudinal direction. This

movement is a local movement and can not be included in AVS since there is no measurement at that location.

4.5.5. Fifth Step in Calibration

Although rigid diaphragm action is out of question for the structure, the walls are interconnected to each other by timber elements. For this reason alteration of modulus of elasticity is effective on not only the modal period of the wall itself but also the overall structural modes. In that respect a final revision should be made to catch the appropriate periods with three different modulus of elasticity. The final values are; $E_1=2315$ MPa, $E_2=8000$ MPa and $E_3=3100$ MPa.

In the calibration process the most important challenge is that; one mode of the AVS is formed by one or few consecutive modes of the NM whose periods are close enough to each other. Further alterations are possible to catch the exact mode shape of the AVS by NM but it requires working with many modulus of elasticity which is not an engineering approach. In the study it was determined that, the first mode of the calibrated NM is exactly the same as the first mode of AVS, the second, third and fourth mode of calibrated NM are forming the second mode of AVS, the fifth mode of calibrated NM is the third mode of AVS and finally the fourth mode of AVS is the combination of sixth and seventh mode of calibrated NM.

The second important parameter is the period of the modes, seen as separate modes in CNM. For the calculation of mutual period, each mode period and mass participation ratios were accounted since mass participation ratio refers to active mass in the mode. The period was obtained by weighted average as shown below;

$$T_a = \left(\frac{T_1 * PF_1 + T_2 * PF_2 + \dots + T_n * PF_n}{PF_1 + PF_2 + \dots + PF_n} \right) \quad (4.3)$$

At the end of the final revision Calibrated Numerical Model (CNM) is obtained with three different modulus of elasticity (Figure 4.30). Dynamic parameters of the model are

summarized in Table 4.6. Calibrated model's mode shapes and respective AVS modes are summarized through Figure 4.31 – 4.34.

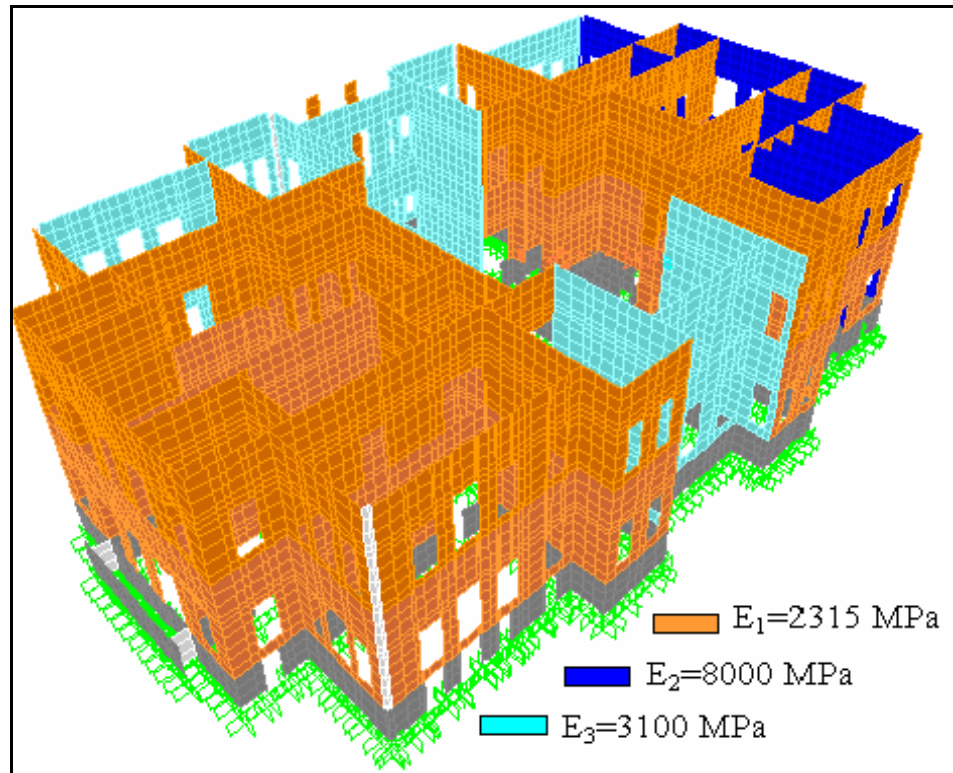


Figure 4.30. Determined modulus of elasticities

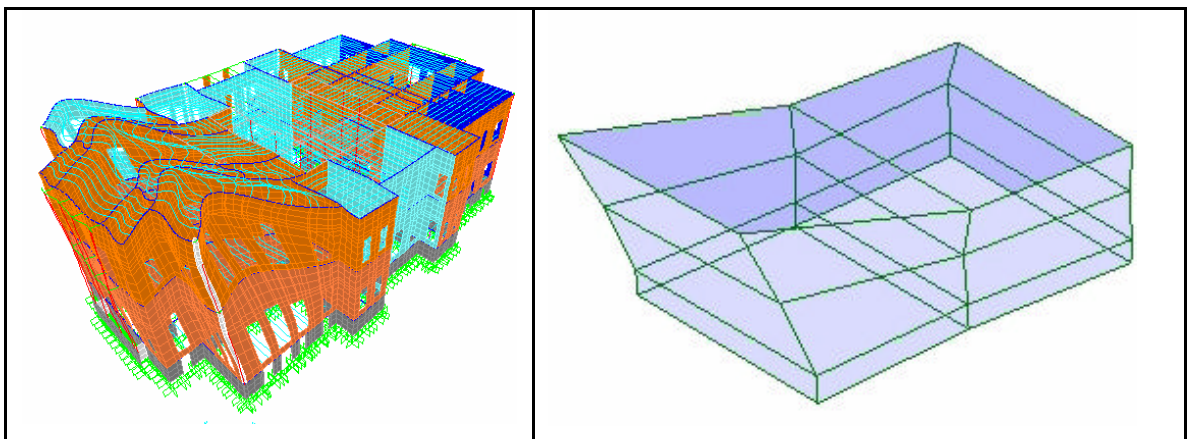


Figure 4.31. The first mode of calibrated model is exactly same as the first mode of AVS
($T=0.371 \text{ Sec}$)

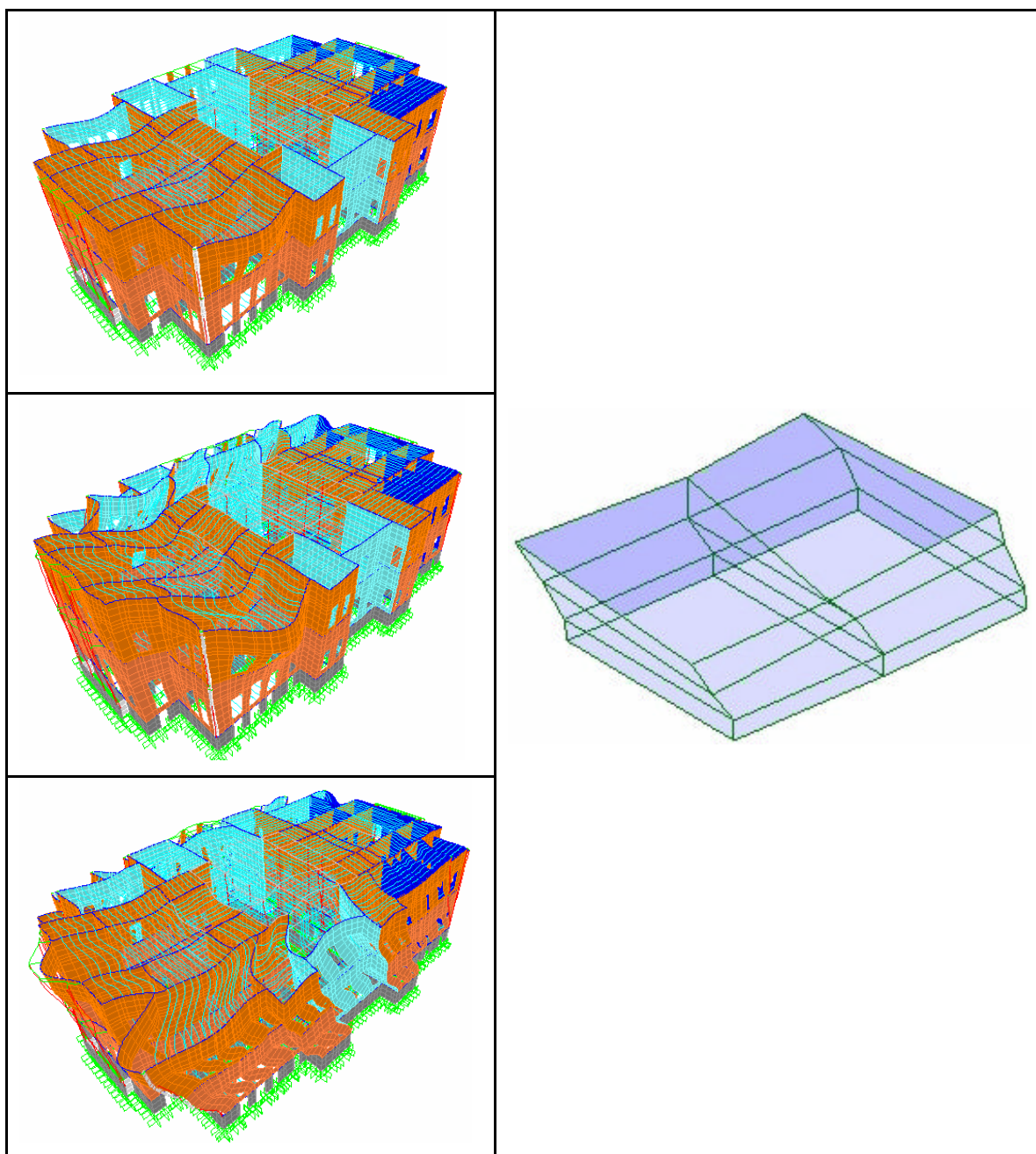


Figure 4.32. Three consecutive modes (second, third and fourth modes) of calibrated model form the second mode of AVS ($T=0.274$ Sec)

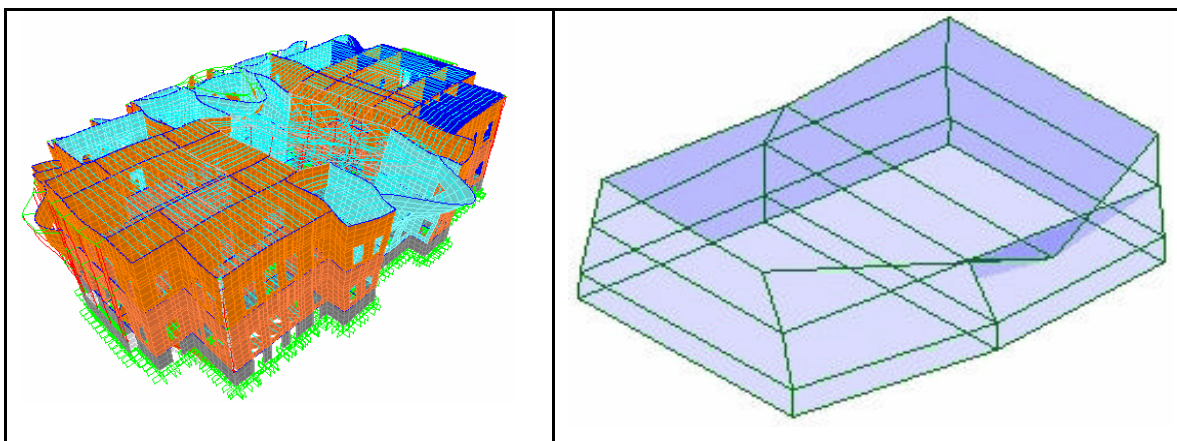


Figure 4.33. The fifth mode of the calibrated model is the same as the third mode of the AVS ($T=0.260$ Sec)

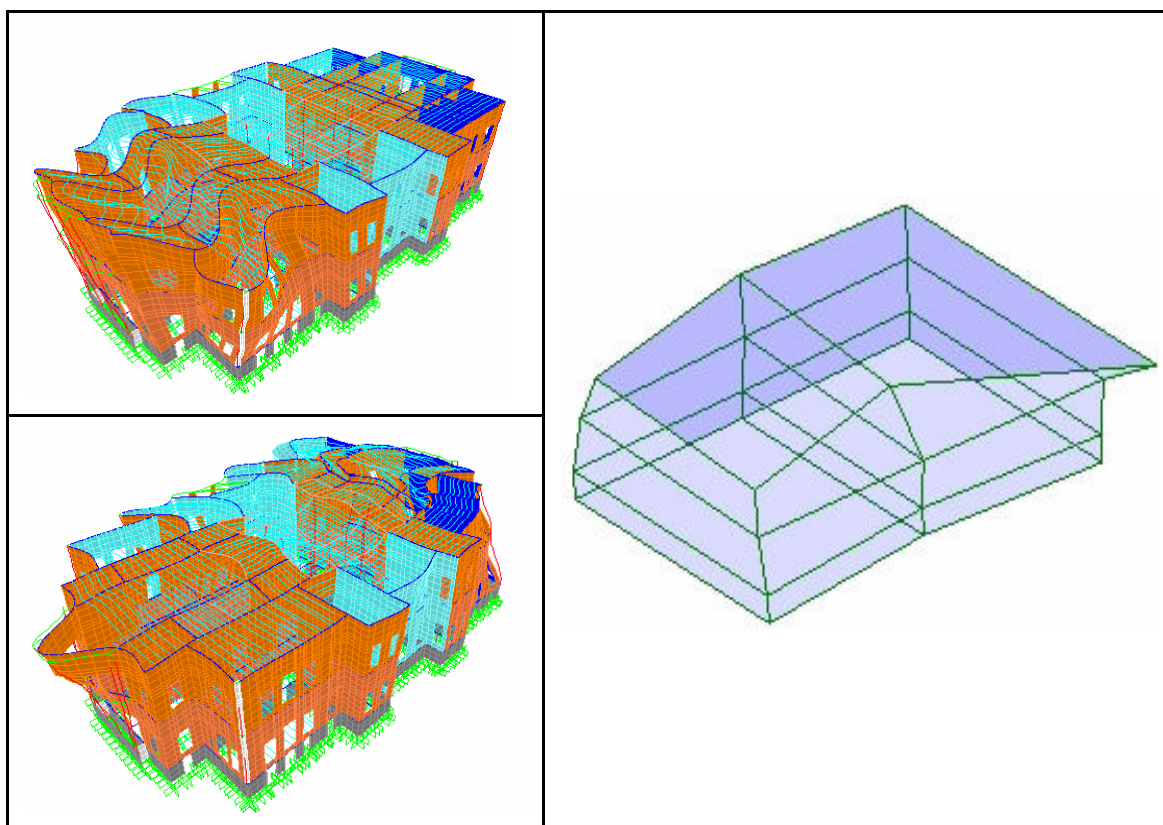


Figure 4.34. Two consecutive modes (seventh and eighth modes) of calibrated model form the fourth mode of AVS ($T=0.230$ Sec)

Table 4.6. Obtained modes at the end of the calibration process

Ambient Vibration Survey			Numerical Analysis					
Mode	Period (Second)	Definition of Mode	Mode	Period (Second)	Mass PF (%)	Combined Mode	Period (Second)	Mass PF (%)
1	0.371	Movement of the left hand side in Y direction	1	0.371	12-Y	1	0.371	12-Y
2	0.278	Movement of the structure in X direction	2	0.289	0.5-X	2	0.274	32-X
			3	0.281	12-X			
			4	0.270	19-X			
3	0.241	Movement of the mid part in Y direction	5	0.260	8-Y	3	0.260	8-Y
			6	0.253	3-X			
4	0.192	Movement of the left and right part in Y direction	7	0.231	1-Y	4	0.230	13-Y
			8	0.230	12-Y			

4.6. Interpretation of the Results

The calibration process showed that, one mode of AVS is seen as separate one or more mode of numerical analysis. This is related to sensitivity of the Ambient Vibration Survey and numerical analysis. Through calibration process the first four modes of the AVS were obtained. The sixth mode of the NM could not be defined as a part of AVS. The reason is the lack of the local measurements in the active part.

The general dynamic properties, such as lack of rigid floors, distributed mass through the height, local modes and small mass participation ratios for single modes, for the calibrated model were the same as those of rough model. At least 60 modes were required to have 90% mass participation in longitudinal and transversal direction.

Calibration process has showed that the walls in the left hand side of the structure (Mabeyn part) have smaller modulus of elasticity those of in the right hand side (Harem part). It is well known that iron reinforcements were used within the masonry walls and different use of iron reinforcement may be the first reason.

Secondly the difference may stem from the existing damage in the structure. During the calibration process the observed cracks were accounted and the moduli of elasticity of the walls which have serious cracks were not increased. Moreover no restoration works were carried-out in the Mabeyn part on which walls have smaller modulus of elasticity.

Furthermore there are three rooms whose interior sides are covered by wood in the Mabeyn part. These rooms are the active part in the first mode of the AVS and calibrated NM thereby the walls have smaller modulus of elasticity. Because of the timber covering, the existing condition of the masonry could not be investigated. Deterioration or cracks may be the main reason for weaker material.

Finally it is concluded that the numerical model was corrected by ambient vibration survey to be used for further assessment techniques. Although the calibration process was illustrated in SAP2000, the same results were obtained in LUSAS model. Hereafter all analysis would be performed over the calibrated model in order to determine the earthquake performance of the structure. For a correct assessment the next step is the determination of the earthquake parameters for the structure.

5. SEISMIC HAZARD AND EARTHQUAKE RISK OF THE MARMARA REGION

In order to have an appropriate safety assessment for a structure not only a well-prepared computer model but also the nature of the risk is required. In this respect special care should be spent to determine the seismic risk of the structure.

There are generally two well-known philosophies for the quantification of earthquake hazard. One of them is the probabilistic seismic hazard analysis, which accounts for all possible earthquake scenarios that could affect the site and results in hazard represented by ground motions parameters at reference ground conditions, such as peak ground acceleration and spectral accelerations. The other one is the deterministic earthquake hazard assessment. Probabilistic hazard assessment is generally conducted prior to the deterministic one since, for the deterministic assessment the composite probabilistic hazard is de-aggregated to find the earthquake scenarios (magnitude, distance and the factored standard deviation) at a particular site that would contribute most to the particular hazard. This scenario constitutes the basis of the deterministic hazard assessment approach, which also provides the ground motion parameters or simulated strong ground motion time histories [1].

5.1. Earthquake Ground Shaking Hazard Levels

The most common and significant cause of earthquake damage to building is ground shaking. Thus, the effects of ground shaking form the basis for most building code requirements for seismic design. Three levels of earthquake hazard are used to define ground shaking in Applied Technology Council document (ATC-40). These are serviceability earthquake, Design Earthquake (DE) and Maximum Earthquake (ME) [9]. Federal Emergency Management Agency (Fema-356) defines two level of ground shaking as Basic Safety Earthquake-1 (BSE-1) and Basic Safety Earthquake-2 (BSE-2). BSE-1 has the same meaning as DE and BSE-2 is named as Maximum Considered Earthquake (MCE) [8].

5.1.1. Serviceability Earthquake

The serviceability earthquake (SE) is defined as probabilistically as the level of ground shaking that has a 50 percent chance of being exceeded in a 50-year period. This earthquake is about 0.5 times of the level of ground shaking of the design earthquake. The SE represents a frequent level of ground shaking that is likely to be felt during the life of the building. The SE has a mean return period of approximately 75 years [9].

5.1.2. Site Specific Design Earthquake

The design earthquake (DE) is defined as probabilistically as the level of ground shaking that has a 10 percent chance of being exceeded in a 50-year period. The DE represents an infrequent level of ground shaking that can occur during the life of building. The DE has a mean return period of approximately 500 years [7]. The DE earthquake has the same definition as the level of ground shaking currently used as basis for the seismic design of new buildings by the Uniform Building Code, (UBC) and the Turkish Earthquake Code (TEC). The DE is one of the two levels earthquake ground shaking hazards that must be used for Basic Safety Objective (BSO) [8].

5.1.3. Maximum Earthquake

The maximum earthquake (ME) is defined deterministically as the maximum level of earthquake ground shaking which may ever be expected at the building site within the known geological framework. This level of ground shaking is typically about 1.25 to 1.5 times of the level of ground shaking of the DE [7]. In probabilistic terms the ME has a mean return period of about 1000 years and it has a 5 percent chance of being exceeded in a 50-years period [9].

5.1.4. Maximum Considered Earthquake

The Maximum earthquake (MCE) is defined as probabilistically as the level of ground shaking that has a 2 percent chance of being exceeded in a 50-year period. The MCE has a mean return period of approximately 2500 years [8].

Considering the uncertainties associated with earthquake occurrences it is more prudent to use probabilistic characterization of earthquake ground motion than to use scenario based deterministic characterizations. Current adoption of the performance based earthquake resistant design requires the definition of ground motion (seismic demand) associated with different average return periods for each performance objective [1].

5.2. Seismic Risk of the Marmara Region

For more than two millennia the Marmara region has been the crossroads between east and west. Being a continuously populated region and having as its center Istanbul, the capital of both Byzantine and Ottoman empires, the historical seismicity record is continuous and relatively complete. Earthquake records spanning two millennia indicate that, on average, at least one medium intensity ($I_0 = \text{VII–VIII}$) earthquake has affected Istanbul in every 50 years. The average return period for high intensity ($I_0 = \text{VIII–IX}$) events has been 300 years [1].

Western portion of the North Anatolian Fault zone controls the tectonic regime in the Marmara region. Toward the Marmara Sea region the North Anatolian Fault begins to lose its single fault line character and splays into a complex fault system. Based on recent findings a fault segmentation model for the Marmara Sea region is developed by Erdik et al (Figure 5.1). This model is based on the tectonic model of the Marmara Sea, defining the Main Marmara fault, a thoroughgoing dextral strike-slip fault system, as the most significant tectonic element in the region [1].

When the earthquakes history of the Marmara region is examined, it is seen that; there exist some potential seismic gaps. The rupture associated with the Kocaeli earthquake leaves the only remaining gap across the Marmara Sea, to the south of Istanbul. This gap is well defined implies increased probabilities for a strong earthquake (Figure 5.1) [1].

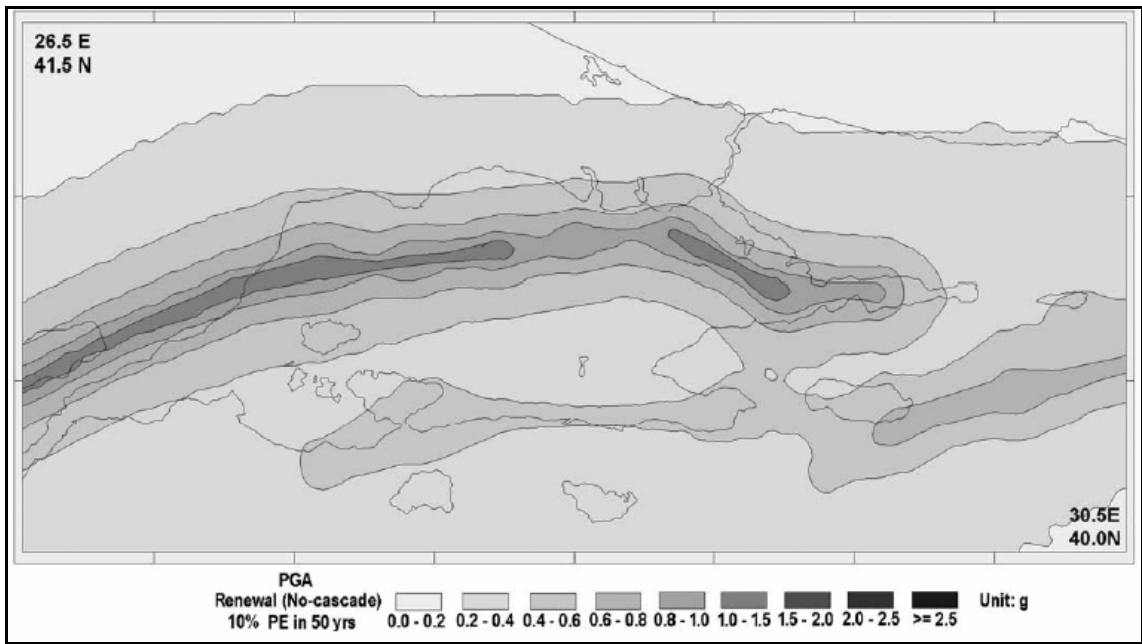


Figure 5.2. PGA contour map for 10% probability of exceedence in 50 years [1]

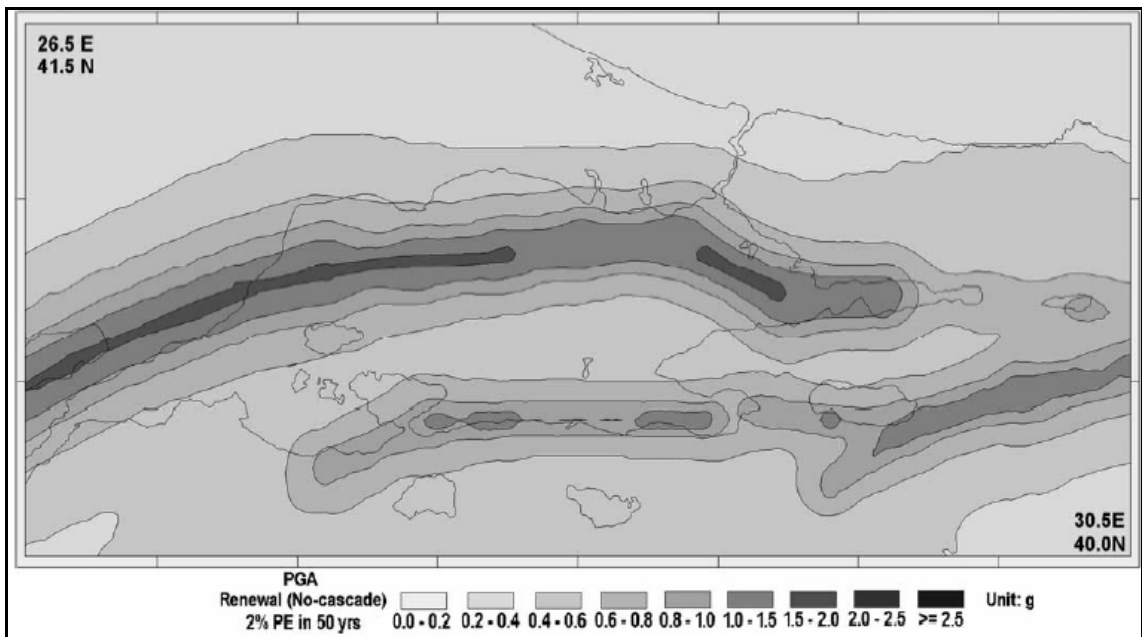


Figure 5.3. PGA contour map for 2% probability of exceedence in 50 years [1]

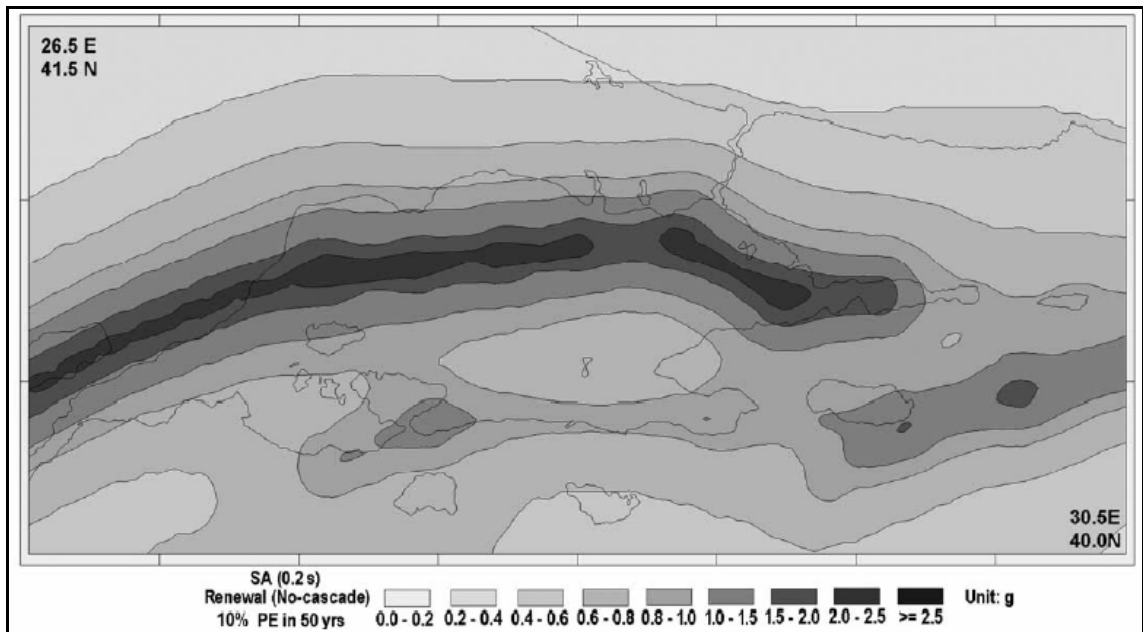


Figure 5.4. Sa ($T = 0.2$ s) contour map for 10% probability of exceedence in 50 years [1]

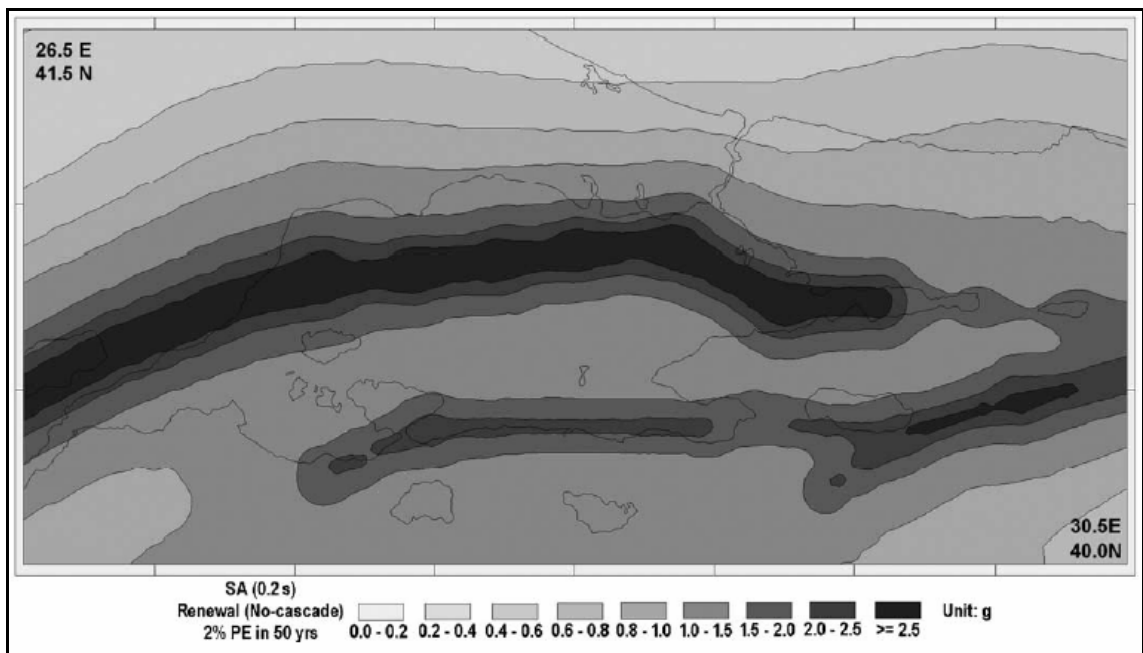


Figure 5.5. Sa ($T = 0.2$ s) contour map for 2% probability of exceedence in 50 years [1]

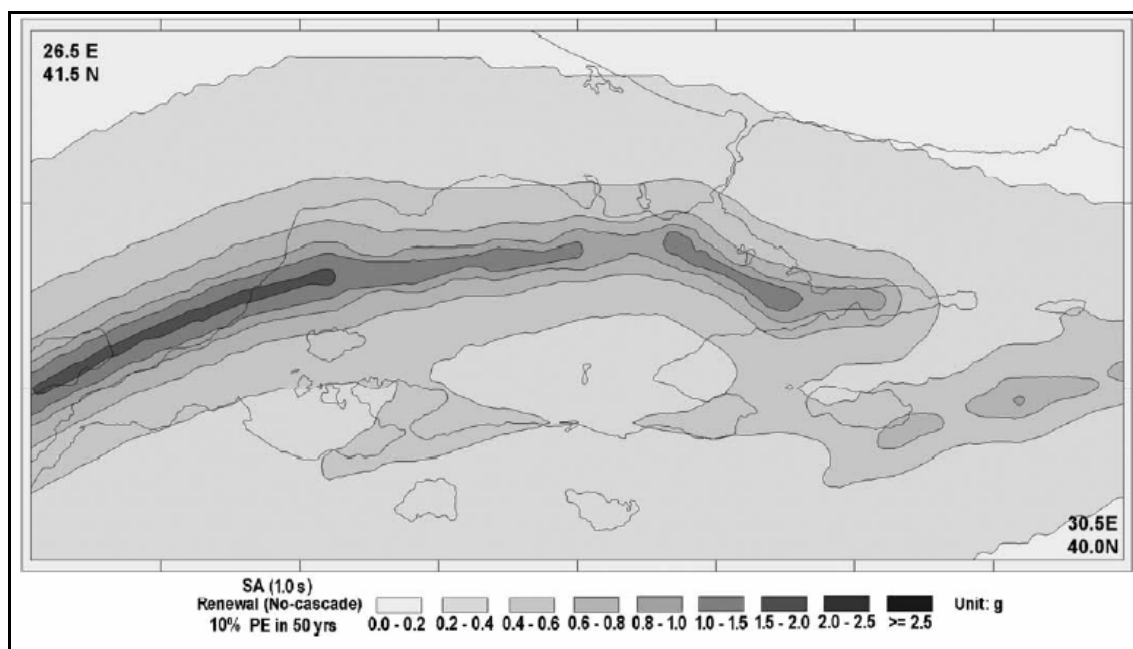


Figure 5.6. Sa ($T = 1.0$ s) contour map for 10% probability of exceedence in 50 years [1]

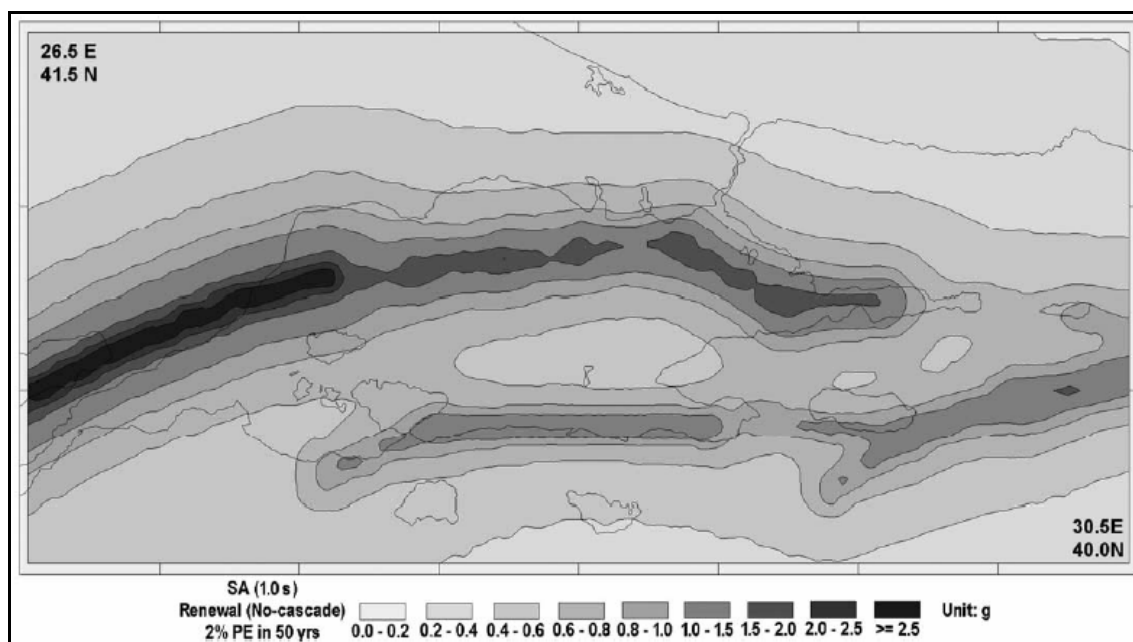


Figure 5.7. Sa ($T = 1.0$ s) contour map for 2% probability of exceedence in 50 years [1].

5.4. Geological and Geotechnical Properties of the Site on which Beylerbeyi Palace is Located

Detailed soil investigation has been performed by Regional Directorate of National Palaces. In order to determine the geological and geotechnical properties of the site on which the palace complex is located, fourteen mechanical drilling and laboratory testing process were performed. Seismicity of the site is investigated by performing Vertical Electricity Drilling on eight different points. Moreover through seven different lines Seismic Refracting Analyses were performed [6].

Figure 5.8 shows the locations of the mechanical drillings and seismic refraction analysis performed for the site of the main building of the palace complex [6].

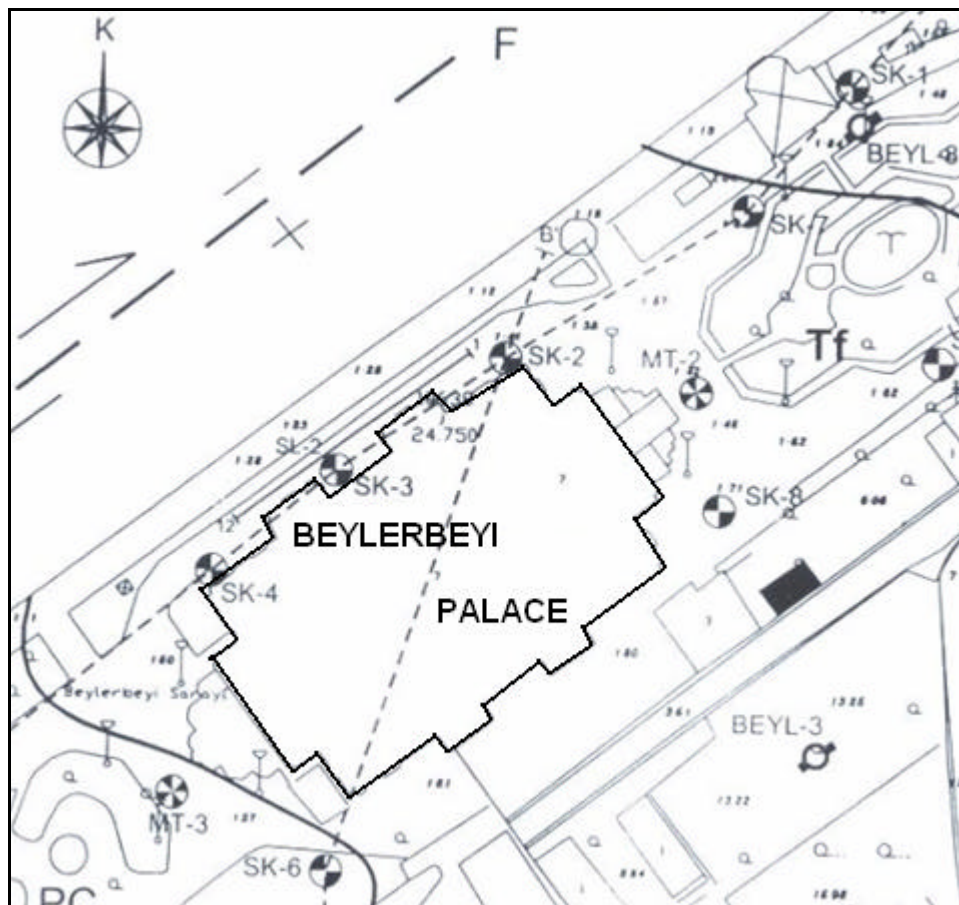


Figure 5.8. Code of the Drillings and lines of Seismic Refraction Analysis [6]

At the end of the specified analysis three soil layers are identified under the main structure. Thickness of each layer, P wave and S wave velocities and classification of the layers according to NEHRP, 1997 are summarized in Table 5.2 [6].

Table 5.1. Identified soil layers under the main palace [6]

Layer	Thickness (m)	V _P (m/s)	V _S (m/s)	NEHRP, 1997
1	4	659	528	C
2	15	2616	920	B
3	30	7320	3064	A

Because of the basement floor of the palace, it is thought that, the weak soil profile is removed and the palace is constructed on the second layer which can be classified as B type according to NEHRP classification.

The bearing capacity of the site is determined as 3-4 kg/cm², and the site is categorized as Z2 type soil according to Turkish Earthquake Code [5]. For this type soil spectrum Characteristic Periods are given as T_A=0.15 second and T_B=0.40 second [7]. With this information response spectrum can be constructed according to seismicity and soil characteristics of the Beylerbeyi region.

5.5. Concluding Remarks

Since the site class of the structure is the same as that used in the study to determine the hazard maps, ground shaking characteristics can be used in the assessment of the structure. Ground shaking parameters, namely, Peak Ground Acceleration (PGA) and Spectral Accelerations (S_a) at natural periods of 0.2 and 1 s can be obtained according to geographic coordinates of Beylerbeyi Palace, 41° 02' 33" N, 29° 02' 33" E.

For the performance assessment of the structure, probabilistic seismic hazard assessment approach is going to be used since they totally fulfill the need of a serious performance assessment due to importance of the structure and potential seismic risk. Ground motion parameters have 10% probability of exceedence in 50 years is called as Design Earthquake (DE) and ground shaking parameters have 2% probability of

exceedence in 50 years is called as Maximum Considered Earthquake (MCE) [8-9]. The ground shaking parameters are summarized in Table 5.2. Parameters were determined according to geometrical coordinates of Beylerbeyi Palace (private communication with Prof. M. Erdik of Kandilli Observatory and Earthquake Research Institute).

Table 5.2. Ground shaking parameters for DE and MCE

Ground Shaking Parameters	Probabilistic Seismic Hazard Assessment	
	10 % probability of exceedence in 50 years	2 % probability of exceedence in 50 years
PGA	0.353 g	0.499 g
$S_a(0.2 \text{ s})$	0.773 g	1.143 g
$S_a(1 \text{ s})$	0.371 g	0.567 g

Obtained earthquake parameters enable to construct the response spectrum for Design Earthquake (DE) and Maximum Considered Earthquake (MCE). Thereby the performance of the palace can be assessed with respect to two different earthquake ground shaking. The response spectrum is going to be constructed according to NEHRP procedure and it depends on the spectral acceleration values at 0.2 s and 1 s periods.

6. ANALYSIS UNDER STATIC AND DYNAMIC LOADS

6.1. Analysis of the Structure under Static Loads,

Before evaluating the stress values, developed under seismic loads, it is appropriate to search about those of under vertical loads. Dead loads, induced by the self weight of the structural elements and live load values were applied to the structure. The analyses have showed that; the stresses along with vertical and horizontal direction are quite low to conclude that the palace is safe under vertical loads. Even if the dead loads are increased by 1.4 and live loads are increased by 1.6, the safety is guaranteed. Figure 6.1 shows the horizontal stress, S11 variation in the structure while Figure 6.2 shows the vertical stresses, S22 variation. Through the structure the maximum compression stress is at around 0.5 MPa while the maximum tension stress is about 0.3 MPa. Thereby it was concluded that the structure is safe under vertical loads.

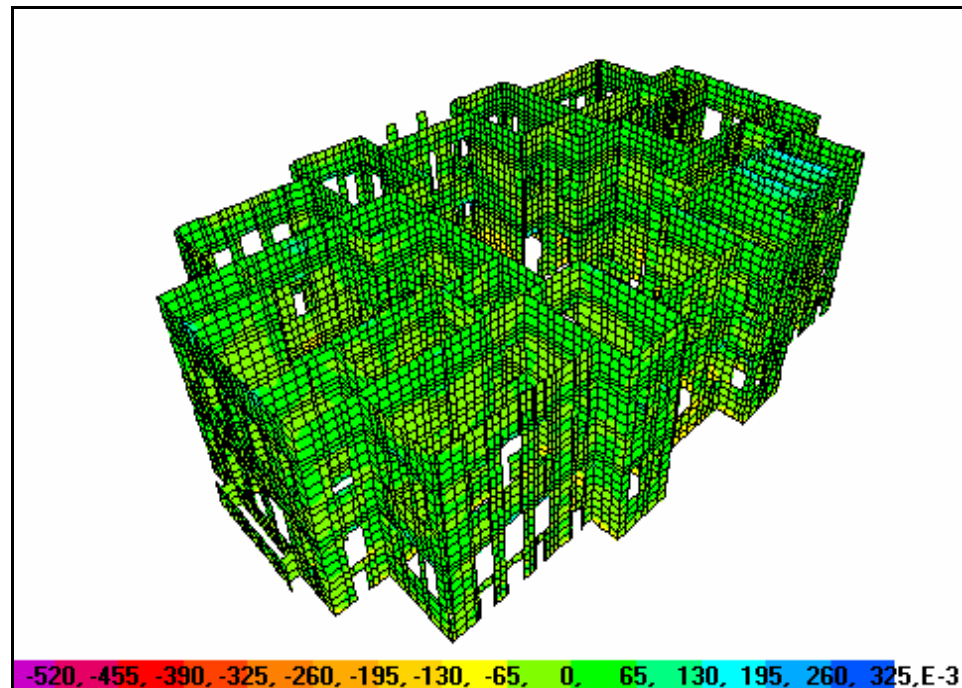


Figure 6.1. S11 stresses under vertical loads

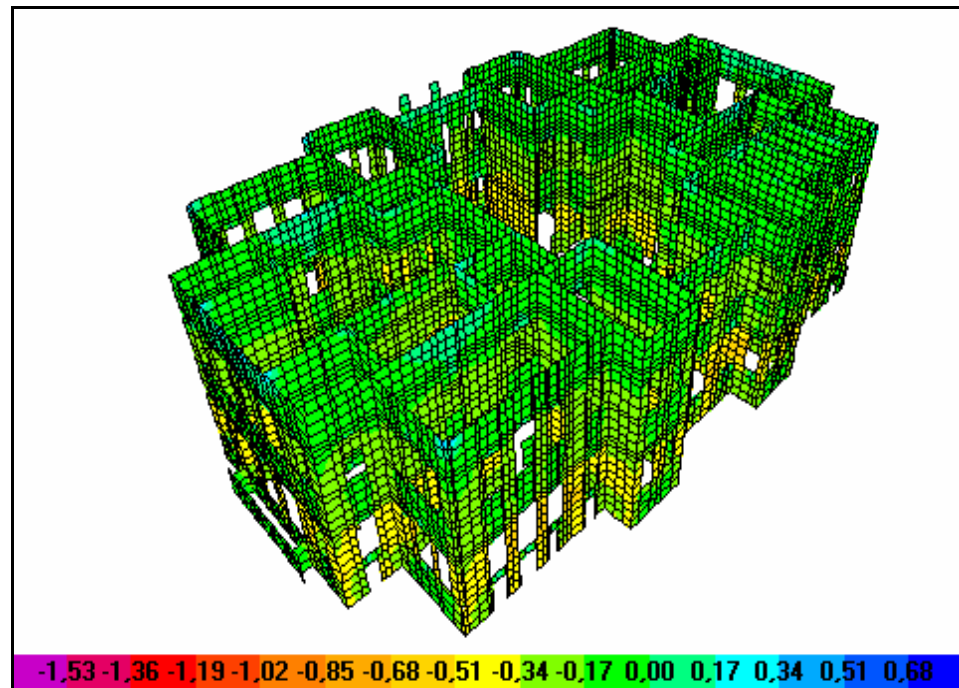


Figure 6.2. S22 stresses under vertical loads

6.2. Analyses of the Structure under Dynamic Loads,

The earthquake safety of Beylerbeyi Palace was assessed by Response Spectrum Analysis (RSA). The method involves the calculation of only the maximum values of the displacements and member forces in each mode using smooth design spectrum that usually the average of several earthquake motions [31-32].

The earthquake ground acceleration in each direction is given as a digitized response spectrum curve of pseudo-spectral acceleration response versus period of the structure. RSA is performed using mode superposition method. Modes may have been computed using eigen vector analysis or Ritz vector analysis. Ritz vectors are recommended since they give more accurate results for the same number of modes [28].

In this study three different RSA will be performed. The first analysis is based on Turkish Earthquake Code. The code gives the response spectrum according to earthquake zone of the structure and soil type of the region on which the structure sits (Figure 6.3) [7]. The required parameters had been given in chapter 5 for Beylerbeyi Palace.

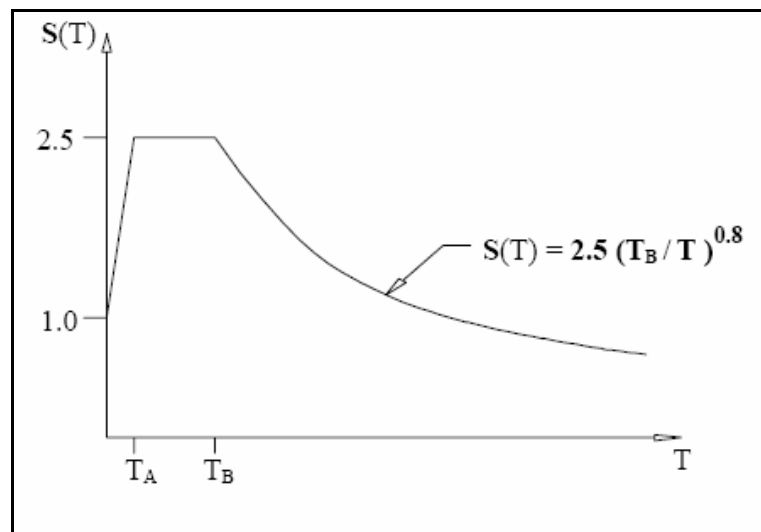


Figure 6.3. Turkish Earthquake Code based response spectrum [7]

The second and third RSA will be performed according to Design Earthquake (DE) and Maximum Considered Earthquake (MCE) [8]. NEHRP based response spectrum would be used [33]. The required values were obtained from site specific hazard assessment, explained in the third chapter and they are the spectral acceleration values at 0.2 s and 1 s periods. The study has accounted the regional seismicity and geology, the expected recurrence rates and maximum magnitudes of events on known faults and source zones, the location of the site with respect to these, near source effects if any, and the characteristics of subsurface site conditions. The construction of the response spectrum is summarized in Figure 6.4 [33].

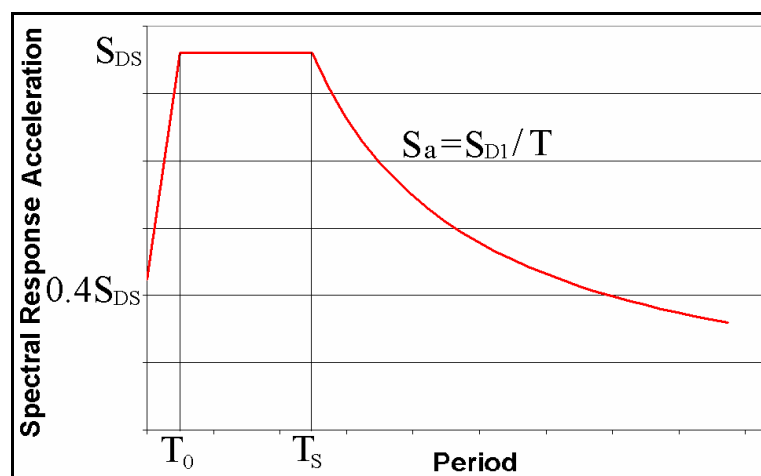


Figure 6.4. Construction of the response spectrum (33)

As can be understood, two important parameters to construct the response spectrum are S_{D1} and S_{DS} . These parameters are available for probabilistic approaches to quantify the hazard in Beylerbeyi region. T_0 and T_s periods can be obtained by the formulas below [33];

$$T_0 = 0.2 \frac{S_{D1}}{S_{DS}} \quad (6.1)$$

$$T_s = \frac{S_{D1}}{S_{DS}} \quad (6.2)$$

where S_{DS} is the design spectral response acceleration at 0.2 second period, S_{D1} is the design spectral response acceleration at 1 second period and T is the fundamental period of the structure (Second)

On the other hand, new developments in application of response spectra concept are witnessed. Classical and well-known seismic response is considered in production of spectral diagrams is based on a linear motion of the earth and pendulum moving with. But the earth and the structural blocks represented by a pendulum move planarly at various direction on the soil surface in very short laps of time. An investigation of the response spectrum based on the concept of planar motion was accomplished by a group of Turkish specialist. The problem was respected likely being under consideration of international institutions, including ATC [34, 35, and 36]. It yields from these efforts that the rules of response spectra could be modified in the future but linear response spectra are still valid practically.

RSA would be performed for both transversal and longitudinal directions of the structure with two opposite directions. In order to include at least 90% of the mass 60 dynamic modes were accounted. The outputs of the modal effects were combined by CQC, Complete Quadratic Combination method [32].

In this study the safety of the masonry walls, which are the main structural elements were concerned. The vertical and horizontal stress values were compared to the strength of

the masonry walls, identified from the laboratory tests as 10 MPa under compression and 0.85 MPa under tension. For the non-structural elements including the exterior façade, stairs, timber slabs and roof system no performance evaluation was performed (e.g. see Figures 2.9 - 2.12 for structural elements). Moreover due to the lack of required connection details and strength parameters exterior and interior columns have been excluded from the safety assessment. After performing the analyses the following results were obtained;

6.2.1. RSA according to Turkish Earthquake Code

The site of Beylerbeyi Palace was categorized as Z2 type soil according to Turkish Earthquake Code and soil spectrum characteristic periods were given as $T_A=0.15$ second and $T_B=0.40$ second in the third chapter. With this information response spectrum can be constructed according to seismicity and soil characteristics of the Beylerbeyi region. Effective ground acceleration coefficient is given as 0.4. The constructed response spectrum is shown in Figure 6.5 [7].

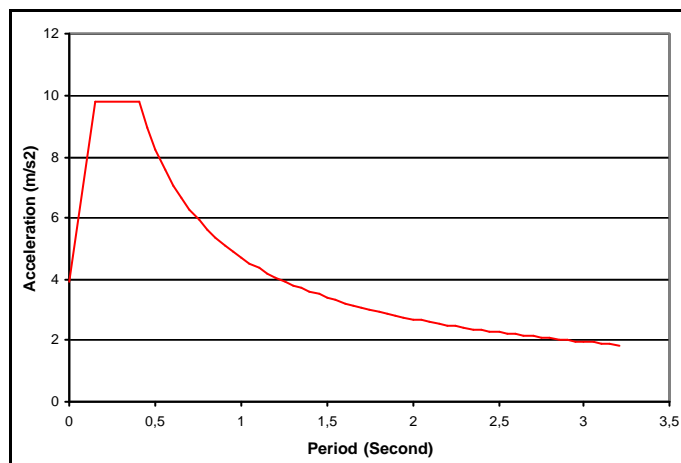


Figure 6.5. Response spectrum of Turkish Earthquake Code [7]

Combined effect of the vertical loads and earthquake load was examined. In that respect the RSA was performed over the calibrated numerical model. Figure 6.6 and 6.7 illustrates the stress along with horizontal and vertical direction for the application of RSA in longitudinal direction. On the other hand Figure 6.8 is the shear stresses. Since the tensile strength is more critical than the compressive strength of the masonry, the maximum stress face was illustrated in the figures.

With respect to S11 stresses, the structure is obviously under risk, since the stresses reach to 5 MPa. The high stress concentration regions are clearly seen in Figure 6.6. These regions occupy the upward portion of the structure which is important for the global safety. S22 stresses are beyond 4 MPa. In a few corner opening and wall, stress concentrations have been identified. Shear stresses, S12 have similar variation to that of S22 (Figures 6.7 and 6.8). As a conclusion it can be said that the most critical stresses are the horizontal stresses. Mainly the walls in the transversal direction are affected from the ground motion along with longitudinal direction.

Figure 6.9, 6.10 and 6.11 shows the S11, S22 and S12 stresses for the combined effect of the vertical loads and RSA along with the transversal direction. The same interpretations are valid for the application of RSA along with transversal direction as those of longitudinal directions. Again the critical stress direction was identified as horizontal direction. In order to have a clear illustration S22 and S12 stresses were plotted to the two dimensional illustration belongs to external sea side of the structure.

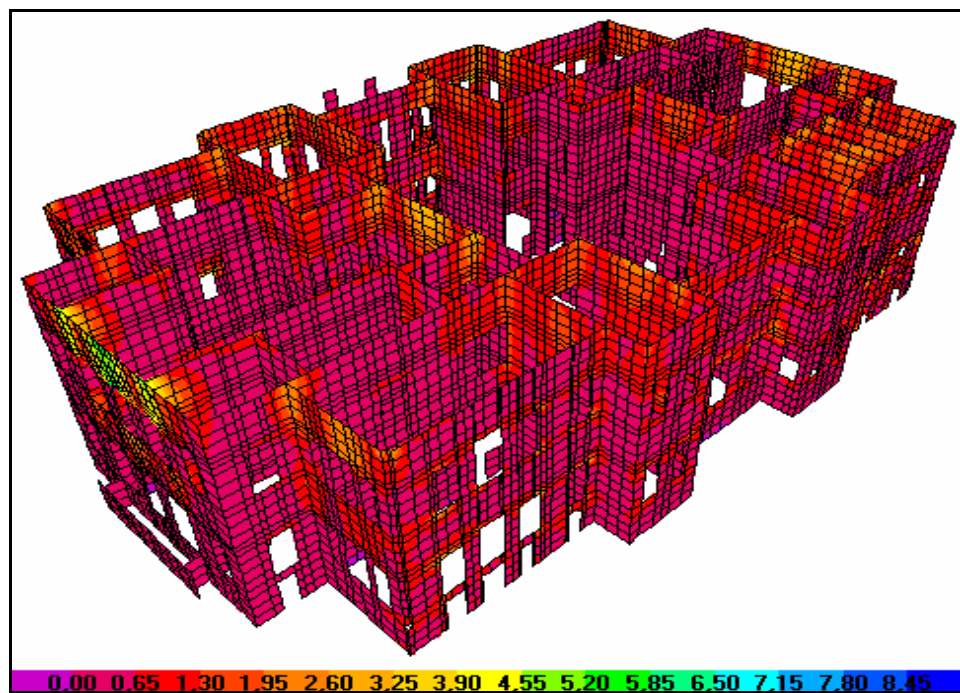


Figure 6.6. S11 stresses under RSA according to TEC, in longitudinal direction

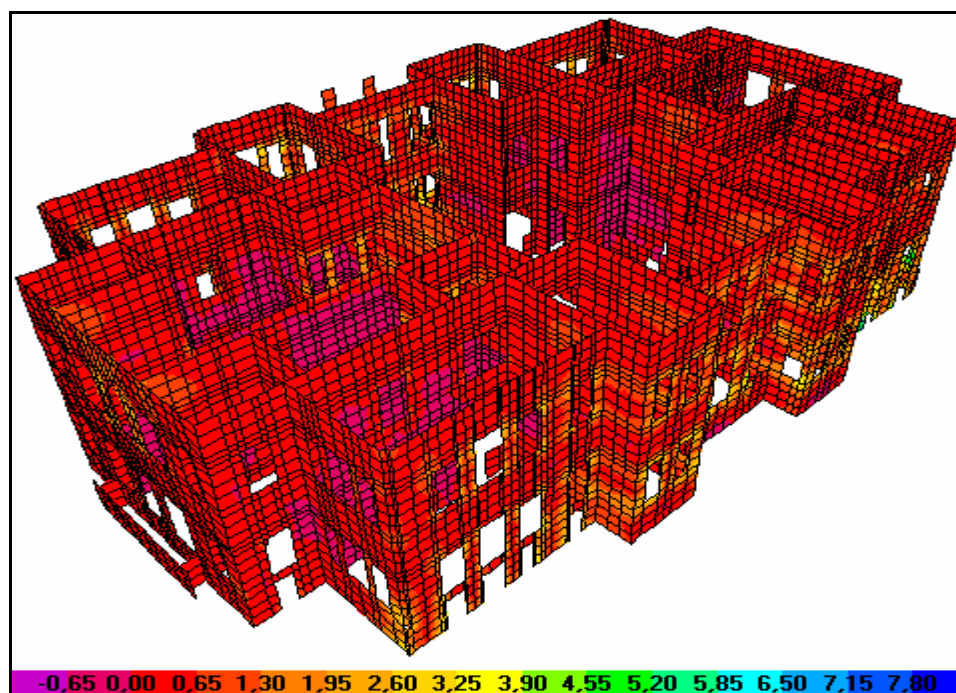


Figure 6.7. S22 stresses under RSA according to TEC, in longitudinal direction

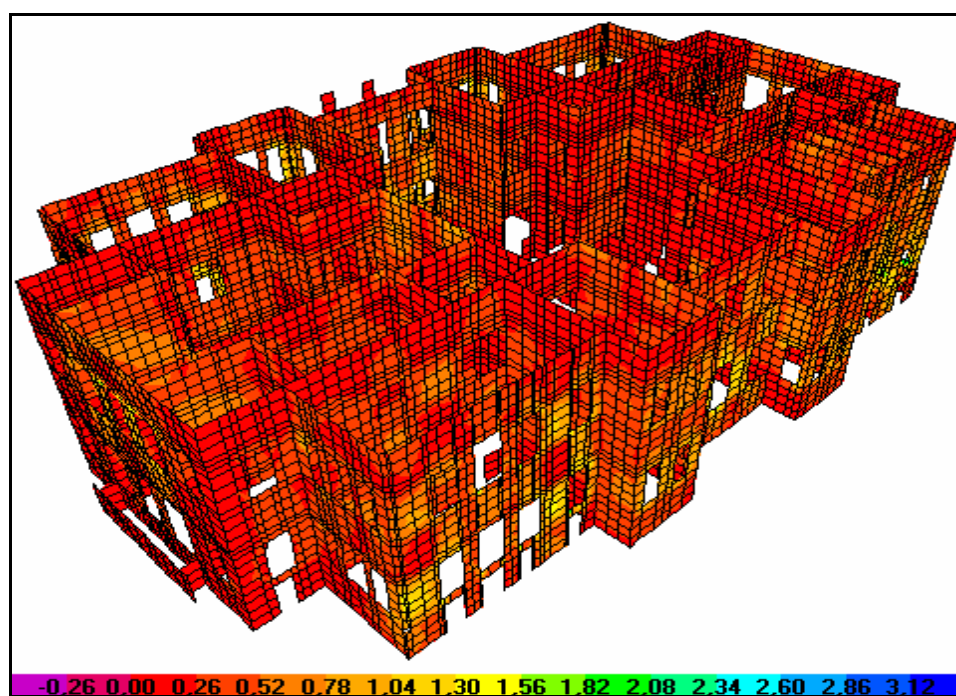


Figure 6.8. S12 stresses under RSA according to TEC, in longitudinal direction

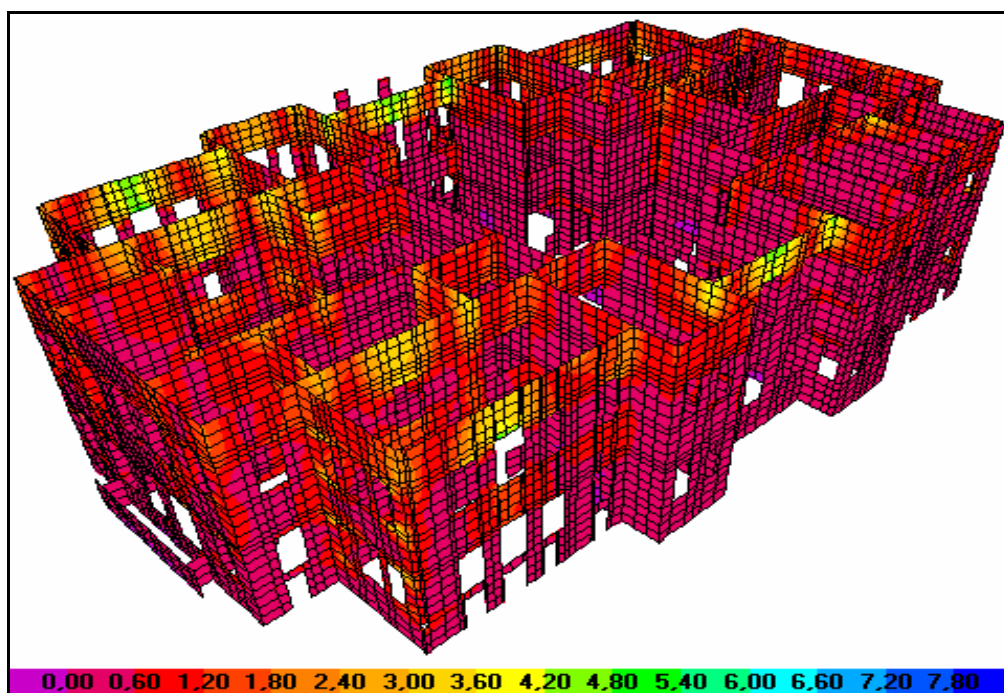


Figure 6.9. S11 stresses under RSA according to TEC, in transversal direction

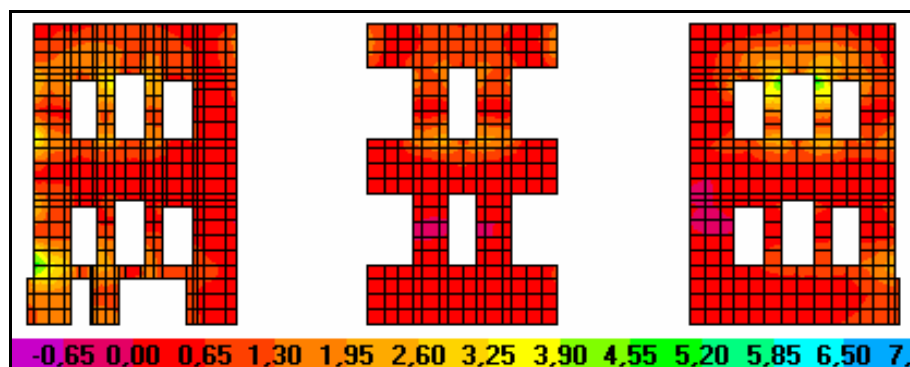


Figure 6.10. S22 stresses under RSA according to TEC, in transversal direction

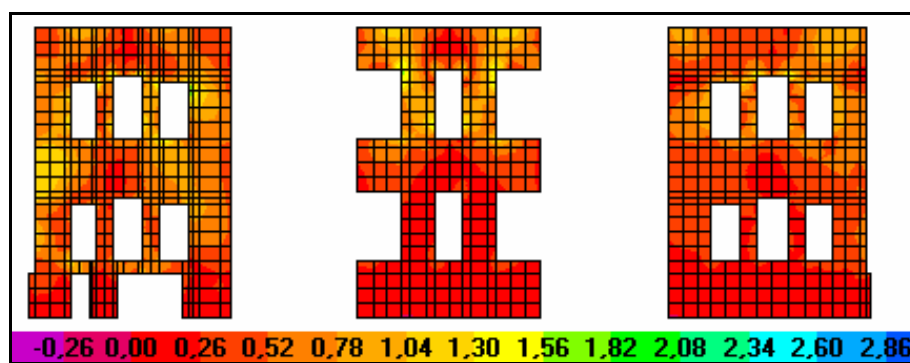


Figure 6.11. S12 stresses under RSA according to TEC, in transversal direction

6.2.2. RSA, according to Design Earthquake (DE)

The earthquake, has 10% chance of exceedance in 50 years is defined as the design earthquake [8-9]. The response spectrum is illustrated in Figure 6.12. In the construction S_{D1} and S_{DS} values were obtained as 0.371g and 0.773g respectively [1].

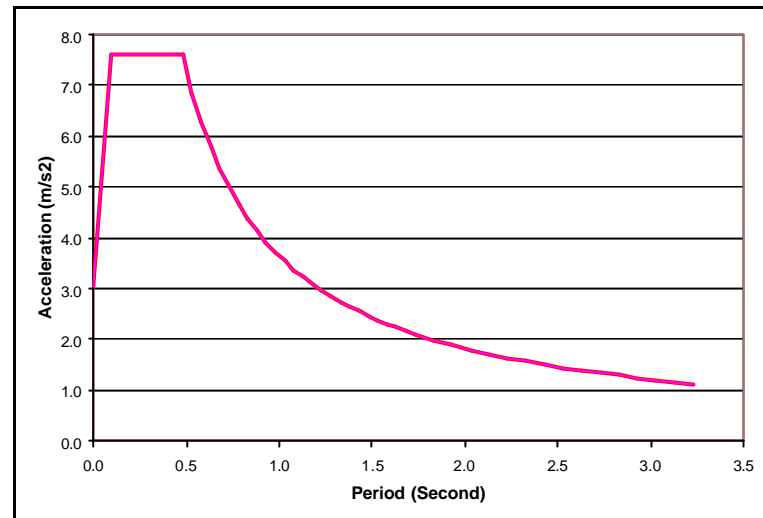


Figure 6.12. Response Spectrum obtained for Design Earthquake

Figures 6.13 and 6.14 shows the S11 stresses for the vertical loads and RSA performed along longitudinal and transversal directions respectively. Since S11 stresses are more critical than S22 and S12 stresses, interpretation of the results will be based on S11 stresses. The lack of rigid floors and out of plane modes has caused the high stress concentration on the roof level. Application of ground shaking caused stress concentration on the walls whose direction is perpendicular to the application direction of the ground shaking.

The value of the maximum stress is unacceptable for design earthquake. Maximum stress value has been determined as 4.0 MPa. When it is compared to tensile strength of the masonry, which had been determined as 0.85 MPa, obviously the structure is under risk.

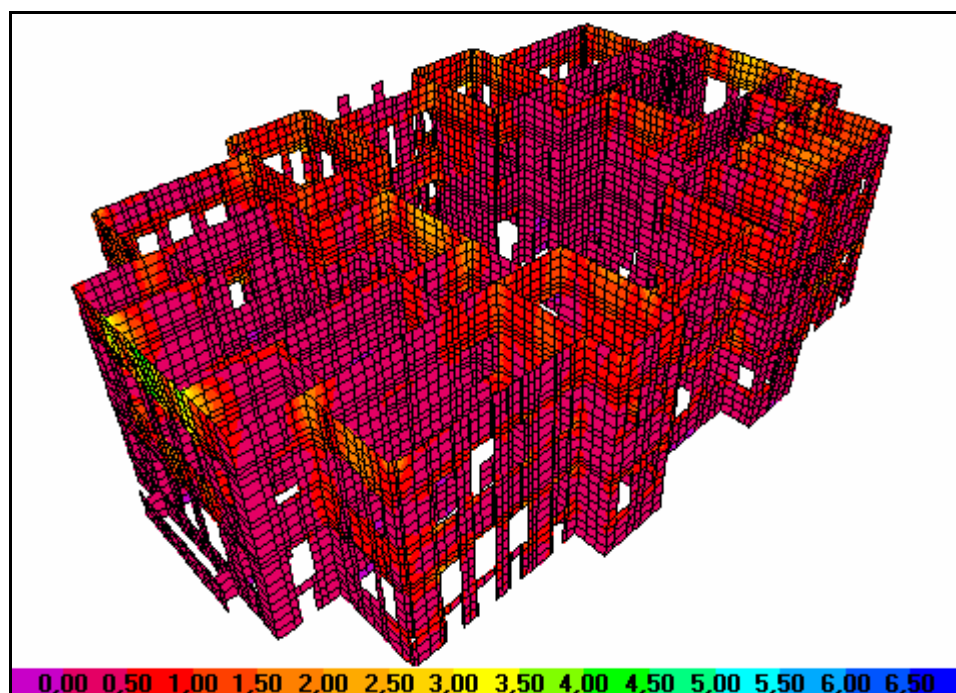


Figure 6.13. S11 stresses under RSA of DE in longitudinal direction

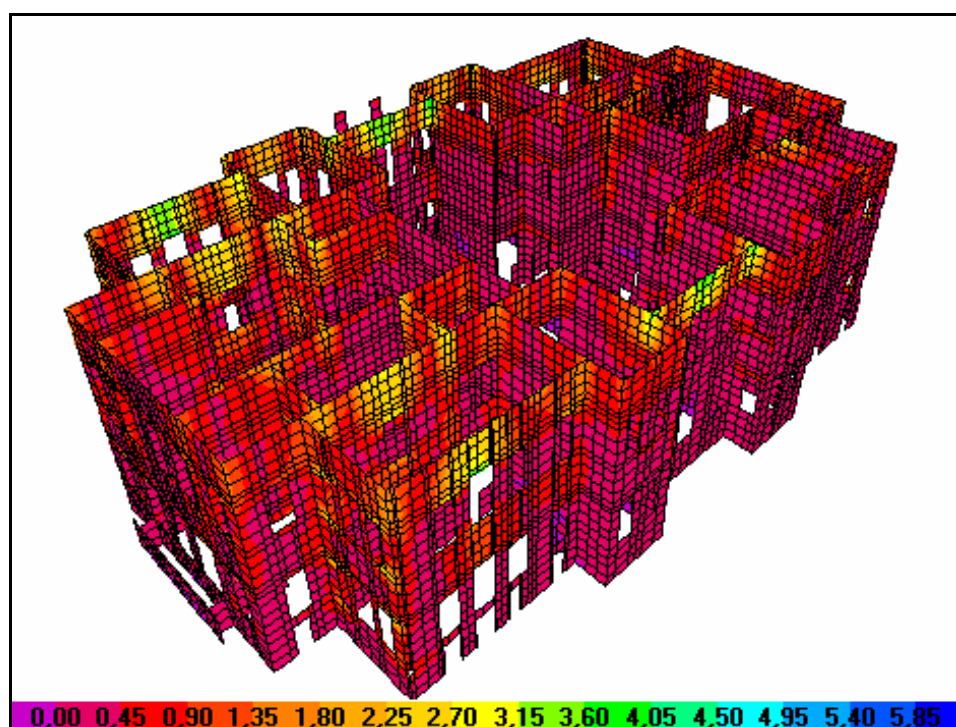


Figure 6.14. S11 stresses under RSA of DE in transversal direction

6.2.3. RSA according to Maximum Considered Earthquake (MCE)

The earthquake, has 2% probability of exceedance in 50 years is referred as the maximum considered earthquake [8]. The response spectrum is illustrated in Figure 6.15. In the construction, S_{D1} and S_{DS} values were used as 0.567g and 1.143g respectively [1].

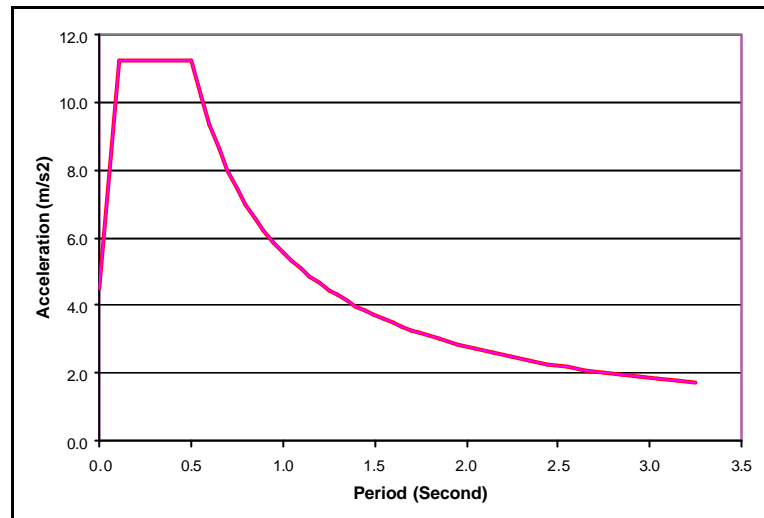


Figure 6.15. Response Spectrum obtained for Maximum Considered Earthquake
MCE

Having a return period of 2500 years, Maximum Considered Earthquake has caused high levels of stresses on the structure. Maximum stress value has reached to 6.5 MPa. Almost all of the structure is under risk since the stress values have exceeded the tensile strength of the masonry. Figure 6.16 and 6.17 shows the S11 stress contours under dead load, live load and RSA performed along with longitudinal and transversal direction.

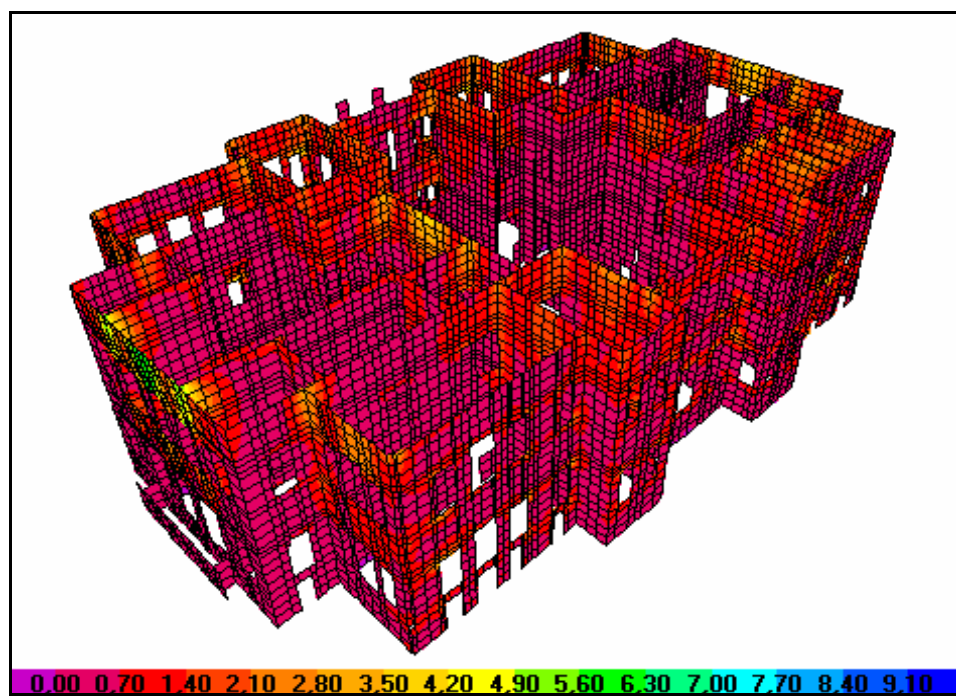


Figure 6.16. S11 stresses under RSA of MCE in longitudinal direction

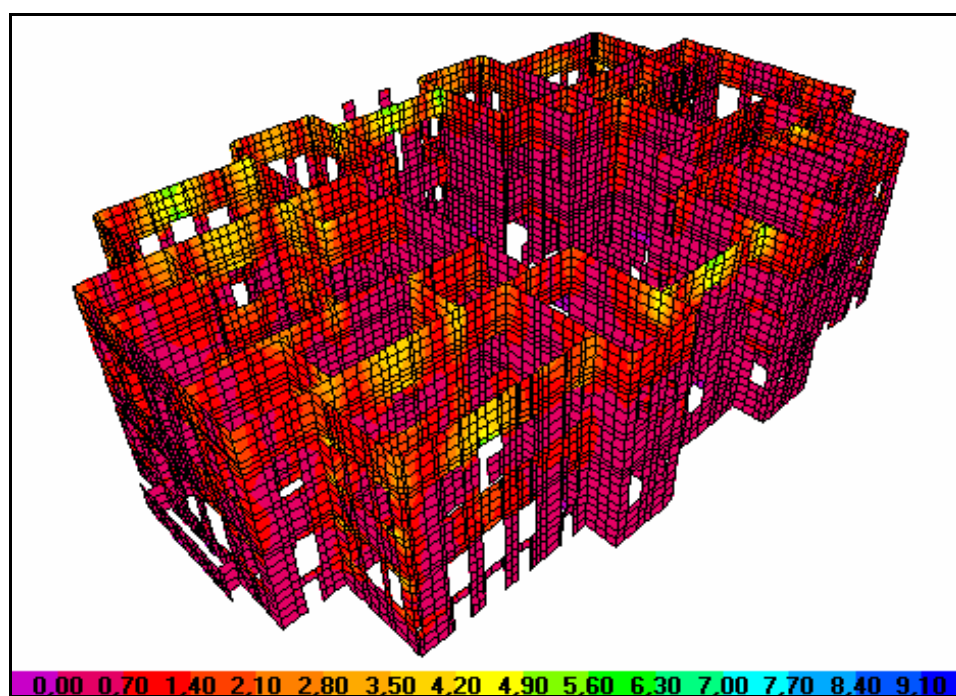


Figure 6.17. S11 stresses under RSA of MCE in transversal direction

6.2.4. Concluding Remarks

Since RSA is a linear method based on mode superposition method, application of different response spectrum to a structure results with similar stress distribution with different magnitudes. For the RSA of Beylerbeyi Palace the earthquake stresses are mainly depend on the magnitude of acceleration on the flat plateau of each response spectrum since modal periods of the structure are gathered on this horizontal line.

It is interesting to note that in the application of the earthquake loads along with the longitudinal direction, transversal walls were under high level of tension stresses (yellow and green colors in Figure 6.6, 6.13 and 6.16). Moreover similarly when the earthquake was applied in transversal direction longitudinal walls were predominantly under stressed (yellow and green colors in Figure 6.9, 6.14 and 6.17). In other words stress concentrations were settled on the walls whose direction perpendicular to the direction of ground motion. This observation reveals the lack of rigid floor action and proves the existence of out of plane action. Figure 6.18 explains the out of plane behavior and stress concentration in detail.

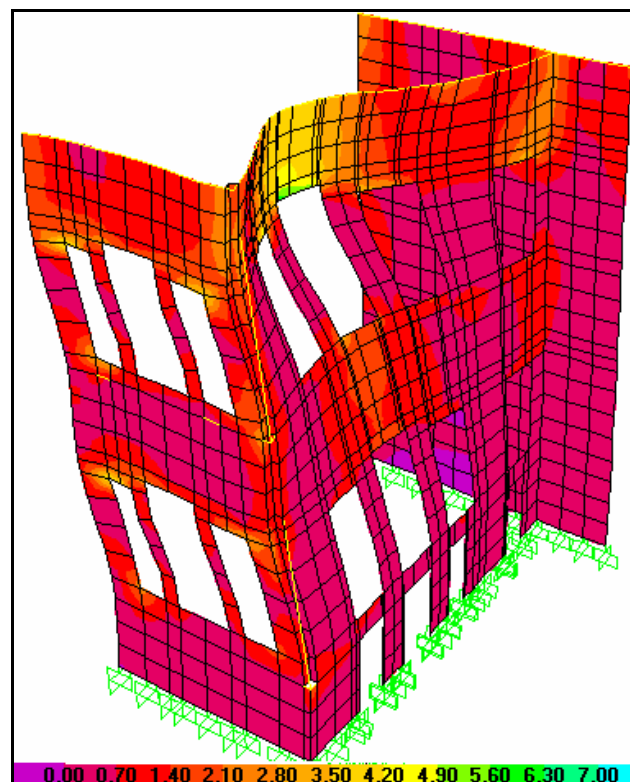


Figure 6.18. Out of plane behavior and related stress concentration

The obtained stress values are also in good agreement with the dynamic behavior of the structure. Many out of plane modes had been identified in the previous section of the study. Additionally left hand side of the structure is more under stressed than the right hand side for both walls, along with longitudinal and transversal directions, as expected due to dynamic analysis.

The stress contours have showed that highest stress values were formed on the second storey of the Mabeyn part due to out of plane behavior. Although the structure was not subjected to an earthquake as strong as MCE, the existing damages should match stress concentration region. On the other hand these walls are covered by timber covering which hide the existing damages.

For in-plane loading of the walls important stress concentration was determined at the corners of openings in the structure. Both horizontal and vertical stress concentrations are effective for the corners of openings. As described in the third chapter damage survey, there were inclined cracks at those regions. In other words these stresses are in good agreement with the damage of the palace. Figure 8.19 shows the computed horizontal stresses under MCE and an example of the corner cracks in the palace.

Another type of stress concentration was the vertical stress related on the wall segments between two openings. In the palace that type of walls are on the exterior side of the palace and they are generally between the windows. The corners of these walls were also subjected to high stress concentration. Damage survey of the palace had revealed the existence of the vertical cracks. One of the most important cracks near the sea side window is seen in Figure 8.20 with respective stress contours under MCE.

Although the timber covering of the rooms in the Mabeyn part did not allow a full comparison of the obtained numerical results and existing damages in the structure, it can be concluded that the obtained stresses are in good agreement with the damages in the palace.

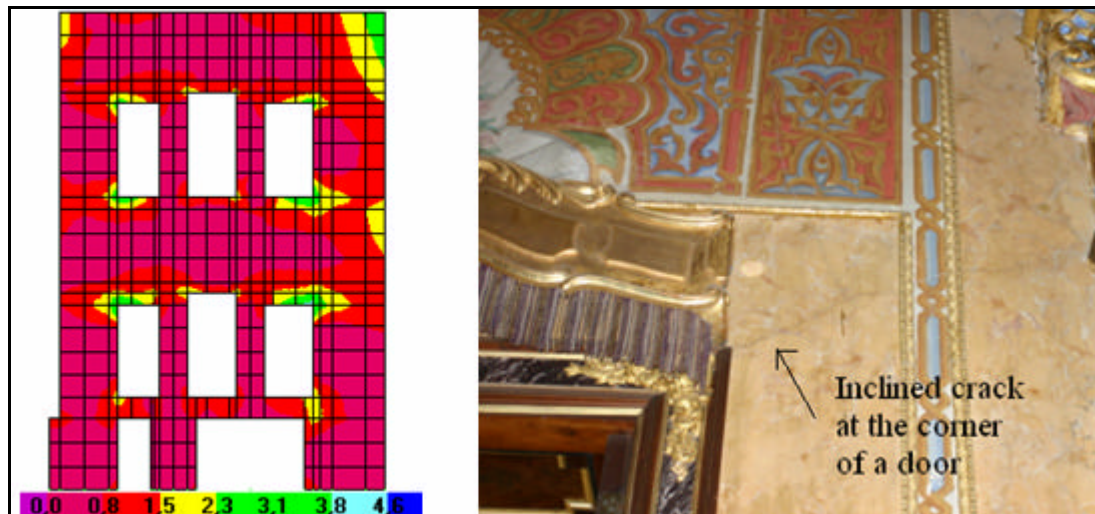


Figure 6.19. Stress concentrations at the corner of openings and a corner crack from the structure

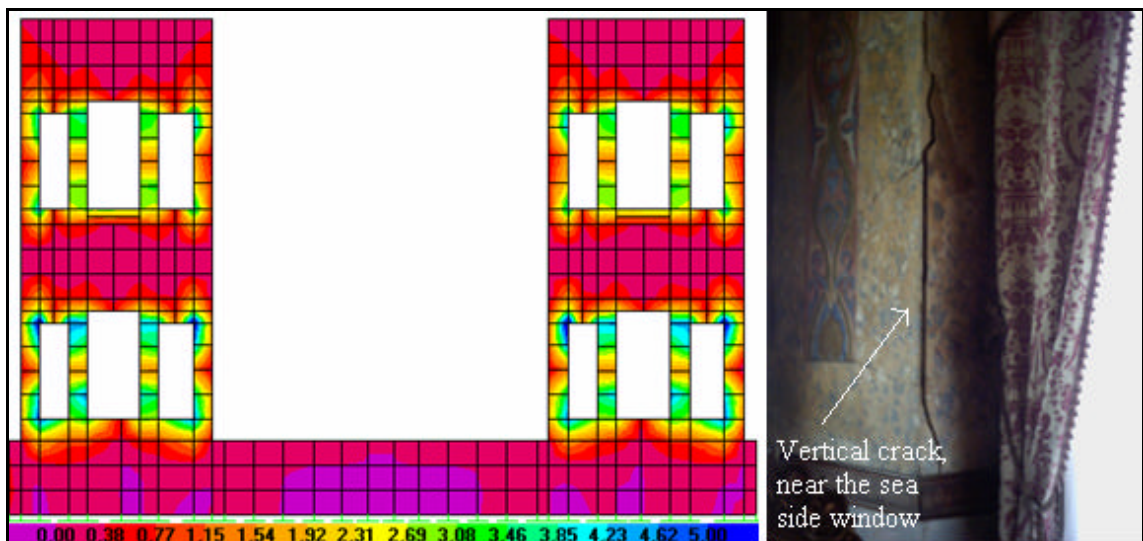


Figure 6.20. Vertical stress concentration and respective crack from the structure

For the performance evaluation of the palace under earthquake loads, it can be concluded that, the structure is not capable to resist the earthquake ground motion, according to design response spectrum of Turkish Earthquake Code and Design and Maximum Considered Earthquake. The effects of RSA analysis according to TEC is between those of DE and MCE.

7. NONLINEAR PUSHOVER ANALYSIS

7.1. Lateral Load Pattern and Non-linear Material Properties

In order to identify the behavior of the structure under horizontal loads, nonlinear pushover analysis was performed. In the response spectrum analysis it had been shown that the stress values were exceeded the strength of the masonry material, meaning the structure went to the nonlinear range. For this reason it is a must to identify the behavior of the structure by nonlinear analysis.

There is no doubt that the nonlinear analysis can reflect the actual behavior of the structure. Moreover the weak elements can be recognized directly [37]. In this study the pushover analysis methodology was used to obtain the capacity curve of the structure. However it is a challenging task to perform the pushover analysis in a structure like Beylerbeyi Palace.

Since the pushover analysis is a nonlinear analysis it requires long computation time and high computer capacity for the analysis of huge structures like Beylerbeyi Palace. The modal analysis of the palace has shown that the basement storey of the structure is much stiffer than the upper stories. For the first fifty modes there is no contribution of the basement floor since basement floor composed of thick stone material with high modulus of elasticity. For this reason the basement floor can be neglected and the model can be assumed as two-storey structure. This enables us to reduce the size of the model and decrease the solution time.

The pushover analysis requires applying a bunch horizontal load pattern to the structure and measuring the respective horizontal displacement. In a regular structure the floor levels are the location of application of the horizontal loads since the mass of the floor is mainly gathered at those levels. Yet it is known that there is no mass concentration in the floor levels due to timber slabs and the mass is distributed through the height of the structure. Moreover the lack of rigid slabs prevents the application of load on a single point

like centre of gravity or stiffness center of the floor. Due to timber slab the applied horizontal forces could not be distributed to the walls.

Furthermore the load pattern is a problem. The modal analysis of the structure revealed the complex behavior with local modes. Like a regular structure load pattern can not be assumed as proportional with the first mode shape of the structure.

As a solution of the pushover load there is no doubt that it should be proportional with the mass of the structure and secondly the elevation of the structure should be accounted. In that respect each piece of wall should be loaded proportional with its mass and its altitude. As a result the lateral load is to be applied to the structure as body force by a definition of acceleration to start to mass to be forced. In order to account the different altitude, the body force would be defined in four different levels. The applied loads are shown in Figure 7.1.

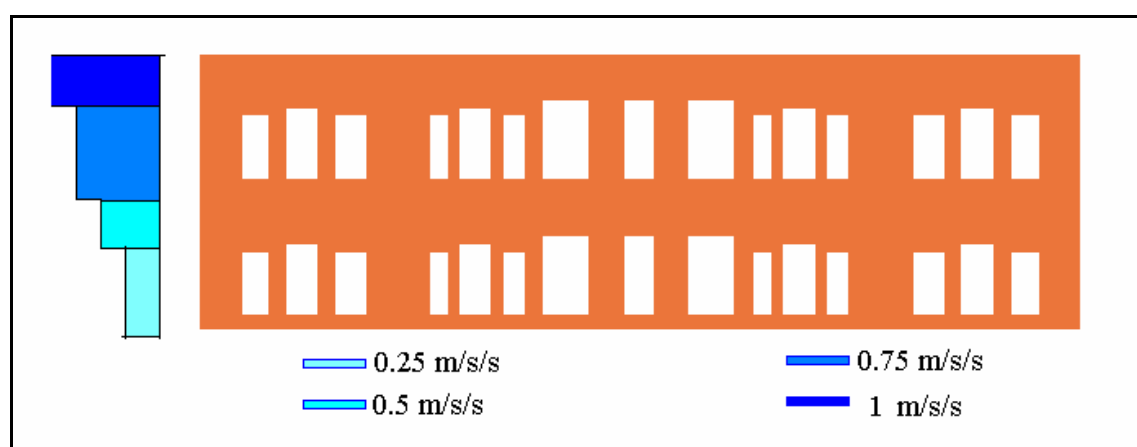


Figure 7.1. Application of the horizontal loads

The pushover analysis was performed by LUSAS finite element computer program. Within the package many nonlinear material models are available to use for different materials. Unfortunately there is no specific material model defined for the nonlinear analysis of the masonry. On the other hand a few material models were assessed as compatible since the experimental tests and numerical models gave the accurate enough results [38]. In that respect the pushover analysis was performed with Drucker-Prager Material Model (DPMM) and Cracking-Crushing Concrete Model (CCCM) [29].

The Drucker-Prager elasto-plastic model may be used to represent the ductile behavior of materials which exhibit volumetric plastic strain (for example, granular materials such as concrete, rock and soils). The model incorporates isotropic hardening. The required material characteristics are initial cohesion, c , friction angle, F , and limit plastic strain values [29].

Initial cohesion and friction angle directly depend on the compression and tension strength of the material and they can be calculated by the formulas below [39];

$$c = \frac{s_c}{2\sqrt{m}} \quad (7.1)$$

$$\sin f = m^{-1/m+1} \quad (7.2)$$

$$m = \frac{s_c}{s_t} \quad (7.3)$$

By using the formulas the cohesion is computed as 1.46 MPa and friction angle is 57° , the plastic strain was restricted to 0.003. In order to account the discrepancy between the structural material, masonry, and material model the cohesion value is decreased 50% and used as 0.73 MPa.

The multi-crack concrete with crushing material model is based on a multi-surface plasticity approach to represent the nonlinear behavior of concrete in both tension and compression [29].

The model simulates directional softening and crushing in compression using the same yield functions. Cracks in tension are assumed to form when the major principal stress reaches the tensile strength, after which a permanent crack plane is formed. Multiple cracks can form at non-orthogonal directions to one another. The model simulates nonlinear behavior in compression with hardening and softening functions applied to the local yield surfaces [29].

In tension zones permanent crack planes result in directional loss of strength, whereas in compression zones the planes are not permanent but rather may rotate and result in an isotropic loss of strength. In both tension and compression unloading from the yield surface is assumed to be elastic [29].

The following material properties are required to define the mode and they can be extracted from uni-axial stress-strain curves in tension and compression. Obtained from the laboratory tests, described in chapter 3, the numerical values were also given below. The parameters are illustrated in Figure 7.2 [29].

- Compressive strength (s_c), the maximum uni-axial compressive stress after which softening in compression begins. Compressive strength had been determined as 10 MPa.
- Tensile strength (s_t) the maximum uni-axial tensile stress after which softening in tension begins. Tensile strength had been determined as 0.85 MPa.
- Strain at peak compressive stress (e_{cp}), the uni-axial strain at the peak uni-axial compressive stress. It had been determined as 0.008.
- Strain at end of compressive softening curve (e_{c0}), the uni-axial strain at the end of the uni-axial compressive softening curve. It had been determined as 0.014.
- Strain at end of tensile softening curve (e_{t0}), the uni-axial strain at the end of the uni-axial tensile softening curve. This should be defined for cases of distributed fracture, which is typically the case for reinforced concrete. In such cases the fracture energy per unit area, G_f , should be set to zero. It was set to zero since the material is assumed as unreinforced masonry
- Fracture energy per unit area (G_f), for concrete that does not contain reinforcement the strains will tend to localize in the crack zones. In this case the fracture energy per unit area (to fully open the crack) should be specified rather than the strain at the end of the tensile softening curve. It was assumed as 100 units.

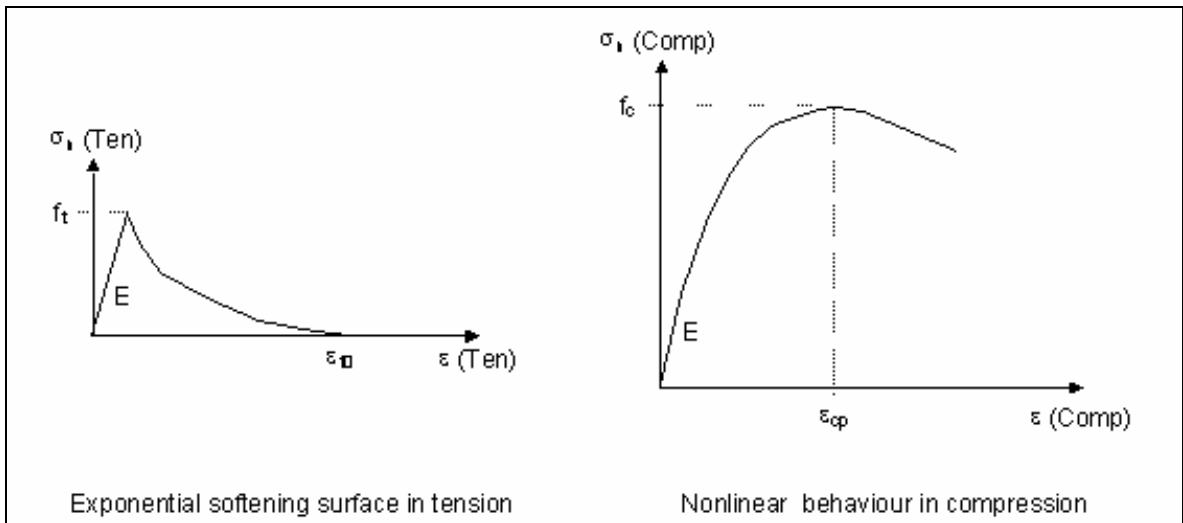


Figure 7.2. Nonlinear material properties for CCCM [28]

Nonlinear analysis was performed with two consecutive analyses. The first one is conducted for the application of the vertical loads, induced by dead and live loads whereas the second load case accounts the application of the horizontal load pattern. For each load case incremental nonlinear analysis was performed. For the first analysis manual incrementation is performed although the analysis remains in linear range. Because the defined limits of the materials could not be exceeded by the stresses. For the second analysis automatic incrementation was preferred. No limit was set for the maximum change for the load factor [29].

After the definition of the nonlinear material properties, the pushover analysis was performed along with longitudinal and transversal direction after application of the vertical loads induced by gravity. In order to assess the behavior and weak parts of the structure the capacity curves were drawn by using two different material models. The results are discussed below. Numerical model of the palace is illustrated below on Figure 7.3 with used terminology.

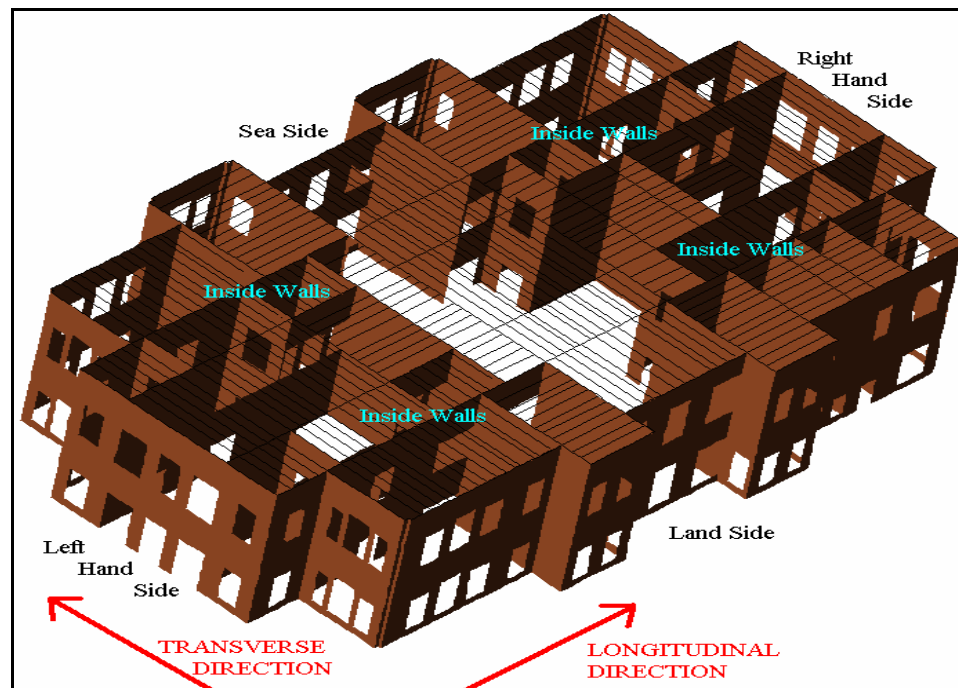


Figure 7.3. Terminology through the discussion.

7.2. Pushover Analysis along with Longitudinal Direction

The pushover analysis was performed along with longitudinal direction first. For both DPMM and CCCM it was observed that; the lack of rigid diaphragm causes to have different displacement values for each increment of the loading. For the reason the global behavior is out of question and capacity curve should be drawn for a portion of the wall. Figure 7.4 shows the deformed shape of the structure. It proves the different movement of the wall. The most flexible part is seen as the sea side of the structure

Pushover curves were also drawn for the walls along with sea side, walls along with land side and inside walls of the palace. In order to examine the out of plane behavior pushover curves were also drawn for the left hand side and right hand side wall of the palace. Lateral load and especially displacement capacity for the wall segments were obtained apparently higher with DPMM than those of CCCM. The maximum displacement value for DPMM is about 13 cm and masonry cannot be expected to sustain that amount of displacement. For this reason it can be concluded that; CCCM is more appropriate than DPMM for masonry material. Figure 7.5 shows the pushover curves for the wall, exhibits

in-plane behavior while Figure 7.6 shows the pushover curves of the left and right side walls which are loaded along with out of plane direction.

As can be understood from both deformed shape of the palace and pushover curves, sea-side wall of the palace is weaker than land-side wall and the inside walls are the stiffest portion of the palace. Out of plane mechanism was observed significantly for the left and right hand exterior walls. All of the findings are compatible with the dynamic behavior of the structure.

The main reason of flexibility of the sea-side and land-side walls can be shown as discontinuous orientation of the walls and windows openings. The lack of rigid slabs causes independent and unrestricted movement of these walls and makes them vulnerable under horizontal ground motion since as masonry they can not sustain with high level of lateral displacement.

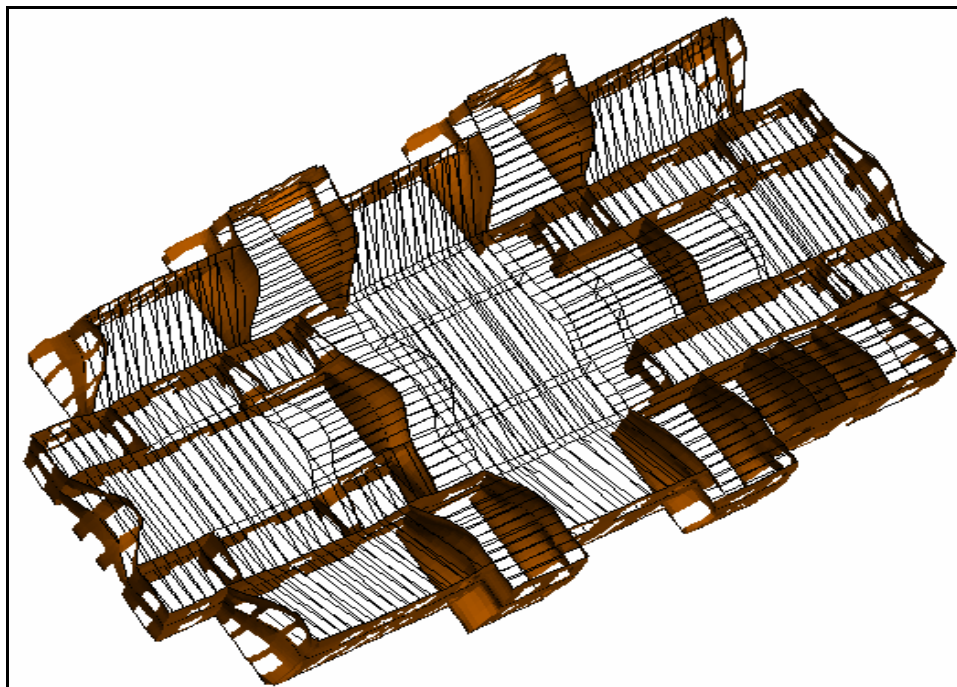


Figure 7.4. Deformed shape of the palace after pushover analysis in longitudinal direction

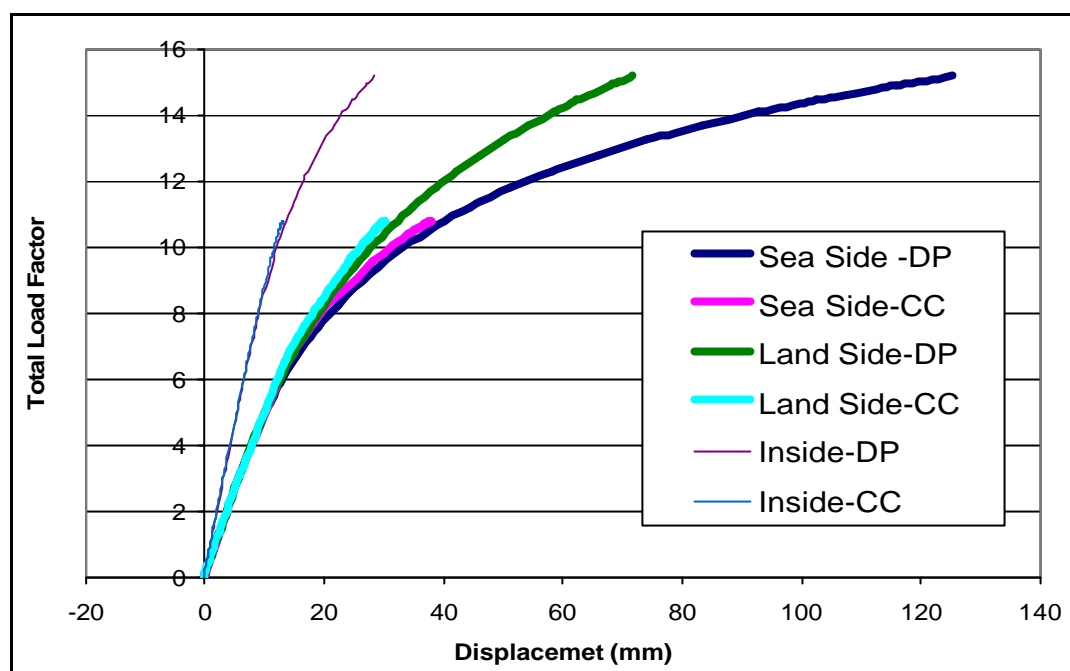


Figure 7.5. Pushover curves for the walls loaded by in-plane loads along with longitudinal direction

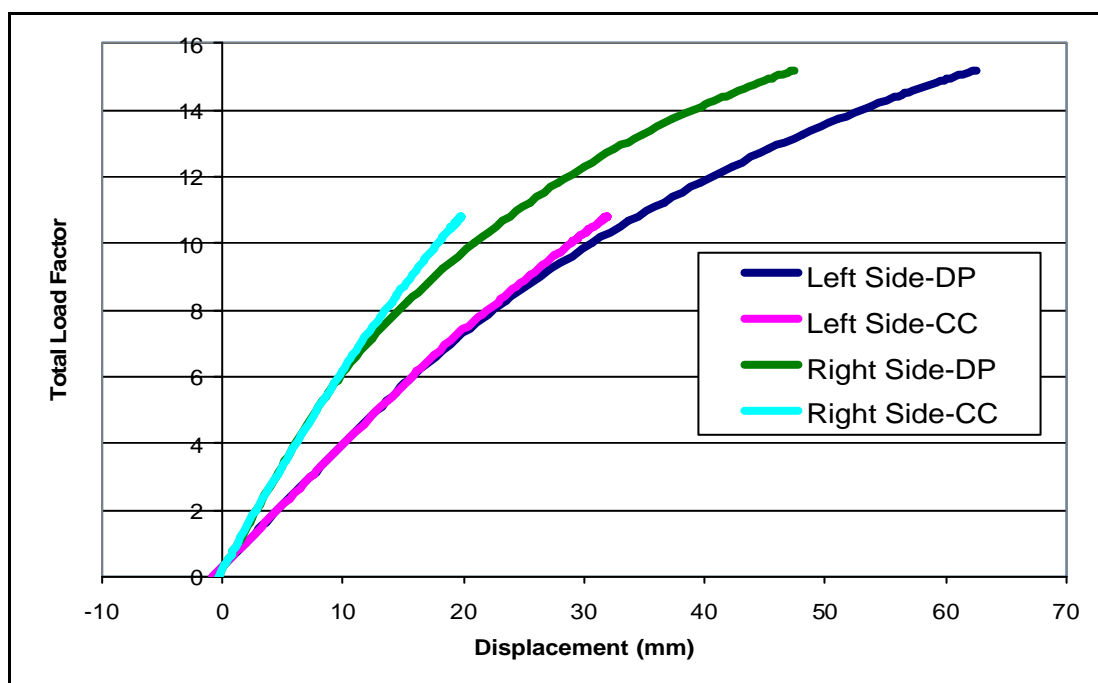


Figure 7.6. Pushover curves for the walls loaded by out of plane loads along with longitudinal direction

7.3. Pushover Analysis along with Transversal Direction

Secondly pushover analysis has been applied along with transversal direction. Figure 7.7 shows the deformed shape of the palace. The lack of rigid floors causes again independent movement of the wall segments as expected.

Almost the same deformed shape configuration is observed for DPMM and CCCM with different force and deformation values. The deformation and load values of the pushover curves of DPMM are much more than those of CCCM. The pushover curves are drawn to quantify the different movement of the wall segments. Figure 7.8 show the pushover curves for the walls loaded by in-plane direction. These walls are Left side walls, right side walls and inside walls. Figure 7.9 illustrates the pushover curves of the walls loaded by out of plane loads. These walls are sea side walls and lend side walls.

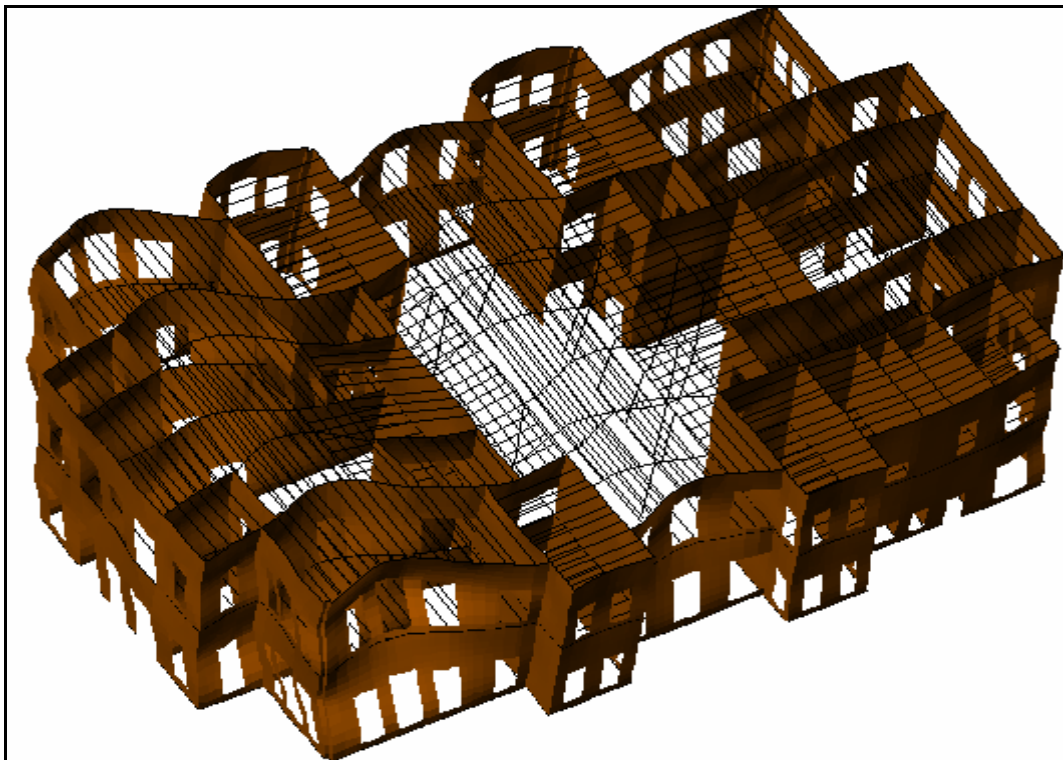


Figure 7.7. Deformed shape of the palace after pushover analysis in transversal direction

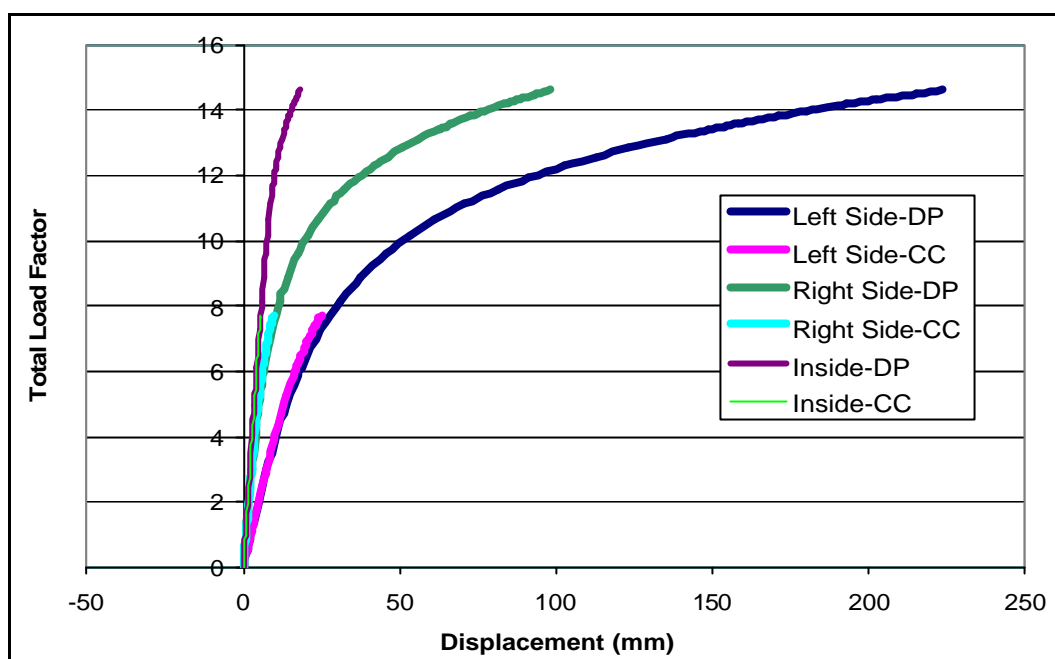


Figure 7.8. Pushover curves for the walls loaded by inplane loads along with transversal direction

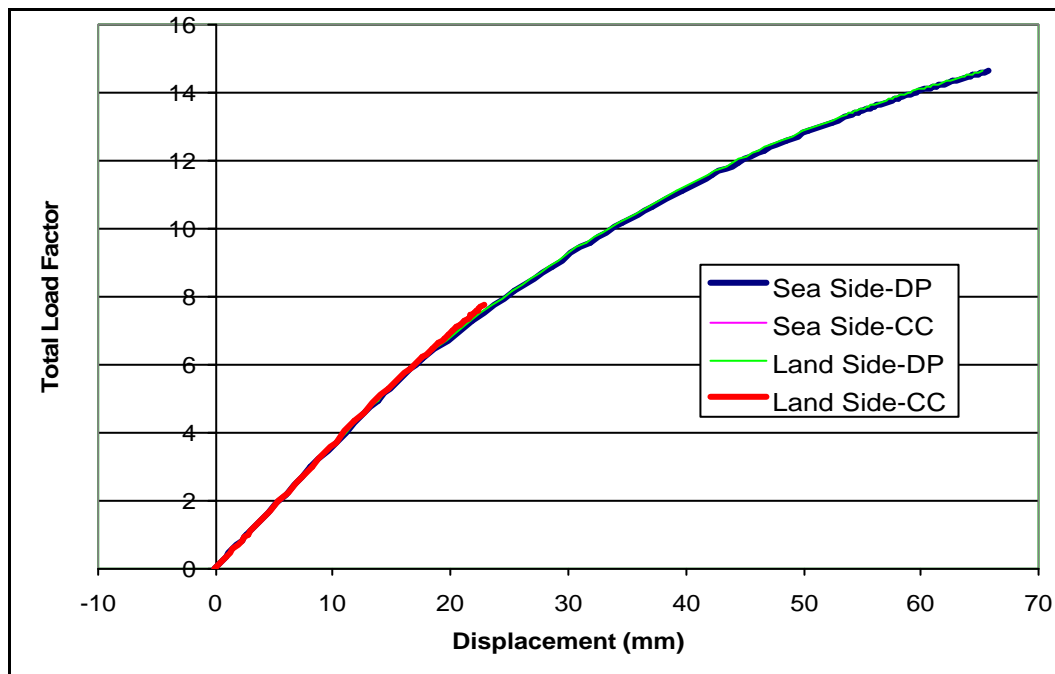


Figure 7.9. Pushover curves for the walls loaded by out of plane loads along with transversal direction

7.4. Concluding Remarks

A bunch of pushover analyses were applied to the structure along with two perpendicular directions and with two different nonlinear material models, namely Drucker Prager Material Model (DPMM) and Cracking Crushing Concrete Model (CCCM). The followings are the most important results of the performed analyses.

The required material properties for CCCM were directly obtained by uni-axial and flexure tests performed over laboratory made specimens while parameters of DPMM were computed with formulas of elasticity. Thereby material properties of CCCM are more realistic than those of DPMM. Moreover the results showed that DPMM gives unrealistically high level of lateral displacement up to 23 cm. For these reasons it is obvious that the CCCM reflects the nonlinear behavior better than DPMM does.

Nonlinear pushover analysis enabled to identify the vulnerable parts of the structure and possible techniques to recover those vulnerabilities realistically. Both the deformed shape of the palace and the pushover curves alerted the lack of rigid floor diaphragms. Since the loads could not be transferred among the walls the exterior wall of the palace has much more displacement than inside walls.

The application of the lateral load pattern was tried to be similar to earthquake effect. For this reason, when a ground motion hits the palace the same behavior can be expected. In that condition during a strong earthquake the exterior walls of the palace are the most vulnerable parts of the structure.

8. RETROFIT OF THE STRUCTURE

The response spectrum analyses have shown that the palace is not capable to resist the earthquake forces. Moreover the nonlinear pushover analysis revealed the vulnerable parts of the structure. In that manner it is clear that the palace should be strengthened by an appropriate strategy. The applied upgrading strategy should have the following superiorities over a common one.

- The efficiency of the strategy should clearly be set with respect to application and final performance. The strategy should give the desired performance level.
- Historical value of the structure is always in great importance. For this reason any application should be appropriate and must not disturb the cultural value of the structure.
- As the key parameter of the study, the strategy should be reversible. Reversible Mixed Technologies, (RMT), are based on the integration of structural members of different materials and/or construction methods into a single construction. The basic feature of RMT is that their application should be always completely recoverable, that is reversible, if required. This is considered as an essential design requirement in order to prevent historical and monumental buildings from unsuitable rehabilitation operations [3].

In this study any proposed technology has been assessed with respect to technical description, practical methodologies and structural detailing, reversibility and aesthetic appearance aspects. These terms were clearly identified for each upgrading strategy.

In general for the rehabilitation of masonry structures the exterior bracing with hysteretic dissipation, the application of fiber reinforced polymers, the consolidation of the timber slabs to have rigid diaphragm action, base isolation, the use of steel/aluminum plates and steel wire meshes and the addition of exterior supports based on the concept of reversible technologies are the basic rehabilitation techniques. However within the scope of this thesis three different strategies have been selected to maintain the original characteristics of Beylerbeyi Place with the least alterations historical and aesthetics

appearance aspects. These strategies are the use of fiber reinforced polymers, installation of base isolation systems and consolidation of the slab of the second storey (Roof level).

8.1. Fiber Reinforced Polymer Overlays (FRP)

Structural intervention with FRP overlays is one of the most widely used strategies to upgrade the performance of masonry structures. The application increases the strength and ductility of the masonry. They can be regarded as innovative because the FRP material is new in seismic retrofitting, because it's very good mechanical characteristics and because it offers a wide range of attractive technical solutions [40-41].

There are two basic approaches to FRP strengthening of the masonry walls. The first one is the application of FRP overlays on the surface of the wall (for normal masonry walls) and the second one is the application of FRP overlays on both surfaces and connecting the overlays with metallic tie rods to induce larger confinement action (more suitable for two-leaf walls with a lower quality infill in between) [41]. For the protection of Beylerbeyi Palace the first approach was accounted because the original masonry configuration in the palace is compatible with the application.

8.1.1. Technical Description,

One of the most modern technologies for the seismic rehabilitation/upgrading of masonry structures is constituted by the use of fiber reinforced materials. Fiber reinforced polymers (FRP) are composite materials constituted by two core materials, namely fiber material with high mechanic properties and matrix acting as a binder [41].

The role of the fiber is to resist the external loads, while the matrix has both the function of guarantying the adhesion to the support and transfer the stress: the result is a lightweight material with high strength capacity [41].

A wide range of mechanical properties can be covered by selecting different types of fiber and matrix (i.e.: Young modulus and strength capacity). Commonly, fibers used for the realization of composite materials are glass, carbon and aramid fibers. Figure 8.1 and

Table 8.1 show the main characteristics of carbon fibers. They exhibit not only high tensile strength and stiffness but also good fatigue behavior, good performance under cyclic loads, high resistance to chemical products and corrosion immunity [41].

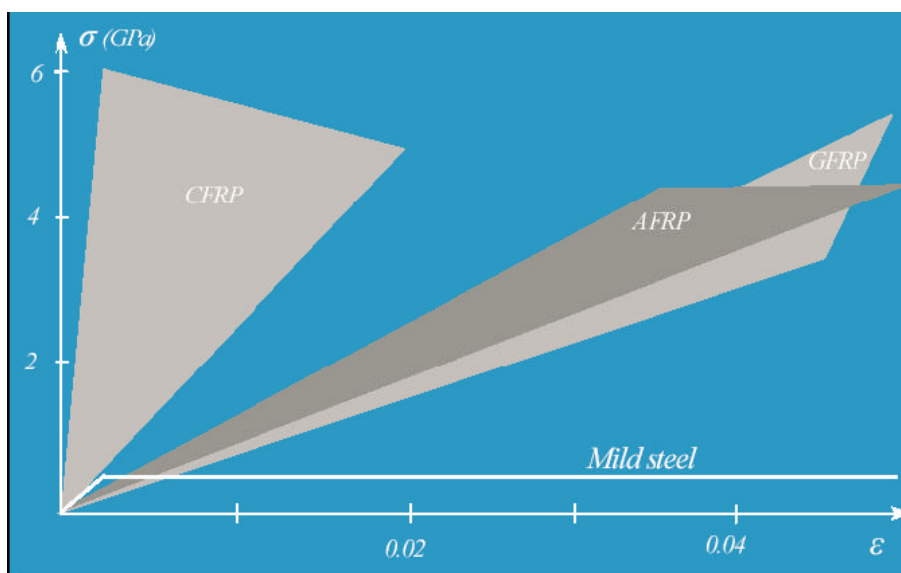


Figure 8.1. Stress-strain relationship of different FRPs [41]

Composite materials are commercialized in several forms; they can be found in form of strips, fabric sheets and rods. In general, FRP strips can be used for upgrading the elements having a plane surface while fabrics can be used where the surface is not regular because they can more easily be adapted to irregular surfaces. FRP strips, fabrics and rods can be used in both concrete and masonry structures [40]. The possibility of selecting the fiber typology, the architecture of sheets, and the number of FRP layers give to the designer flexibility in the choice of the reinforcement (Figure 8.2).

Externally bonded FRP reinforcement is an efficient technique that can be applied for a wide range of structures and materials, in particular in the case of the design of masonry structures. Both FRP and masonry show a brittle behavior, what allows considering, as failure control mechanism, either FRP rupture/debonding or masonry crushing. Masonry strengthened with FRP systems typically fails due to crushing of the masonry [42] or debonding of the FRP [43 and 44]. The state of the structure prior to strengthening should be taken as a reference for the design of the FRP reinforcement. The strengthening design has to provide sufficient resistance capacity for the ultimate and

service loads, and it has to guarantee the required durability taking into account the characteristics of the structure itself and the environment conditions. The FRP system has to be considered working only in tension.

Table 8.1. Tension characteristics of fibers [40]

Fibre Type	Elasticity Modulus (GPa)	Ultimate Strength (MPa)	Ultimate Deformation (%)
Carbon			
High Strength	215 – 235	3500 - 4800	1.4 - 2.0
Very High Strength	215 – 235	3500 - 6000	1.5 - 2.3
High Elasticity Modulus	350 – 500	2500 - 3100	0.5 - 0.9
Very High Elasticity Modulus	500 – 700	2100 - 2400	0.2 - 0.4
Glass			
Glass E	70	1900 - 3000	3.0 - 4.5
Glass S	85 – 90	3500 - 4800	4.5 - 5.5
Aramid			
Current	70 – 80	3500 - 4100	4.3 - 5.0
High Performance	115 – 130	3500 - 4000	2.5 - 3.5

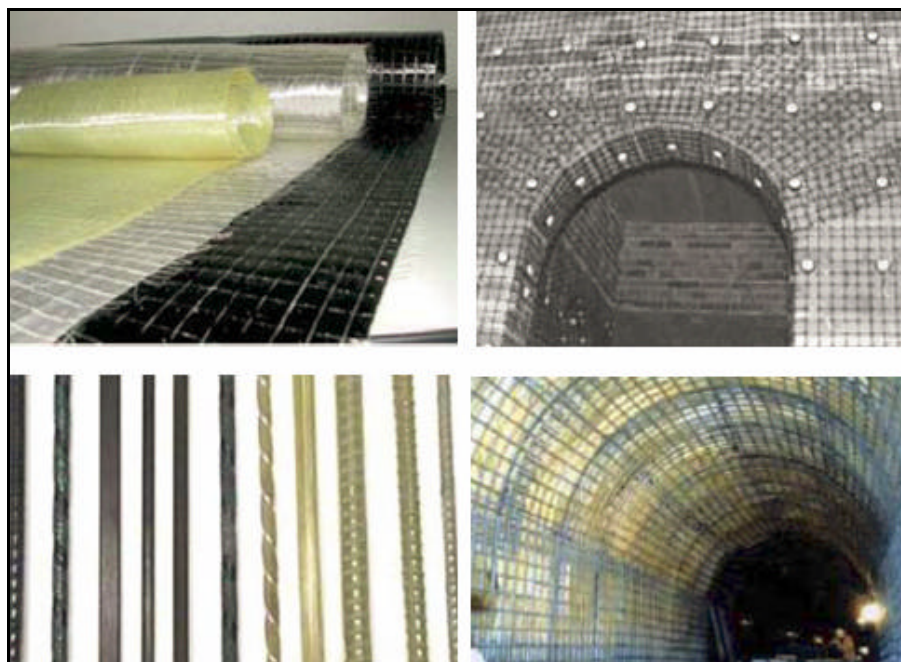


Figure 8.2. Different types of FRP and their applications [41]

Masonry may be strengthened with epoxy-bonded laminates or fabrics made of FRP, as shown in Figure 8.3. When out-of-plane bending response dominates (as in the case of upper levels of masonry buildings), horizontally applied FRP laminates may offer

considerable increase in strength [40]. Most important in the case of in-plane bending is the amount and distribution of reinforcement: high reinforcing ratios placed near the highly stressed zones give significant strength increase. The achievement of full in-plane flexural strength depends on proper anchorage of the laminates at their ends. The in-plane shear capacity of masonry walls strengthened with FRP laminates may be quite high too, especially in the case of low axial loads [40].

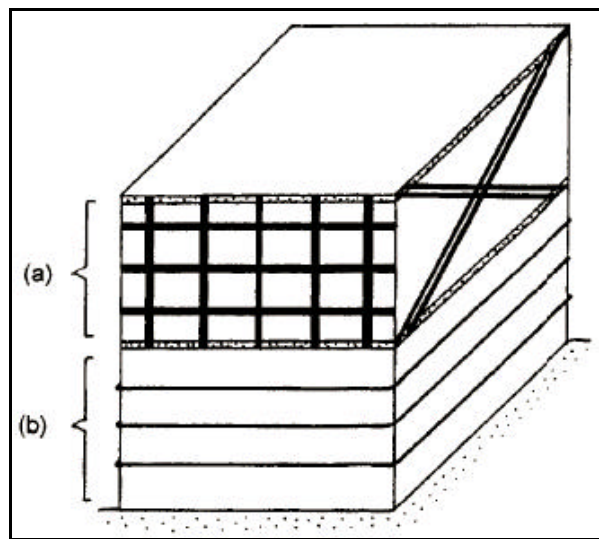


Figure 8. 3. Strengthening of masonry with FRP (a) bonded strips to improve flexural and in-plane shear strength, (b) circumferentially applied unbonded strip-like tendons, providing confinement [40].

In order to prove the useful effect of FRP many tests have been carried out and there are many ongoing projects. In the framework of PROHITECH, WP7, Experimental Research, full scale model of Mustafa Pasha Mosque has been tested on tri-dimensional shake table. The strengthened model by FRP has shown very good performance. The other one relates to tests on masonry walls [45] where first walls were tested in as-built condition up to failure and then retrofitted on one side with FRP overlay (glass and carbon fibers, different orientations of fibers, different resins). The test set up is shown in Figure 8.4 for Un-reinforced Masonry (UM) wall and 8.5 shows one of the reinforced walls prepared for testing. Figure 8.6 and Figure 8.7 illustrates the results of the tests for vertically and horizontally applied CFRP. Increase of strength and especially ductility is evident.

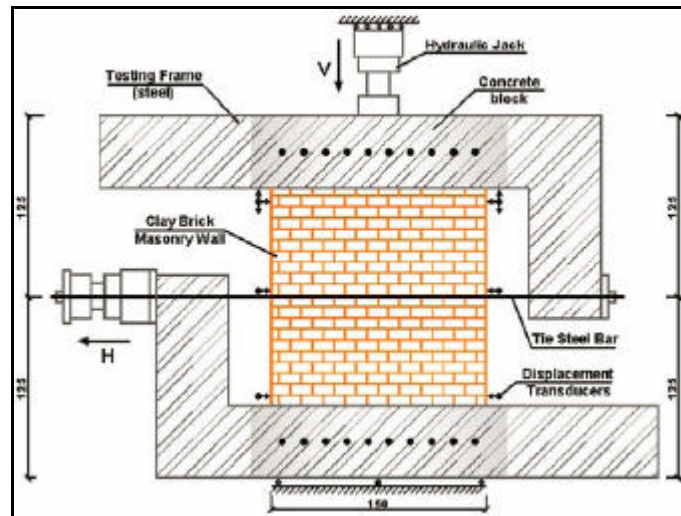


Figure 8. 4. The specimen test set-up [45]



Figure 8. 5. The tested RM3 wall (vertical applied CFRP) [45]

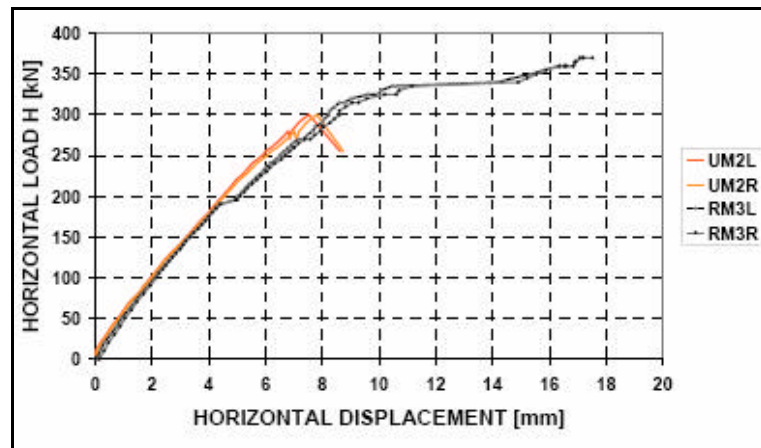


Figure 8. 6. Load-displacement diagram of the wall for vertically applied CFRP [45]

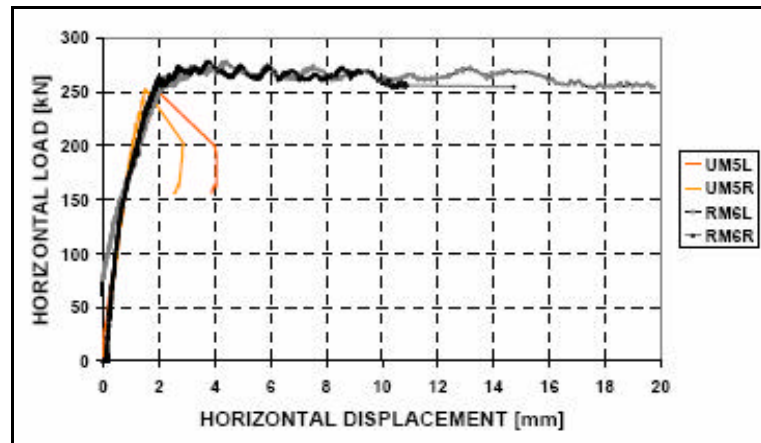


Figure 8. 7. Load-displacement diagram of the wall for horizontally applied CFRP [45]

8.1.2. Practical Methodologies and Structural Detailing

Until 1997 the major number of applications of FRP materials has been studied with reference to RC structures, with some but few applications to masonry structures and historical monuments. In Italy, the use of FRP for the refurbishment of masonry structures increased after the well known Umbro-Marchigiano earthquake (1997). This earthquake had interested the area of Perugia, an important cultural and religious city in the middle part of Italy, rich of monumental buildings and ancient churches. The earthquake caused several damages to masonry structures with the subsequent need of rehabilitation [41].

The FRP application for Beylerbeyi Palace will be based on the computed horizontal and vertical tension stresses by Response Spectrum Analysis (RSA). RSA had been applied for three different response spectrums. In that respect the FRP orientation depends on the expected ground shaking parameters. For each analysis, critical locations of the horizontal and vertical stresses were determined. Critical locations refer to regions on which the tensile strength of the masonry was exceeded. The FRP orientation must be determined according to those regions (Figures 8.8-8.13).

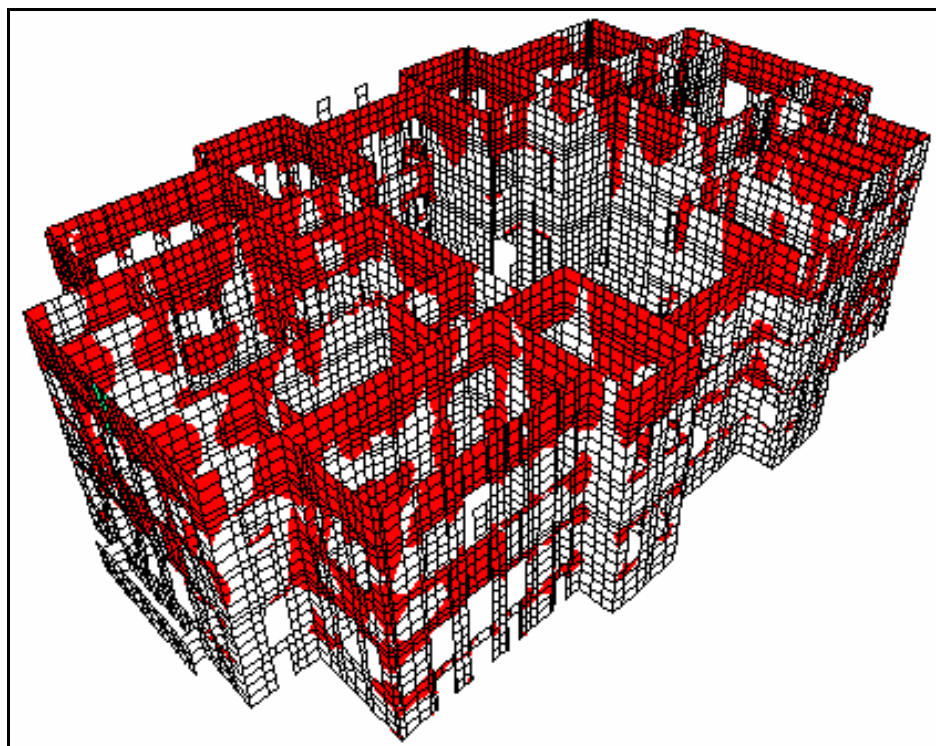


Figure 8.8. Critical regions with respect to horizontal stresses according to TEC

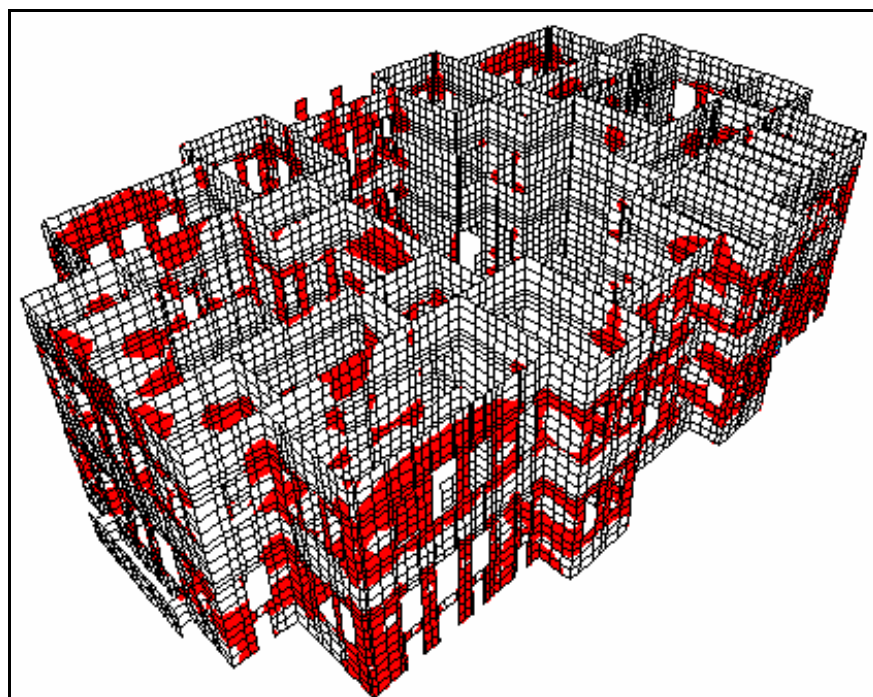


Figure 8.9. Critical regions with respect to vertical stress stresses according to TEC

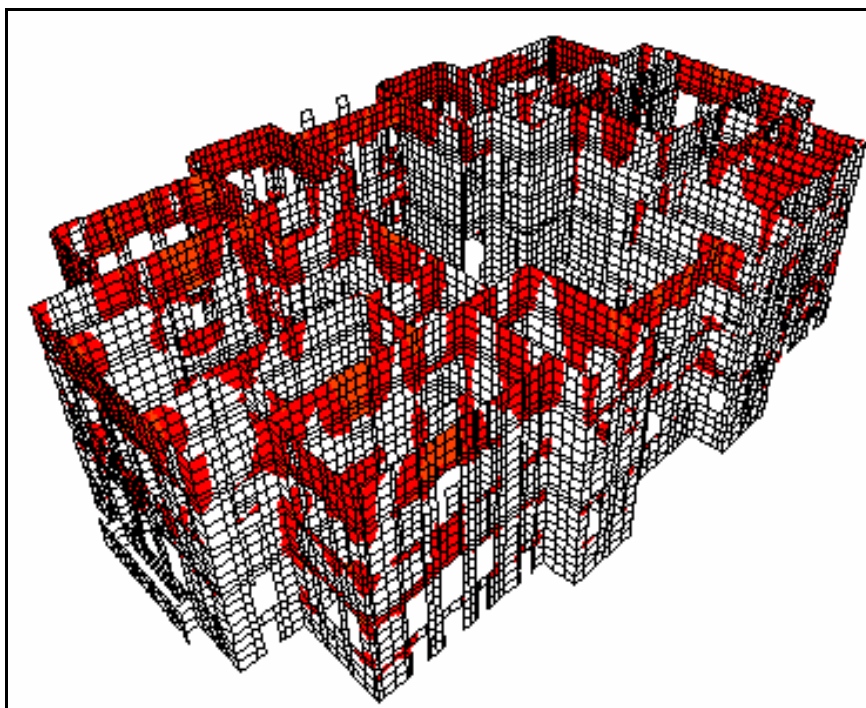


Figure 8.10. Critical regions with respect to horizontal stresses according to DE

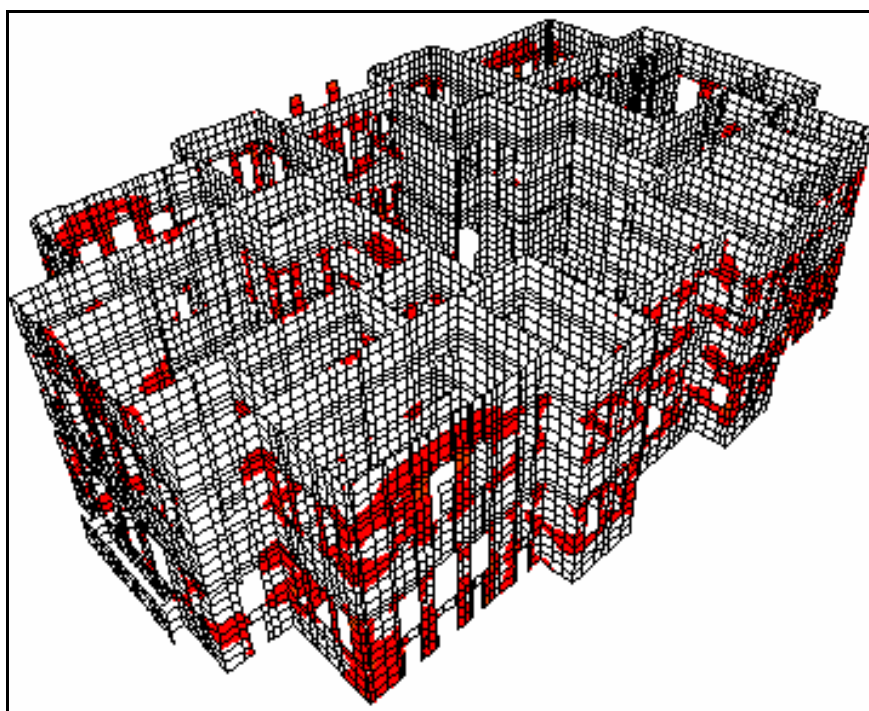


Figure 8.11. Critical regions with respect to vertical stresses according to DE

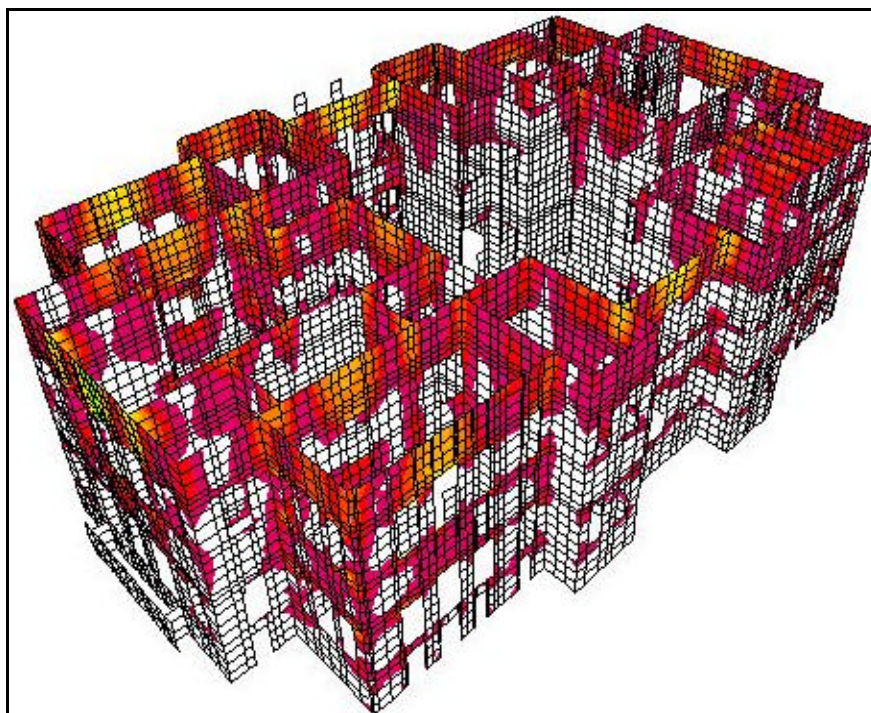


Figure 8.12. Critical regions with respect to horizontal stresses according to MCE

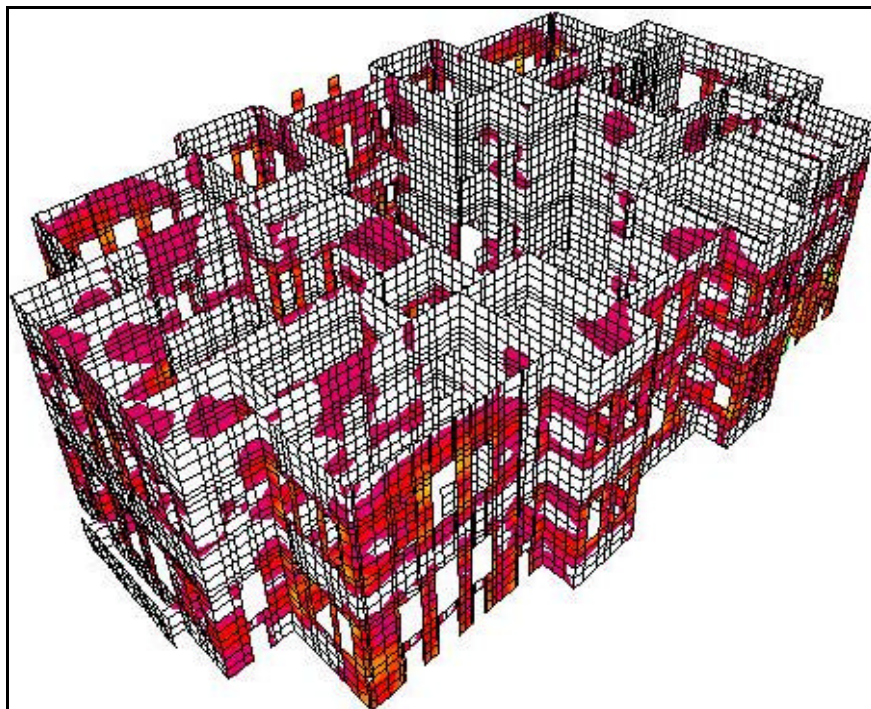


Figure 8.13. Critical regions with respect to vertical stresses according to MCE

The determined critical regions are actually the presentation of the RSA results in a different fashion. For this reason each analysis has different FRP lay-out. In other words different strengthening scheme can be proposed according to desired level of safety. For example application of FRP strengthening technique against the Design Earthquake (DE) requires less effort and less FRP material than application of FRP strengthening technique against Maximum Considered Earthquake (MCE).

On the other hand, the decision of a restoration for a historical structure is a serious task and it is an interdisciplinary issue. The difference between the local application of FRP to a specific part and global application to all walls is not important. If a restoration work had been started, it must give the maximum safety. For this reason in this study FRP orientation would be based on Maximum Considered Earthquake whose return period is about 2500 years.

The critical horizontal and vertical stress regions and their variation are illustrated in Figure 8.14 and 8.15 for external walls in transversal and longitudinal directions respectively. Obviously in the same region there is a need to apply the FRP in both direction and horizontal stresses are more critical than the vertical one. It is clearly seen that the window levels in the first and second stories are vulnerable with respect to vertical stress.

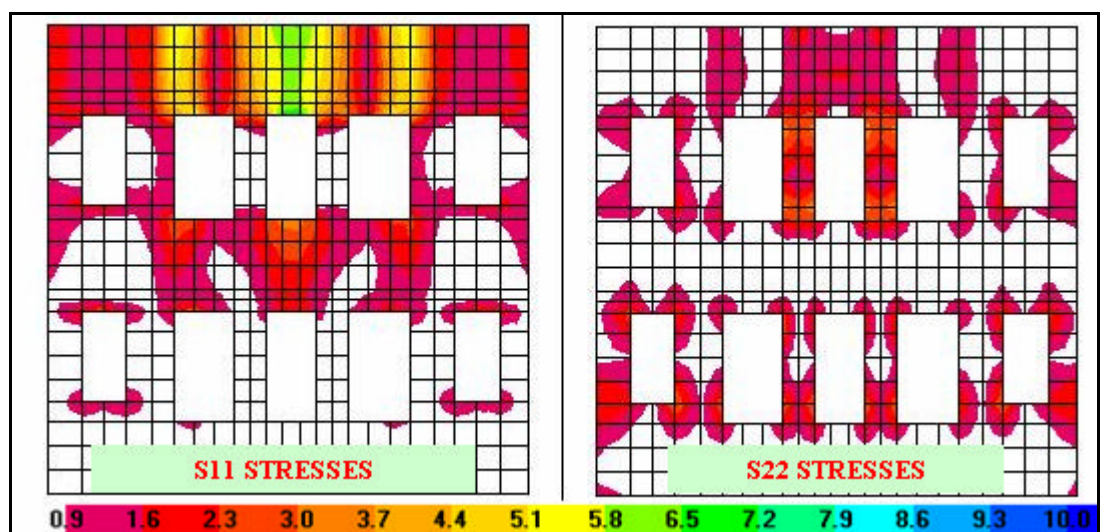


Figure 8. 14. Critical regions with respect to horizontal and vertical stresses under MCE for external left part walls

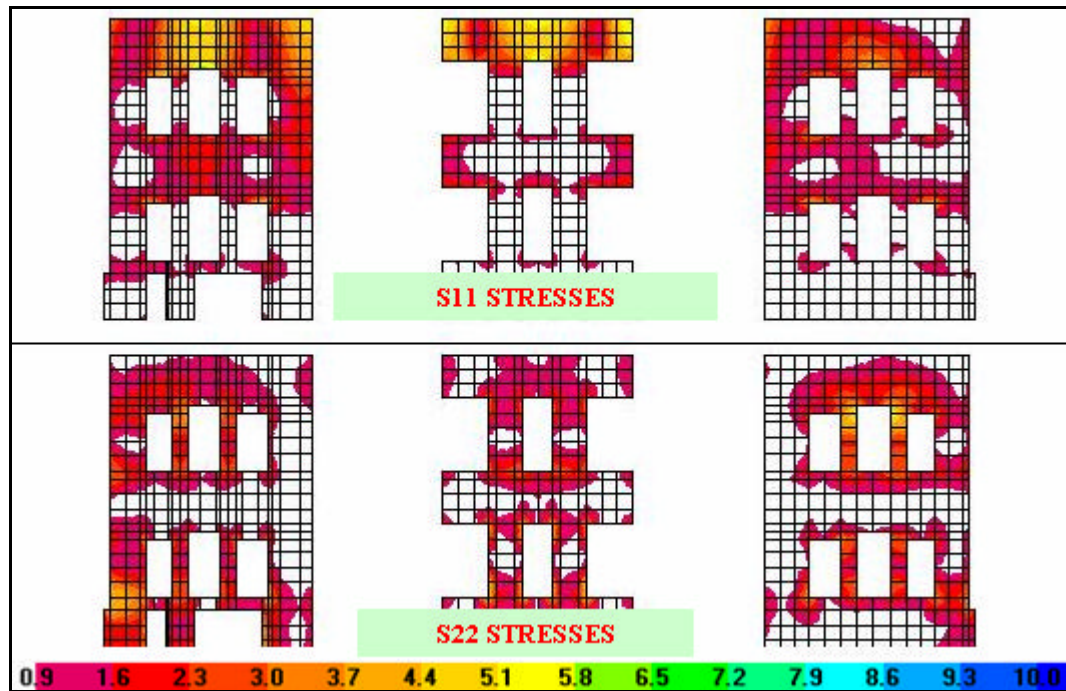


Figure 8. 15. Critical regions with respect to horizontal and vertical stresses under MCE for external sea-side walls

For the strengthening fabrics type of FRP is appropriate because of the simple application. Main fibers of FRP fabrics should be horizontal. Horizontal fibers are effective to carry out of plane stresses on the top part of the structure. The wall between two windows can be treated as a column and it can be fully confined by FRP fabrics. This increase the vertical load capacity and ductility of the wall.

MCE requires that, almost every wall should be covered by FRP. In that respect each wall in the first and second storey of the palace should be covered by FRP along with horizontal direction. Here the FRP is applied to the walls from one face. One face application is important with respect to historical and aesthetics appearance aspects of the palace.

8.1.3. Reversibility

The reversibility of composite materials is a very important aspect. These types of materials, in some cases, reach the “complete reversibility”. Composite materials using different bare materials and construction technologies can reach three different degree of

reversibility (e.g. small, medium and large). The aspect that must be controlled for having a good degree of reversibility is the type of resin used [41].

8.1.4. Aesthetic of Appearance

In the case of seismic upgrading by means of FRP the aesthetic appearance is directly connected with the type of elements to be retrofitted. In case Beylerbeyi Palace, it was noted that the walls are covered from one face. This requirement is very important with respect to aesthetic appearance. For the external walls, FRP can be applied between küfeki stone façade and masonry walls. In that condition all application would be hidden. For the internal walls the stucco plaster is in main concern and application side of the wall depends on this covering. For the timber covered room FRP can be applied underneath the timber surface. Finally for normal plastered walls there is no problem since plaster can be applied over the FRP application.

8.2. Base Isolation

For in-plane and out of plane loading masonry walls are very stiff and brittle. The actual behavior largely depends on the type of brick and the type of mortar involved but small ductility is a very limited factor. Typical inter-storey drifts at the initiation of cracking are in the range of few millimeters (2-3mm). Secondly small periods in the dynamic behavior may cause the structure to be affected from ground motion severely. For this reason, base isolation technique is one of the most effective strategies to upgrade the performance since it restrict the relative displacements of the within the wall and lengthen the period [41].

8.2.1. Technical Description,

Contrary to the traditional concept of seismic design, relying on the ductility resources of structural members and connections, the isolation approach is based on the response control concept, aiming at controlling and limiting the dynamic effects on the structural elements by means of special devices [41].

Seismic isolation approach is based on the reduction of the input energy to the structure, by a filter action of special devices. Structural disconnection may be realized between foundation and superstructure (base isolation) or part of the structure (roof isolation). Insertion of flexible elements at the structure-to-foundation interface modifies the dynamic properties of the system by increasing the global system deformability and reducing the magnitude of the seismic action on the structure. Secondly the energy dissipation capability of the structure under seismic loads is increased.

Isolation devices can be classified as Elastomeric Devices, High Damping Rubber Bearings (HDRB), Lead Rubber Bearings (LRB), Added Damping Rubber Bearings (ADRB), Friction Pendulum System (FPS), Sliding Devices, Flat Slider Bearings, Curved Slider Bearings, Elasto-plastic Bearings and Wire-Rope Bearings (Figure 8.16).

A very high structural performance can be achieved compared with fixed base buildings. However the long-term reliability of the seismic protection system could be impaired by a poor maintenance [41].

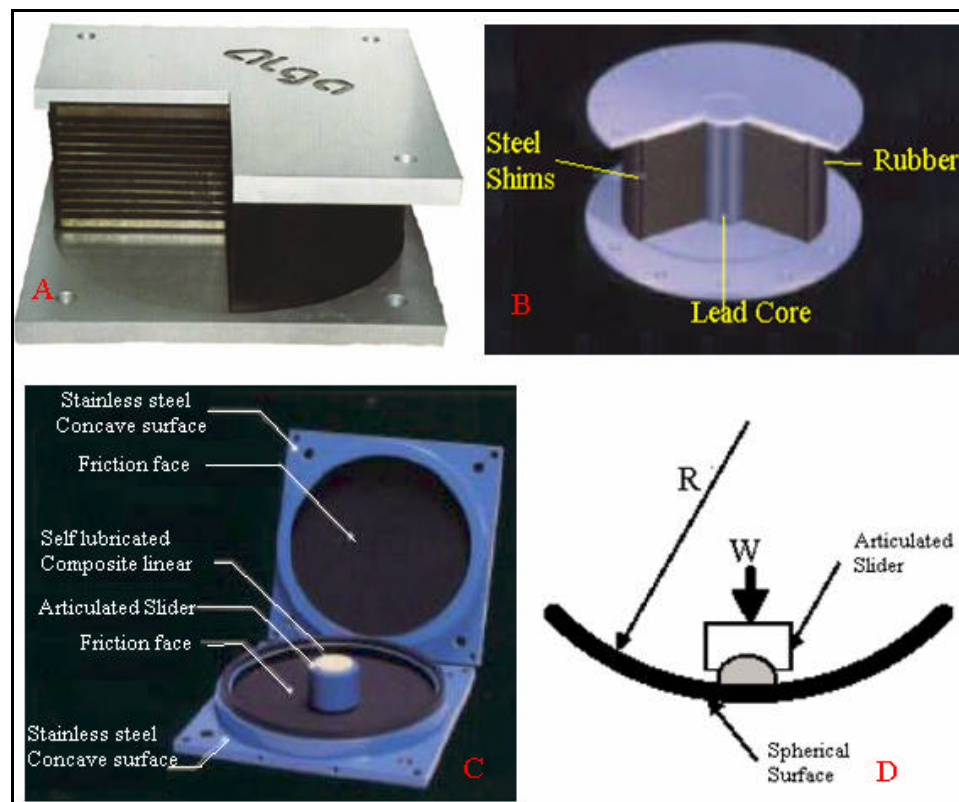


Figure 8. 16. Base isolation devices (A : HDRB, B:LRB, C, D : FPS)

In isolated systems special devices (seismic isolators) are used in order to reduce the amount of the energy transmitted to the structure. Basically, the effect of such devices is to shift the fundamental vibration period of the building upward, so as to reduce the value of the maximum spectral acceleration (Figure 8.17). For this reason seismic isolation is very appropriate for structures with short periods and low damping like masonry buildings. A given amount of input energy can be dissipated by the devices themselves, when these devices possess special dissipative features, or can be absorbed by additional damping devices. The effect of such devices is to increase the overall damping properties of the system. This prevents the structure from an excess of displacements, with a simultaneous control of damage in structural elements [41].

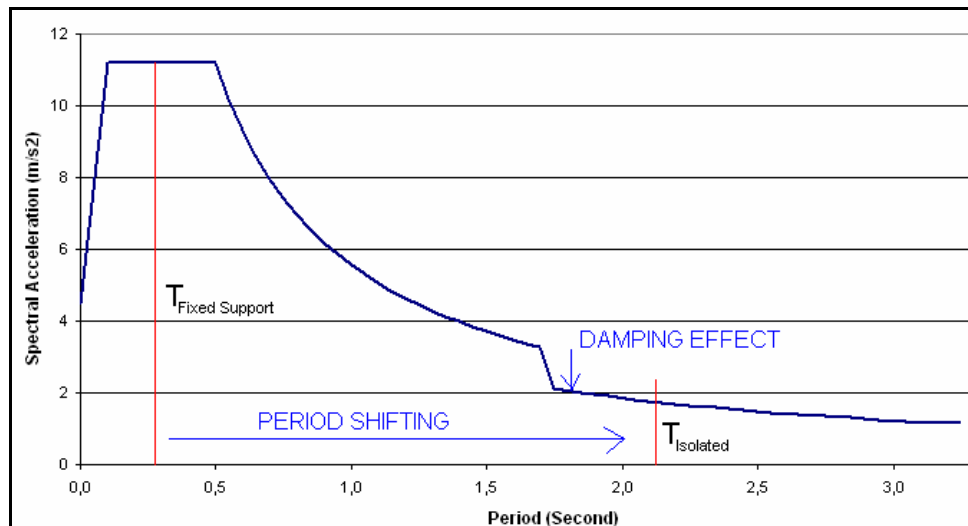


Figure 8.17. Period shifting and damping effect on response reduction

8.2.2. Practical Methodologies and Structural Detailing

The insertion of a seismic isolation system in an existing building needs a cut in the structure at floor chosen as isolation level (most often at the level of foundations). This operation is very delicate because it could induce damages in the structural members, especially in a rigid and brittle structure like Beylerbeyi Palace.

Application of such techniques showed a great convenience compared to other techniques in highly seismic areas. For the design of the base isolation system and for the safety of the super-structure, the maximum earthquake response spectrum is going to be

used. Dynamic modes of Beylerbeyi Palace showed that; all frequencies of 60 modes are on the flat plateau of the response spectrum. For this reason shifting the fundamental periods is going to result in significant reduction in spectral acceleration. Moreover additional damping is another factor to decrease the spectral acceleration value. Within this study High Damping Rubber Bearings (HDRB) would be used (Figure 8.18). These devices are composed of rubber and steel layers. Mechanical properties of each material and geometry of the device are in importance to resist both vertical and lateral forces.

For the base isolation project, initial point is the determination of the target period of the isolated structure. This is directly related to the amount of decrease in the maximum stress levels. In order to reduce the maximum stress values from 6.5 MPa to 0.85 MPa, the period of the isolated structure should be shifted around 2.5 second. With an additional decrease of damping effect the stress values on the structure would be acceptable.

Secondly the isolator should be distributed to the plan of the structure in a way that not to disturb the load flow. In reinforced concrete structure this aspect is not problematic since the isolators are placed under the columns. On the other hand the vertical elements are the masonry walls in Beylerbeyi Palace. The selected distribution of the devices is shown in Figure 8.18. Total number of bearing is determined as 123. For the design of the system the following steps are adopted [46]. Each of the parameters is defined at the place where it is first appears.

1. Select the design shear strain, γ_{max} and effective damping ratio, γ_{eff} for the bearing, and the target design period, T_D for the isolated structure. The former can be obtained from the material supplier. For this study γ_{max} and γ_{eff} were selected as 150% and 20% respectively [46]. T_D was already decided as 2.5 second.
2. Use code formulas, or static or dynamic analysis, to determine the effective horizontal stiffness K_{eff} and maximum horizontal displacement D_M of the bearing.

$$K_{eff} = \frac{P_{DL+LL}}{g} \left(\frac{2p}{T_D} \right)^2 \quad (8.1)$$

$$D_M = \frac{g}{4p^2} \frac{S_D T_D}{B_D} \quad (8.2)$$

where P_{DL+LL} is the vertical load acting on the isolator, S_D is the Spectral displacement B_M is the damping coefficient, given in Table 8.2 [47].

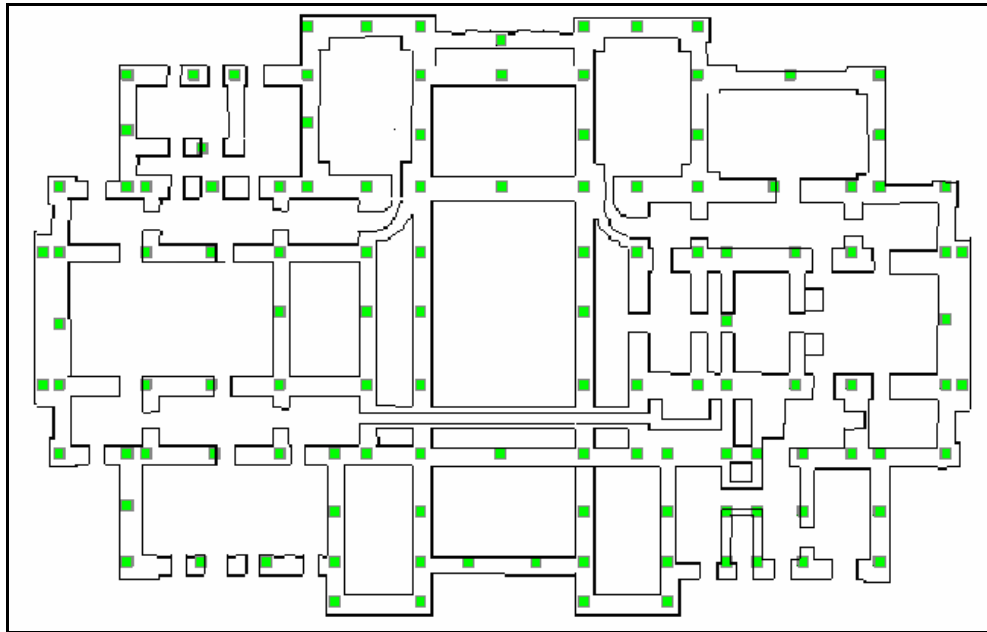


Figure 8.18. Plan lay-out of HDRB in Beylerbeyi Palace

According to number and locations of isolators maximum value of P_{DL+LL} was calculated 3200 kN, S_D was computed from acceleration response spectrum of the Maximum Considered Earthquake as 0.567 and B_M was determined as 1.5 from Table 8.2 [47].

Table 8.2. Damping coefficients B_D or B_M factor [47]

Effective damping γ_D or γ_M (Percentage of critical)	B_D or B_M factor
< 2%	0.8
5%	1
10%	1.2
20%	1.5
30%	1.7
40%	1.9
>50%	2

K_{eff} and D_M have been calculated as 2060 kN/m and 0.223 m respectively by using the formulas above.

3. Select the material properties, including Young's modulus E and shear modulus G , from the manufacturer's test report. These values depend on the hardness of the rubber used in the isolator. Table 8.3 shows the material properties of rubber according to its hardness [48].

Table 8.3. Relation of rubber hardness and material constants [48]

Rubber Hardness IRHD +- 2	Young's Modulus E (N/cm ²)	Shear Modulus G (N/cm ²)	Modified Factor k
30	92	30	0.93
35	118	37	0.89
40	150	45	0.85
45	180	54	0.8
50	220	64	0.73
55	325	81	0.64
60	445	106	0.57
65	585	137	0.54
70	735	173	0.53
75	940	222	0.52

In this study IRHD 60 rubber was selected ($E=4.45$ MPa, $G=1.06$ MPa and $k=0.57$). If no published data are available, G and E should be determined by test.

4. Calculate the total height of rubber, t_r , in the bearing according to the maximum displacement D_M and design shear strain γ_{max} by the formula below [46];

$$t_r = \frac{D_M}{\gamma_{\text{max}}} \quad (8.3)$$

t_r was computed as 0.11 m and selected as 0.15 m.

5. Calculate the effective area A and thickness t of individual rubber layers [46].

- a. Select the shape factor S under no rocking condition:

$$\frac{K_V}{K_H} = \frac{\frac{E_c * A}{t_r}}{\frac{G * A}{t_r}} = \frac{E_c}{G} = \frac{E(1 + 2kS^2)}{G} > 400, \quad (8.4)$$

for $S > 10$

where K_V is the vertical stiffness of the bearing, K_H is the horizontal stiffness of the bearing, G is the shear modulus, in the range of 0.4 to 1.0 MPa, E is Young's modulus, in the range of 1.5 to 5.0 MPa, E_c is the compression modulus of the rubber-steel composite, $E_c = E*(1 + 2kS^2)$, A is the full cross-sectional area (loaded area) of the bearing, t_r is the total height of rubber layers, k is the modified factor, in the range of 1 to 0.5, S is the shape factor = A/A_f and A_f is the load-free area around the bearing (Figure 8.19).

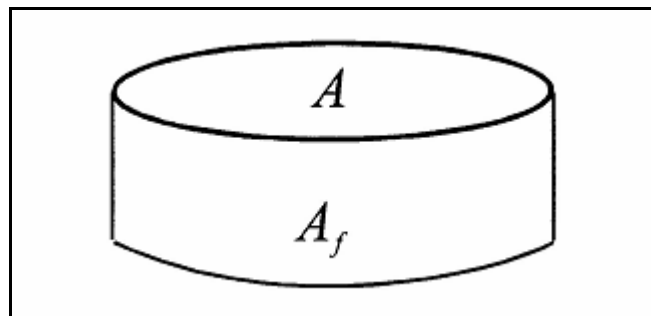


Figure 8.19. Load free area, A_f

In Equation 17.8, the stiffness ratio K_V / K_H is required to be greater than 400 for $S > 10$, since the P-d effect has been ignored in computing the horizontal stiffness K_H . In this study S is required to be greater than 9.1 and it was selected as 20. E_c has been calculated as 2034 MPa.

- b. Determine the effective cross-sectional area A_0 of the bearing based on the allowable stress s_c for the vertical load case P_{DL+LL} . Allowable value of s_c is 7.84 MPa. A_0 value has been calculated as 0.408 m^2 .

$$\mathbf{s}_c = \frac{P_{DL+LL}}{A_0} \quad (8.5)$$

- c. Determine the effective cross-sectional area A_1 of the bearing from the shear strain due to the vertical load P_{DL+LL} (eq). where e_b is the elongation of rubber at break. A_1 value has been calculated as 0.113 m^2 .

$$6S \frac{P_{DL+LL}}{E_c A_1} \left\langle \frac{e_b}{3} \right. \quad (8.6)$$

- d. Obtain the minimum cross-sectional area A_{sf} for shear failure of the bearing:

$$A_{sf} = \frac{K_{eff} * t_r}{G} \quad (8.7)$$

Use A_{sf} to determine the dimensions of the bearing. Then compute the effective cross-sectional area A_2 as the reduced area A_{re} given below (Figure 8.20):

$$A_{re} = L * (B - \Delta S); \text{ for a rectangular bearing}$$

$$A_{re} = \frac{d^2}{4} (\mathbf{b} - \sin \mathbf{b}); \text{ for a circular bearing} \quad (8.8)$$

$$\mathbf{b} = 2 \cos^{-1} \left(\frac{\Delta_s}{d} \right); \text{ for a circular bearing}$$

where L and B are the plan dimensions of the bearing perpendicular and parallel to the displacement respectively, Δ_s is the horizontal displacement of the bearing and d is the diameter of a circular bearing

A_{sf} has been computed as 0.291 m^2 and smaller diameter for the A_{re} has been determined as 0.9 m . Thereby respective A_2 area was decided as 0.636 m^2 for isolator.

- e. The design cross-sectional area A of the bearing is the maximum of the three values computed: A_0 , A_1 , and A_2 .

- f. Select proper dimensions for the rubber layer based on the design cross-sectional area A . Circular cross-section with 0.9m diameter rubber layers were chosen for the isolator geometry.

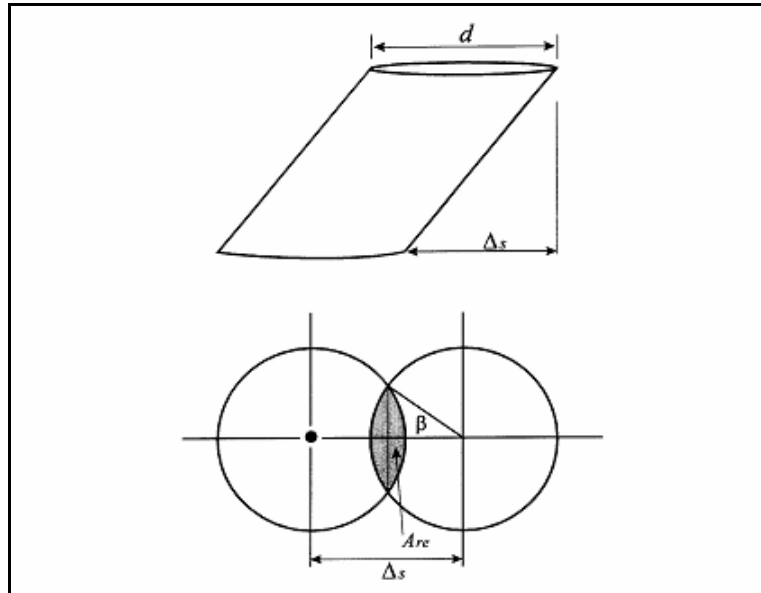


Figure 8.20. Reduced cross-sectional area of circular bearing [46]

6. Calculate the effective area A and thickness t of individual rubber layers [46].

Use the shape factor S and dimensions of the rubber layer to determine the thickness of individual rubber layer, t :

$$S = \frac{L * B}{2(L + B) * t} \quad ; \quad \text{for a rectangular bearing} \quad (8.9)$$

$$S = \frac{\mathbf{p} * d^2 / 4}{\mathbf{p} * d * t} = \frac{d}{4 * t} \quad ; \quad \text{for a circular bearing}$$

The thickness of individual rubber layer, t was calculated as 1.125 cm and selected as 1.2 cm. number of layer depends on the total rubber height ζ and thickness of an individual layer t . In this respect number of layer, N was computed as 13 by the formula below;

$$N = \frac{t_r}{t} \quad (8.10)$$

7. Finally compute the steel plate thickness t_s by the formula below [46];

$$t_s = \frac{2(t_i + t_{i+1}) * P_{DL+LL}}{A_{re} * F_s} > 2mm \quad (8.11)$$

where t_i , t_{i+1} are the rubber layer thickness in top and bottom of the steel plate, F_s is 60% of F_y , yield strength of the steel plates (= 274.4 MN/m²).

As a result the steel plate thickness was calculated as 1.9 mm and used as 2 mm. For the determined rubber and steel geometry a proper device was designed (Figure 8.21). 3.5 cm steel plates were used on the top and bottom-side of the isolator.

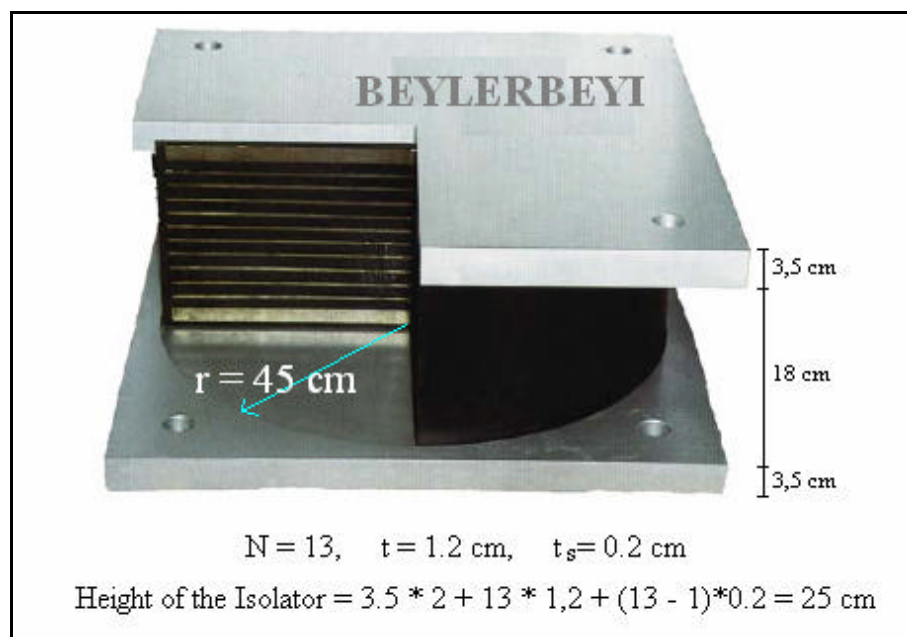


Figure 8.21. Geometry of the HDRB designed for Beylerbeyi Palace

The efficiency of the base isolation has been proved by Response Spectrum Analysis (RSA). The numerical model was revised to contain the determined device properties. The HDRB were modeled by beam elements having 25 cm height, geometrical and material properties of devices. Effect of the damping, in response spectrum of the earthquake

having 2% probability of exceedence within 50 years, was accounted by a reduction in spectral acceleration value of period beyond $0.8T_1$ by B_M . Finally Figure 8.17 has been determined as the response spectrum of the MCE for isolated structure.

The application of isolation has altered overall behavior of the structure significantly. Mode shapes of the structure turned to simple rigid body motions in transversal and longitudinal directions. The first mode is a movement of the all body in transversal direction with a torsional movement while second mode is simple movement is longitudinal direction. The third mode is the final mode to complete the overall mass of the structure to complete 100% of the mass to be included in the dynamic action. The period of the effective modes are beyond 2 second, indicating a great amount of reduction in spectral acceleration. Table 8.4 represents the dynamic characteristics of isolated Beylerbeyi Palace.

Table 8.4. Dynamic properties of isolated Beylerbeyi Palace

MODE	Period (Sec)	Mass Participation Ratio in X	Mass Participation Ratio in Y	Total Mass Participation Ratio in X	Total Mass Participation Ratio in Y
1	2.08	0.04	0.49	0.04	0.49
2	2.05	0.92	0.08	0.96	0.57
3	2.03	0.04	0.43	1	1
4	0.34	0	0	1	1
5	0.29	0	0	1	1

Figure 8.22 and 8.23 show the stress values for RSA in longitudinal and transversal directions respectively. It is clear that, the isolated structure is safe under maximum earthquake. All stress values are less than 0.85 MPa which is the tension strength of the masonry wall of the palace.

On the other hand, the application of base isolation systems as a retrofit strategy to Beylerbeyi Palace is indeed a challenging task. For the construction of two levels of rigid foundation, stone masonry walls are required to be cut. In this process the vertical loads should be supported by smart systems without causing tilting in the structure. For this reason special concern should be spend for the application of the strategy.

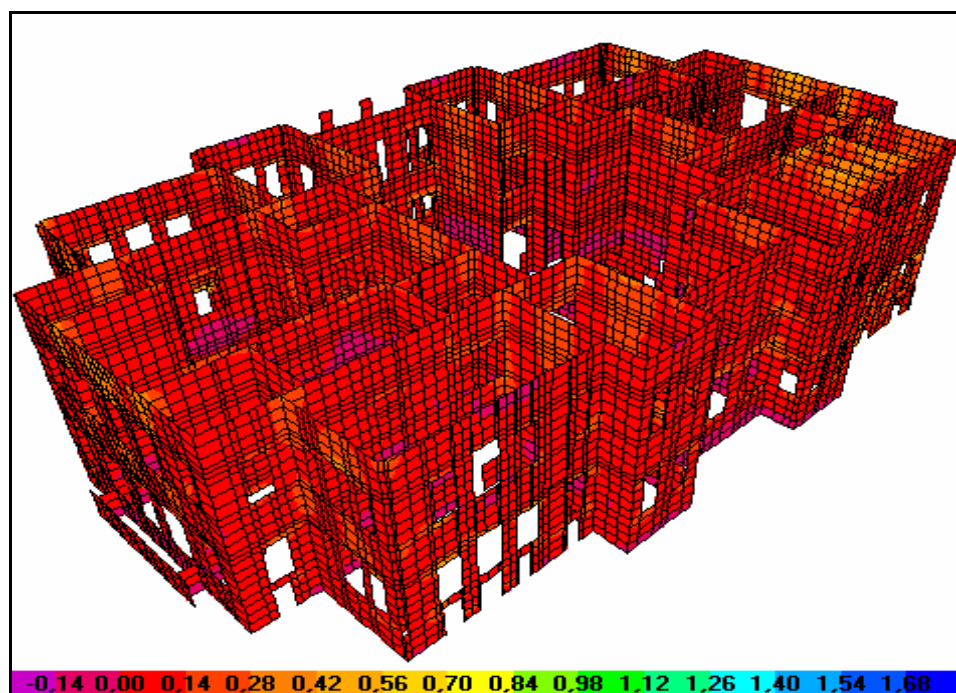


Figure 8.22. S11 stresses under RSA of MCE in longitudinal direction for isolated Beylerbeyi Palace with HDRB

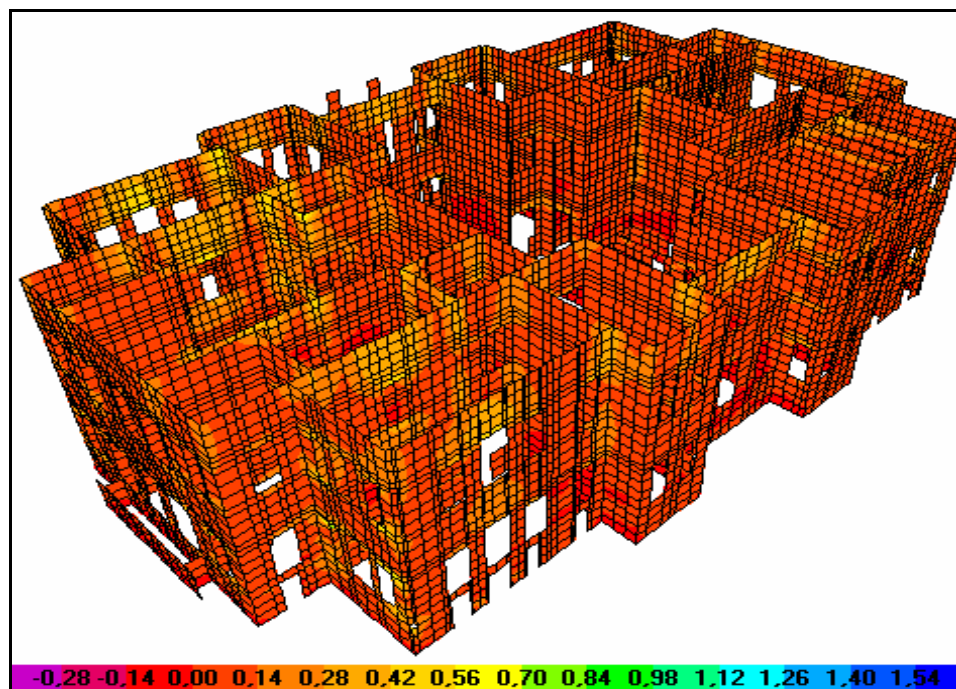


Figure 8.23. S11 stresses under RSA of MCE in transversal direction for isolated Beylerbeyi Palace with HDRB

Another important subject that should be accounted is the effect of the exterior adjacent wall (Figure 4.24) into dynamic behavior of the isolated Beylerbeyi Palace. Isolated structure has a period of 2.08 second with a horizontal displacement of 19 cm. Application requires the separation of the wall from the main structure by at least 19 cm gap.

Many new buildings has been equipped with base isolation systems and also many existing buildings of historical importance has were seismically upgraded by means of seismic isolation (like City and County Building in Salt Lake City, Utah (USA) and Parliament House, Wellington (NZ), see Figure 8.24 and 8.25) [41].



Figure 8.24. Parliament House, Wellington (Seismic retrofit, 1994) [40]

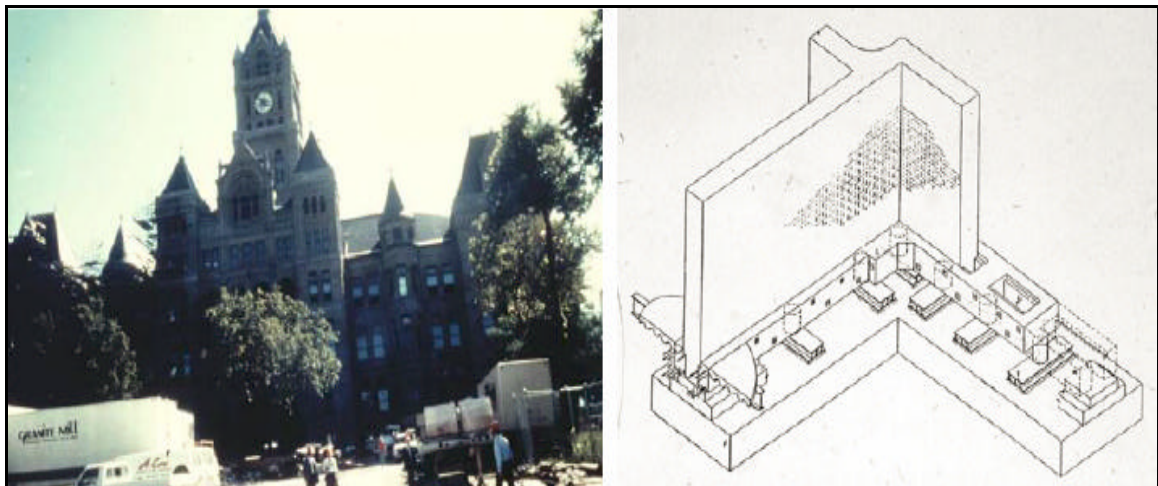


Figure 8.25. City and County Building, Salt Lake City, Utah (Seismic retrofit, 1989) [40]

8.2.3. Reversibility

For a seismic isolation at the level of foundation non-reversible intervention by adding rigid foundation beams is necessary. Seismic protection intervention is limited to the foundation level of the building, where a new reinforced concrete beam should be incorporated together with base isolators. In this way the facade and the interior including frescoes and other architectural elements are fully preserved. A historical layer of soil around the building is disturbed and there is a possibility of an irreparable loss of archaeological site. For this reason the level of reversibility can be rated as very good for the building itself but questionable for the possible archaeological site [41]. In case of Beylerbeyi Palace the application is appropriate with respect to architectural and historical aspects.

8.2.4. Aesthetic of Appearance

Seismic isolation is very convenient in the respect of aesthetic appearance as there are no interventions necessary above the foundation level and the aesthetic appearance is not impaired.

8.3. Consolidation of the Slabs to Have Rigid Diaphragm Behavior

The pushover analysis has proved that the lack of rigid slabs prevents the distribution of the horizontal loads among the masonry walls. It causes out of plane loading and failure for majority of the walls. Moreover the response spectrum analysis showed that the maximum stresses were created due to out of plane loading. In that condition the most logical consolidation technique is to make the timber floors rigid enough to transfer the loads and prevent out of plane loading.

8.3.1 Technical Description

In order to stiffen the timber slabs three techniques may be applied. These are the replacement of the timber slabs by reinforced concrete slab, application of reinforced concrete over the timber slab and use of steel members instead of timber members.

For all strategies the most important aspects is the application process. For this reason the connection of the old and new material should be designed well. For each strategy an extensive experimental and numerical modeling study must be carried out. The efficiency of the strategies should be tested to demonstrate the strategy is capable to connect the wall and transfer the loads between them.

Within the framework of this study no detail would be given except application of the concrete over timber beams. These details belong to a study named as “Innovative steel connection for a composite timber – steel – concrete slab system” [46]. In the study steel devices were used as connector between the timber and concrete. Two point loads are applied and performance of the composite beams with different connectors are tested (Figure 8.26).

In order to work as a rigid diaphragm the concrete slab should have at least 7 cm thickness and should also be connected to masonry walls appropriately [special communication with J. M. Proenca].



Figure 8. 26. Application of concrete over timber beams with steel connector [49]

8.3.2. Practical Methodologies and Structural Detailing

Three slab systems of the palace on each storey level have similar orientation with timber beams. The slab system on basement floor has no effect on the structural and dynamic properties of the structure due to stiff basement walls. On the other hand the first and second storey slabs are effective. For this reason the consolidation should emphasize over these two slabs. Furthermore the consolidation of the first storey slab gives damage to

the historic fabric of the palace and it requires excessive efforts while working in the roof floor do not give any harm to the historical aspects of architectural appearance. For this reason the retrofit technique is restricted to consolidation of only second floor slab, which is the roof floor.

The efficiency of the rigid diaphragm is proved by response spectrum analysis. The numerical model with rigid second floor was subjected to maximum earthquake. Figure 8.27 and Figure 8.28 show the regions of horizontal and vertical stresses beyond the tensile strength of the masonry under Maximum Considered Earthquake. The results showed that;

- The rigid diaphragm reduced the stress values and thereby critical zones on which the tensile strength of the masonry has been exceeded.
- On the other hand the consolidation technique could not save the structure under maximum earthquake.
- For this reason the application itself is not enough but this strategy may be completed by another discussed retrofit strategy which is use of Fiber Reinforced Polymer. Orientation of the FRP can be determined according to critical stress zones, seen in Figure 8.32 and 8.33.
- By the application of the strategy, the dynamic properties of the structure were totally altered. The rigid floor in the second storey causes the wall to act together. In this respect the external adjacent wall (Figure 4.24) will affect the dynamic properties of the palace adversely. For this reason the wall should be separated from Beylerbeyi Palace for the safe application of the strategy.

8.3.3. Reversibility

Reversibility aspect of the strategy is one of the most important strategy that had caused to restrict the application are of the strategy to second floor slab which is also roof of the structure. On this level, ant intervention can be done without touching the historical fabrics since it is totally separated from the palace. On the other the first storey slabs is connected to the historical aspects. For this reason during the installation process and removal process serious damages can be given to the palace. Thereby any consolidation technique, applied to only the roof slabs can be categorized as reversible.

8.3.4. Aesthetic of Appearance

Because of the mentioned characteristics of the strategy in previous reversibility part the retrofit strategy is suitable with respect to aesthetic appearance aspect.

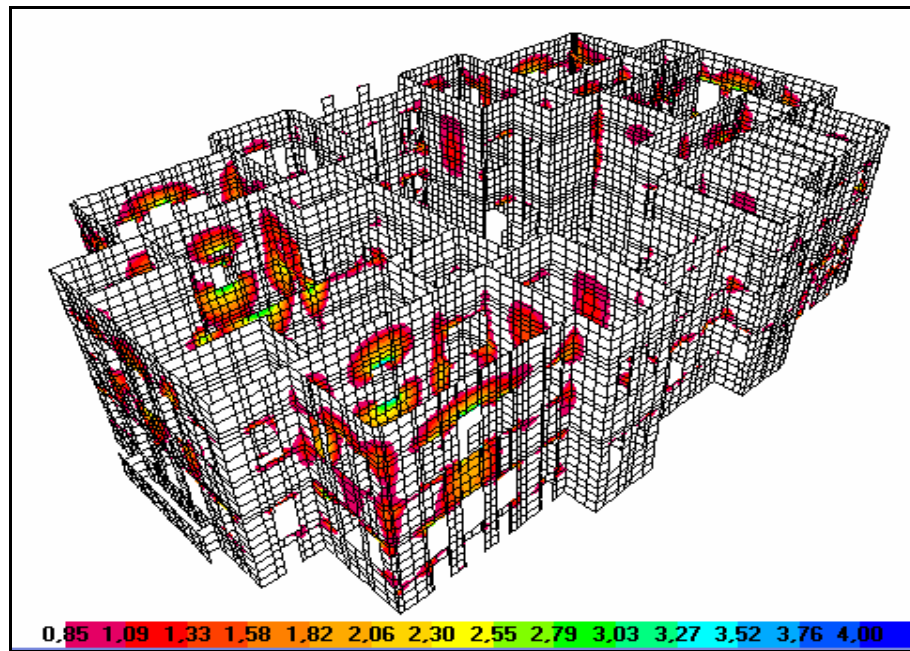


Figure 8.27. Critical horizontal stress zones for rigid diaphragm application under MCE

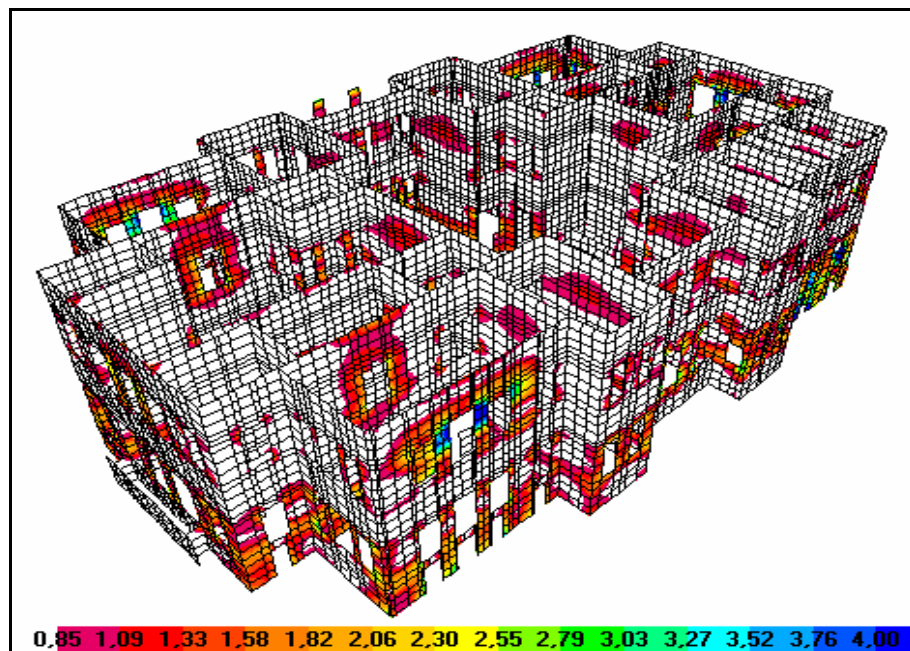


Figure 8.28. Critical vertical stress zones for rigid diaphragm application under MCE

9. CONCLUSION

In one sense Beylerbeyi Palace is a representative of the great buildings in the late of 19th century in Istanbul and elsewhere in the Ottoman Empire. Starting with the study of historical background of the structure and ending with the evaluation of possible retrofit strategies to prolong the life of the structure by centuries, the following important findings have been revealed.

As examined in detail throughout the second and third chapters of this thesis, the construction material is a typical stone, brick and lime mortar combination used in almost all the 19th century Ottoman structures. Thick masonry walls of the structure are the main lateral load carrying members and for the large spans wood truss systems were in use. Chemical and mineralogical surveys, namely Thin Section, SEM-EDX and XRD analyses, of the mortar ruins taken from the palace have revealed the origin of the mortar as Horasan type mortar used in Ottoman time. In order to determine the material characteristics of the palace, laboratory made mortar and masonry specimens were produced with two types of mortar formulas. Compression test was performed and required material characteristics were determined for masonry.

Dynamic properties of the structure have been determined by Ambient Vibration Survey and via numerical model of the structure. Laboratory test results were used for material properties of the masonry in the numerical model. Later numerical model was altered to have the same dynamic properties as the results of AVS. The calibration process proved that, the laboratory tests over reproduced masonry specimen gave sufficiently accurate results for the most of the palace. Since it does not account the effect of iron reinforcement and existing damages, some alterations were required for specific region of the palace. Moreover one mode of AVS has been obtained as two or more mode of the numerical model.

The earthquake performance of the structure was checked by response spectrum analysis. Three different earthquake hazards were used. These are the design earthquake of Turkish Earthquake Code, Design and Maximum Considered Earthquake defined in

FEMA-356 and characterized by site specific hazard estimation. The palace was assessed as weak under all earthquake hazards. The existing damages in the structure and stress concentration regions in the numerical model were compared. For the corners of the openings and at the window edges good agreement has been reached between observed crack patterns and theoretically obtained ones.

In order to identify the nonlinear behavior of the structure pushover analyses were performed with two different material models, namely, Drucker-Prager Material Model (DPMM) and Crushing Cracking Concrete Model (CCCM). The exterior walls in longitudinal and transversal directions were determined as more vulnerable than the interior walls under horizontal loads. Moreover it was also noted that, CCCM gives more suitable results than DPMM applied to masonry structure.

Three possible retrofit strategies have been proposed against MCE. These are the application of fiber reinforced Polymer, Base Isolation and Consolidation of Second Storey Slab to have Rigid Diaphragm Action. Reversibility and aesthetic appearance subjects were clearly explained.

A retrofit strategy best applicable to this type of masonry should add sufficient strength and some ductility to the walls to obtain the required performance level against earthquakes for the weakest parts of the wall sections. For the application of FRP, it was seen that different FRP orientation can be proposed for different ground shaking characteristics and almost every wall should be covered by FRP in order to prove the efficiency of the strategy against Maximum Considered Earthquake. With an appropriate application of the strategy it was concluded that, historical aspects and aesthetic appearance can totally be saved.

Second seismic retrofit technique, the application of base isolation, gave the desired performance with 123 units High Damping Rubber Bearing (HDRB). After the application it was seen that dynamic properties of the structure altered significantly and the maximum stress values did not exceed the strength of the material under MCE. In addition the application of base isolation on the foundation of the structure can be a solution for the decomposition of the stone masonry due to high humidity level. In this respect the affected

masonry walls can be replaced by a wall system which allows the safe application of base isolation system and does not affect the historical value and aesthetic appearance of the structure. It is important to note that, the exterior adjacent wall (Figure 4.24) must be separated from the main structure since it disturbs dynamic properties of the retrofitted structure by the application of base isolation.

The last retrofit strategy aims to allow the force transmissions among the structural walls of the palace by creating rigid slab system. For the consolidation of the floor slabs, the application of the strategy was limited to roof level of the structure due to historical and architectural reasons. For this application, it was seen that, the strategy could not give the desired performance, although it reduced the stresses significantly. However the strategy may be used with another retrofit technique together, such as FRP application. Before the application of this strategy, the exterior adjacent wall must be separated from the main structure.

Once the application details of these retrofit options are produced and the cost/benefit studies are performed for each case, the one most suitable for the expected performance level can be selected.

As the final comment apart from the specific findings of the study related to historical Beylerbeyi Palace, it can be concluded that, the followed scientific approaches of the present study are hopefully expected to serve as a model for the future studies of the engineering assessment of the historical structures.

REFERENCES

1. Erdik, M., M. Demircioglu, K. Sesetyan, E. Durukal and B. Siyahi, ‘Earthquake hazard in Marmara Region, Turkey’, *Soil Dynamics and Earthquake Engineering*, Vol. 24, pp. 605–631, 2004.
2. Lourenco, P. M., “Recommendations for Restoration of Ancient Buildings and the survival of a Masonry Chimney”, *Construction and Building Materials*, Vol. 20, pp. 239-251, 2006.
3. PROHITECH, *Earthquake Protection of Historical Structures by Reversible Mixed Technologies*, Specific Targeted Research or Innovation Project, Abridged Version of Annex-I, 2004.
4. Asteris, P. G., A. D. Tzamtzis, P. P. Vouthouni, and D. S. Sophianopoulos, “Earthquake Resistant Design and Rehabilitation of Masonry Historical Structures”, *Practice Periodicals on Structural Design and Construction*, pp. 49-55, 2005.
5. Krstevska, L. and L. Taskov, *Ambient Vibration Measurements of Beylerbeyi Palace*, IZIIS Report No: 2006-030, Skopje, 2006.
6. Eren, R. H., F. Y. Oktay and O. M. Ilkisik, *Beylerbeyi Sarayi Jeolojik/Jeoteknik Etüt Raporu*, TBMM of National Palaces, Report no. 05-528, Istanbul, 2005.
7. Ministry of Public Works and Settlement, *Specifications for the Buildings to be Constructed in Disaster Areas*, IMO Izmir Subesi, Izmir, 1998.
8. Federal Emergency Management Agency, FEMA-356, *Prestandart and Commentary for the Seismic Rehabilitation of the Building*, FEMA, Washington, 2000.

9. Applied Technology Council, ATC-40 *Seismic Evaluation and Retrofit of Concrete Buildings*, Vol. 1, ATC, Redwood City, California, 1996.
10. TBMM Department of National Palaces, *Beylerbeyi Palace*, Istanbul, 1993.
11. Torres, M. I. M., V. S. Freitas, “Treatment of Rising Damp in Historical Buildings”, *Building and Environment*, Vol. 42, pp. 424-435, 2007.
12. Masonry Structural Design for Buildings, *Departments of the Army, the Navy and the Air Force*, 1992, <http://www.usace.army.mil/publications/armytm/tm5-809-3/chap10.pdf>
13. Sorenson Building Masonry Evaluation, *Atkinson-Noland & Associates INC. Consulting Engineers*, http://www.ana-usa.com/download/sorenson_building/pdf
14. Elsen, J., “Microscopy of Historic Mortars-A Review”, *Cement and Concrete Research*, Vol. 36, pp. 1416-1424, 2006.
15. Böke, H., S. Akkurt, B. Ipekoglu and E. Ugurlu, “Characteristics of Brick Used as Aggregate in Historic Brick-Lime Mortars and Plasters”, *Cement and Concrete Research*, Vol. 36 pp. 1115-1122, 2006.
16. Gülec, A., T. Tulun, “Physico-chemical and petrographical studies of old mortars and plasters of Anatolia”, *Cement and Concrete Research*, Vol. 27 pp. 227–234, 1997.
17. Antonelli, F., S. Cancelliere, L. Lazzarini, “Minero-petrographic characterization of historic bricks in the Arsenale, Venice”, *Journal of Cultural Heritage*, Vol. 3 pp. 59–64, 2002.
18. Bianchini, G., E. Marrocchino, C. Vaccaro, “Chemical and mineralogical characterization of historic mortars in Ferrara (northeast Italy)”, *Cement and Concrete Research*. Vol. 34, pp. 1471–1475, 2004.

19. Yüzer, E., N. Görür, E. Gürdal, M. Vardar, “*Dolmabahçe Sarayında Kullanılan Tasların Korunmuşluk Durumlarının, Ayrısma Nedenlerinin Belirlenmesi ve Koruma ve Onarım Yöntemlerinin Saptanması*”, ITU Gelistirme Vakfi, Report No: 01-103.
20. Akman, M.S., A. Güner, I.H. Aksoy, “The History and Properties of Khorasan Mortar and Concrete”, *Turkish and Islamic Science and Technology in the 16th Century*, ITÜ Research Center of History of Science and Technology, Vol. 1, pp.101–112, Istanbul, 1986.
21. Moropoulou, A., A. Bakalos, S. Anagnostopoulou, “Composite Materials in Ancient Structures”, *Cement and Concrete Composites*, Vol. 27, pp. 295–300, 2005.
22. EN1052, *Methods of Tests for Masonry*, 2000.
23. Eurocode-6, *Design of Masonry Structures*, 1996-3:2006.
24. Tomazevic, M., *Earthquake-Resistant Design of Masonry Structures*, Imperial College Press, London, 1999.
25. Bozkurt, A. Y. and Y. Göker, *Fiziksel ve Mekanik Ağaç Teknolojisi*, Istanbul University Press, Istanbul, 1996.
26. Bozkurt, A. Y. and N. Erdin, *Ağaç Teknolojisi*, Istanbul University Press, Istanbul, 1997.
27. Çeribası, S., *Static and Dynamic of Super-elliptic Homogeneous and FGM Plates*, Ph.D. Thesis, Bogazici University, 2007.
28. Structural Analysis Program, *SAP2000 Integrated Finite Element Analysis and Design of Structures*, Analysis Reference, Vol. 1, Berkeley, California, 2006.

29. London University Structural Analysis System, *LUSAS Finite Element Analysis, Examples Manual*, 2004.
30. TS498, *Design Loads for Buildings*, Turkish Standards Institution , Ankara, 1997.
31. Chopra, A., *Dynamics of Structures*, Prentice Hall, Upper Saddle River, NJ, 2001.
32. Hart, G. C. and K. Wong, *Structural Dynamics for Structural Engineers*, John Wiley & Sons, Inc., New York, 1999.
33. International Code Council, *International Building Code*, 2000.
34. Karaesmen, Er. and C. Erkey, An Approach for the Evaluation of Seismic Action, *10th European Conference on Earthquake Engineering*, Duma, 1995, pp. 1929-1934, Balkema, Rotterdam.
35. Erkey, C. and E. Karaesmen, Site Effects and Considerations for Seismic Code Renewals, *11th European Conference on Earthquake Engineering*, Acapulco, 1996, (in CD format).
36. Erkey, C., En. Karaesmen and Er. Karaesmen, Significance of Spatial Variation of Seismic Motion and Consequences Affecting Design Procedure, *12nd European Conference on Earthquake Engineering*, London, 2002.
37. Aras, F. *Nonlinear Response Analysis of Retrofitted Structures by Different Strategies*, M. S. Thesis, Bo gaziçi University, 2001.
38. Landolfo, R., B. Faggiano and F.P. Portioli, “*Preliminary Studies in Numerical Analysis*”, Earthquake Protection of Historical Structures by reversible mixed Technologies, WP8, Naple, 2006.
39. Lazorav, L. *Theory of Plasticity and Elasticity*, Lecture Notes, Skopje, 2006.

40. Calado, L., J.M. Proença and A. Panão, “*Innovative materials and techniques for seismic protection*”, Earthquake Protection of Historical Structures by reversible mixed Technologies, WP5, Lisbon, 2006.
41. Beg D., P. Skuber and L. Pavlovic, “*Set-up of advanced Reversible Mixed Technologies for Seismic Protection*”, Earthquake Protection of Historical Structures by reversible mixed Technologies, WP6, Ljubljana, 2006.
42. Triantafillou T.C., “Strengthening of Masonry Structures Using Epoxy-Bonded FRP Laminates”, *Journal of Composites for Construction*, Vol. 2, No. 2, pp. 96-103, 1998.
43. Hamilton H. R. and C.W. Dolan, “Flexural Capacity of Glass FRP Strengthened Concrete Masonry Walls”, *Journal of Composites for Construction*, Vol. 5, No. 3, pp. 170-178, 2001.
44. Valluzzi M. R., D. Tinazzi and C. Modena, “Shear behavior of masonry panels strengthened by FRP laminates”, *Construction and Building Materials*, Vol. 16, 2002.
45. Stoian V., T. Nagy-György, D. Dan and J. Gergely, “Retrofitting the Shear Capacity of the Masonry Walls Using CFRP Composite Overlays”, *The SE 40EE International Conference in Earthquake Engineering*, Skopje, Macedonia, 2003.
46. Yang, Y. B., K. C. Chang, and J. D. Yau, “Base Isolation”, *Earthquake Engineering Handbook*, Chapter 17, CRC Press, 2002.
47. Federal Emergency Management Agency, FEMA-302, *NEHRP Recommended Provisions for Seismic Regulations for New Buildings and Other Structures*, FEMA, Washington, 1997.
48. Bridgestone Corporation, *Multi Rubber Bearings*, International Industrial Products Department, Tokyo, 1990.

49. Calado, L., J. M. Proença and A. Panão, “*Innovative Steel Connections for a Composite Timber - Steel - Concrete Slab System*”, Earthquake Protection of Historical Structures by reversible mixed Technologies, WP7, Lisbon, 2007.